4. GEOLOGICAL STRUCTURE & PHYSICAL OCEANOGRAPHY

4.1 Geological Structure

Introduction. The Philippine Islands are situated along the western margin of the tropical North Pacific Ocean, between 6° and 18° North Latitude (see Fig. 4.1). This island chain is one of several island arcs within the western North Pacific Ocean and around its perimeter.

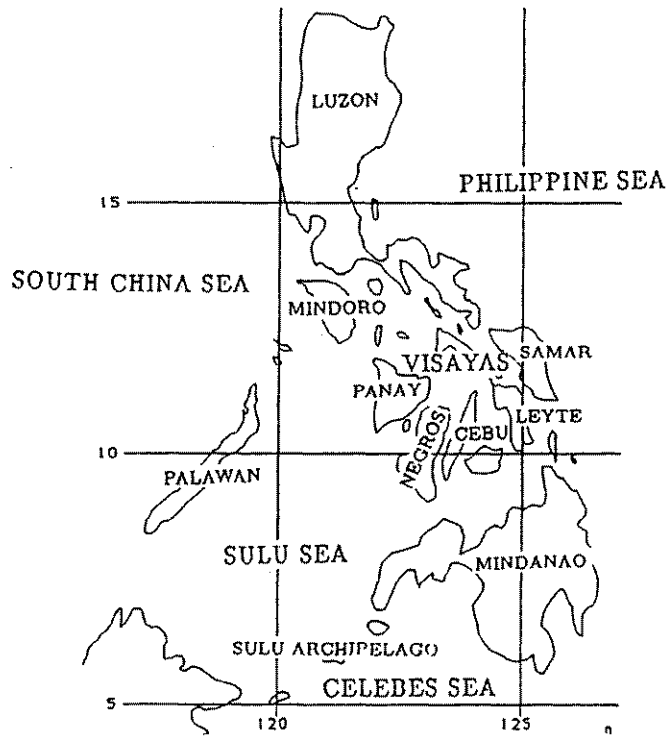

Figure 4.1: Map of the Philippines.

Typically, these island arcs are associated with significant volcanic activity in the mountains along the arc as well as under the sea itself, and with deep ocean trenches along the adjacent ocean (see Fig. 4.2). The Philippine arc displays these typical characteristics. In addition, there are marginal seas that separate the Philippine arc from the Asian continent to the west (see Fig. 4.3).

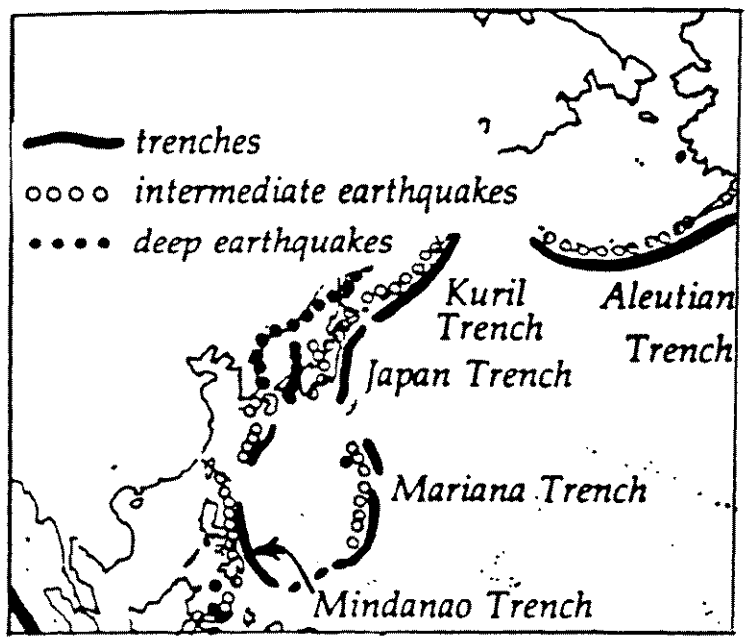

Figure 4.2: Island Arcs showing Earthquake Foci (adapted from Ingmanson and Wallace (1973)).

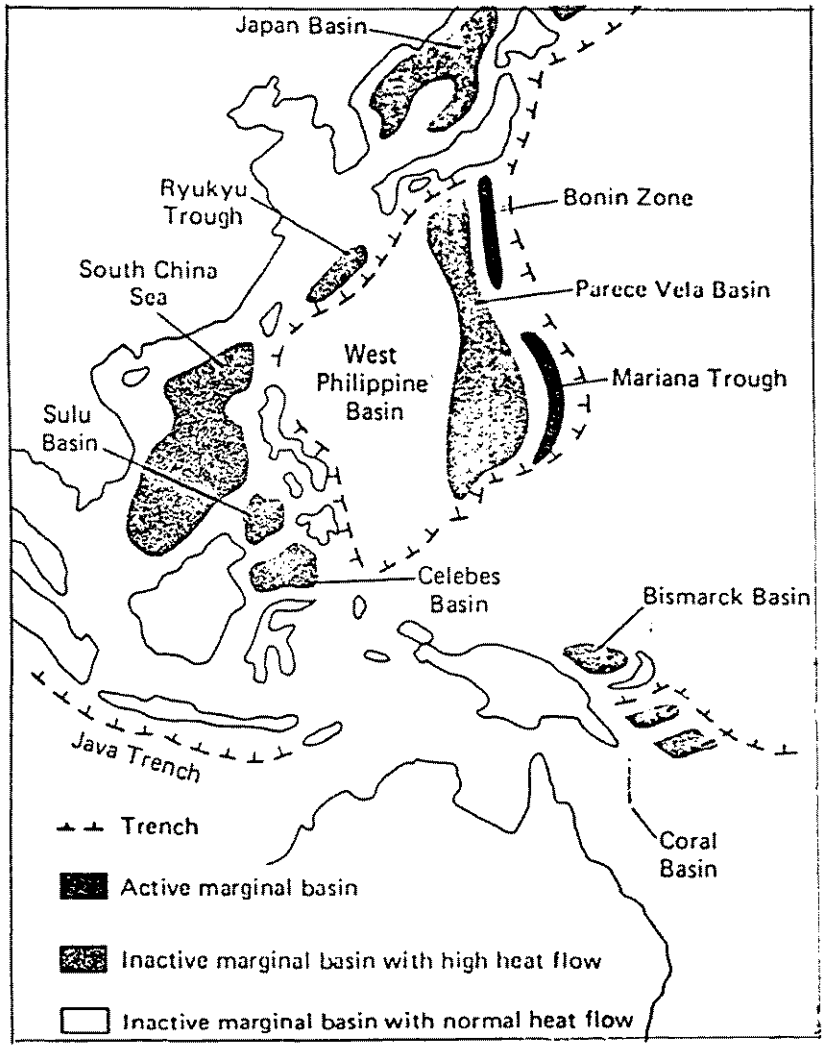

Figure 4.3: Distribution of Marginal Basins in the Western Pacific (adapted from Eicher and McAlester (1980)).

This arc/trench/marginal sea structure has developed in response to geological forces operating within the earth's crust and upper mantle underneath this region; those forces appear to have influenced this region throughout its geological history, continuing into the present. Geologists believe this region has been subject to an unusually large number of such forces.

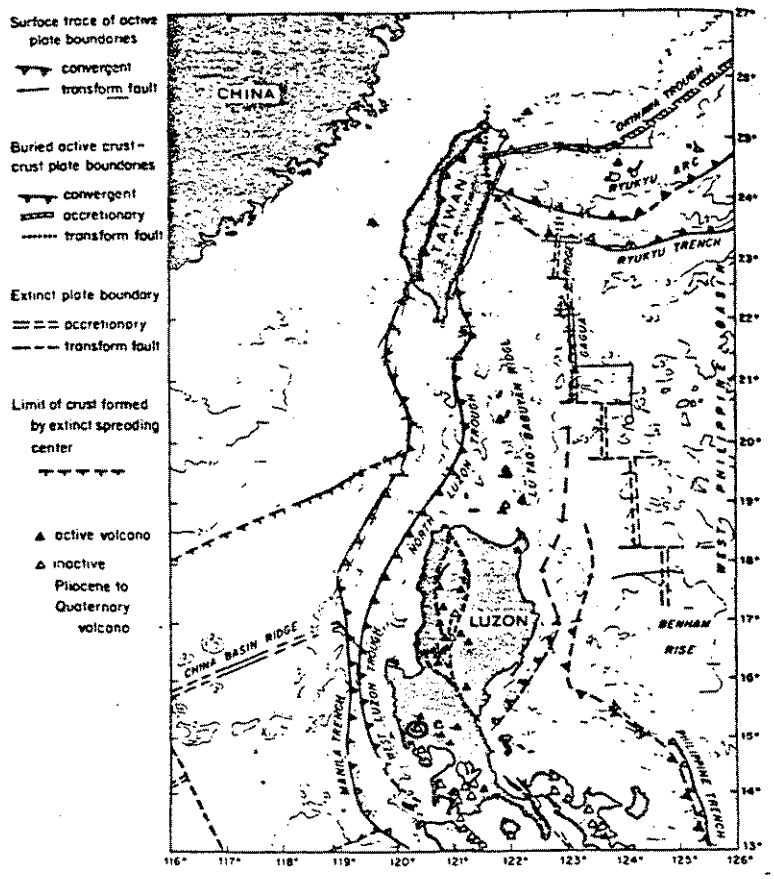

Figure 4.4: Active and Extinct Plate Boundaries in the Taiwan-Luzon Region. The Mount Pinatubo Volcano which became active in June 1991 is circled (adapted from Bowin et al. (1978)).

The earth's crust appears to be made up of numerous large plates on which the present continents and oceans lie (see Dewey 1972, pp 34–35). These plates move in response to forces within the earth's mantle, which lies beneath the earth's outer crustal layer; this motion is often described as "Continental Drift".

Mid-ocean ridges or rises are the surface (or subsurface) features above the upward part of the convective current; subduction zones mark the descending portion of the convection current at the plate boundary. The marginal seas west of the Philippines are on continental crustal plates (see Dewey 1972, p. 40). Subduction zones are associated with volcanoes, deep ocean trenches and earthquakes. The volcanoes observed in the Philippine Islands originate from the subduction zone activity (see Dewey 1972, p.40). The large numbers of active volcanoes on Luzon, as well as inactive volcanic mountains, is shown in Fig. 4.4. The relationship between the convergent plate boundaries, and the Philippine and Manila Trenches is illustrated here as well.

Earthquake activity located off the coasts of northern Luzon and extending across Luzon Strait to Taiwan, for the years 1904–1974, is shown in Fig. 4.5.

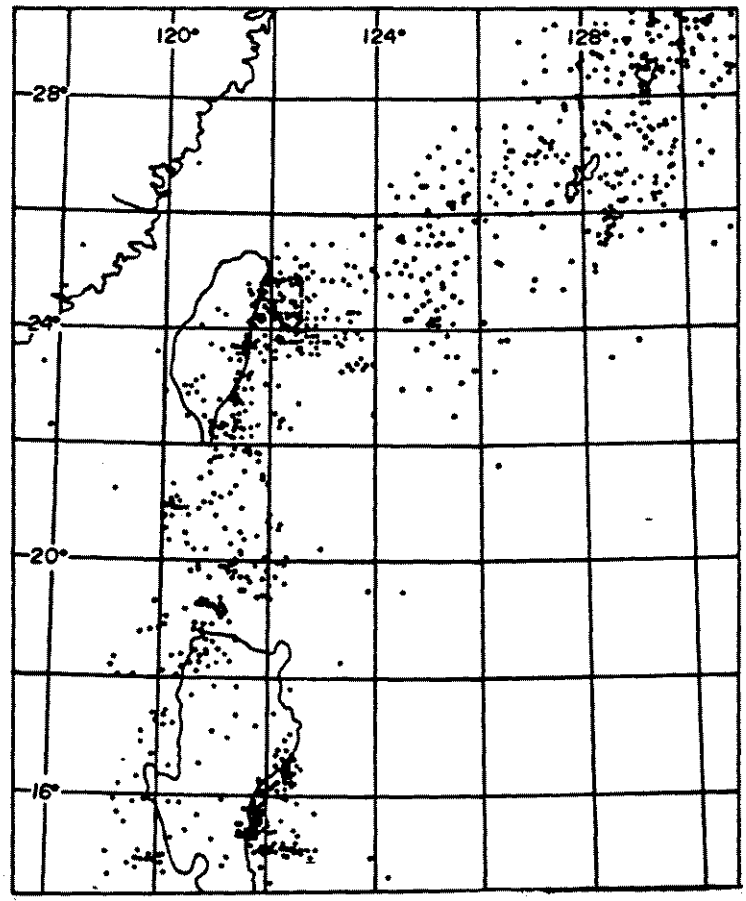

Figure 4.5: Map showing the Epicenters of the Earthquakes occurring between 1904 and 1974 in the Taiwan Region including Parts of the Ryukyus and the Philippines (adapted from Chingchang et al. (1985)).

Shallow-focal depth earthquakes dominate in the region seaward from the Philippine fault zone; this zone is shown as the solid line along the eastern portion of the major Philippine Islands in Fig. 4.6. On the marginal-sea side of the fault zone, deep-focus earthquakes appear; some shallow-focus earthquakes have occurred in this region also.

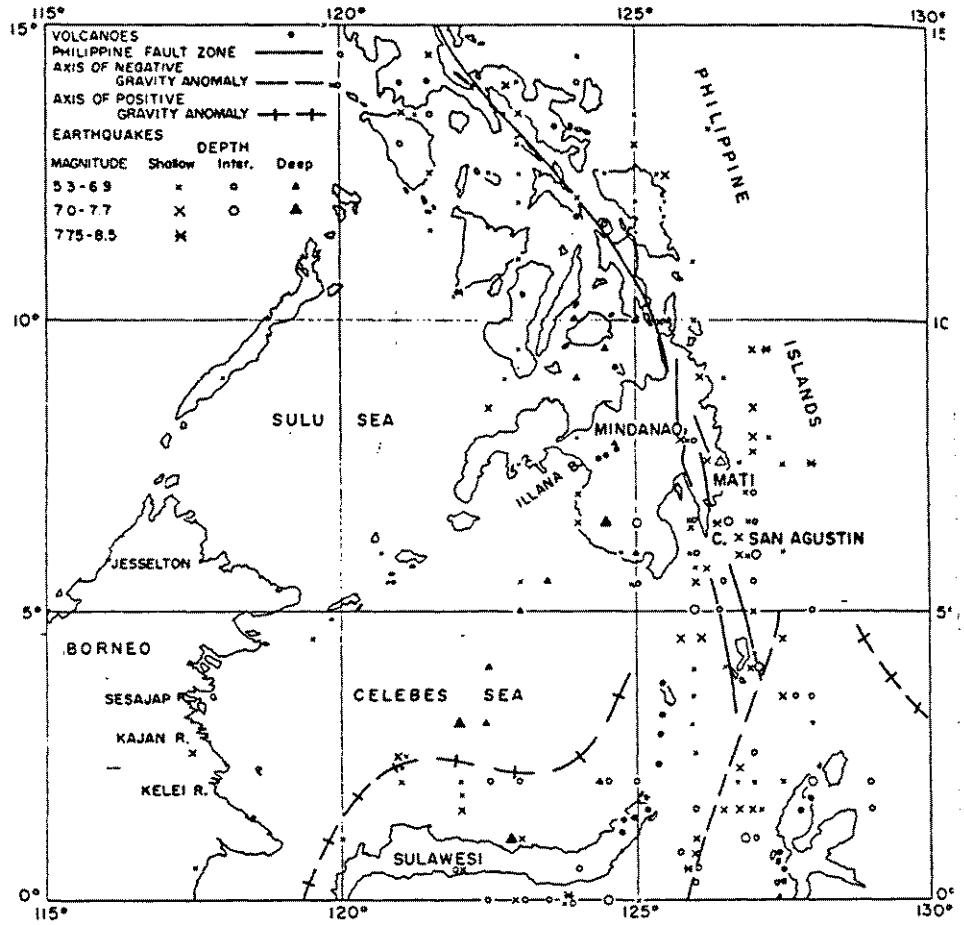

Figure 4.6: Location of Earthquakes, Volcanoes, Gravity Anomalies and Philippine Fault Zone (adapted from Krause (1966)).

All of these influences have given the Philippine Islands region a complex configuration of ocean and marginal sea basins, interspersed with many island chains; see the bathymetric chart of this region (Fig. 4.7).

The complexity of this bathymetry and the many island chain configurations influence the physical ocean characteristics within the marginal seas and the adjacent ocean regions.

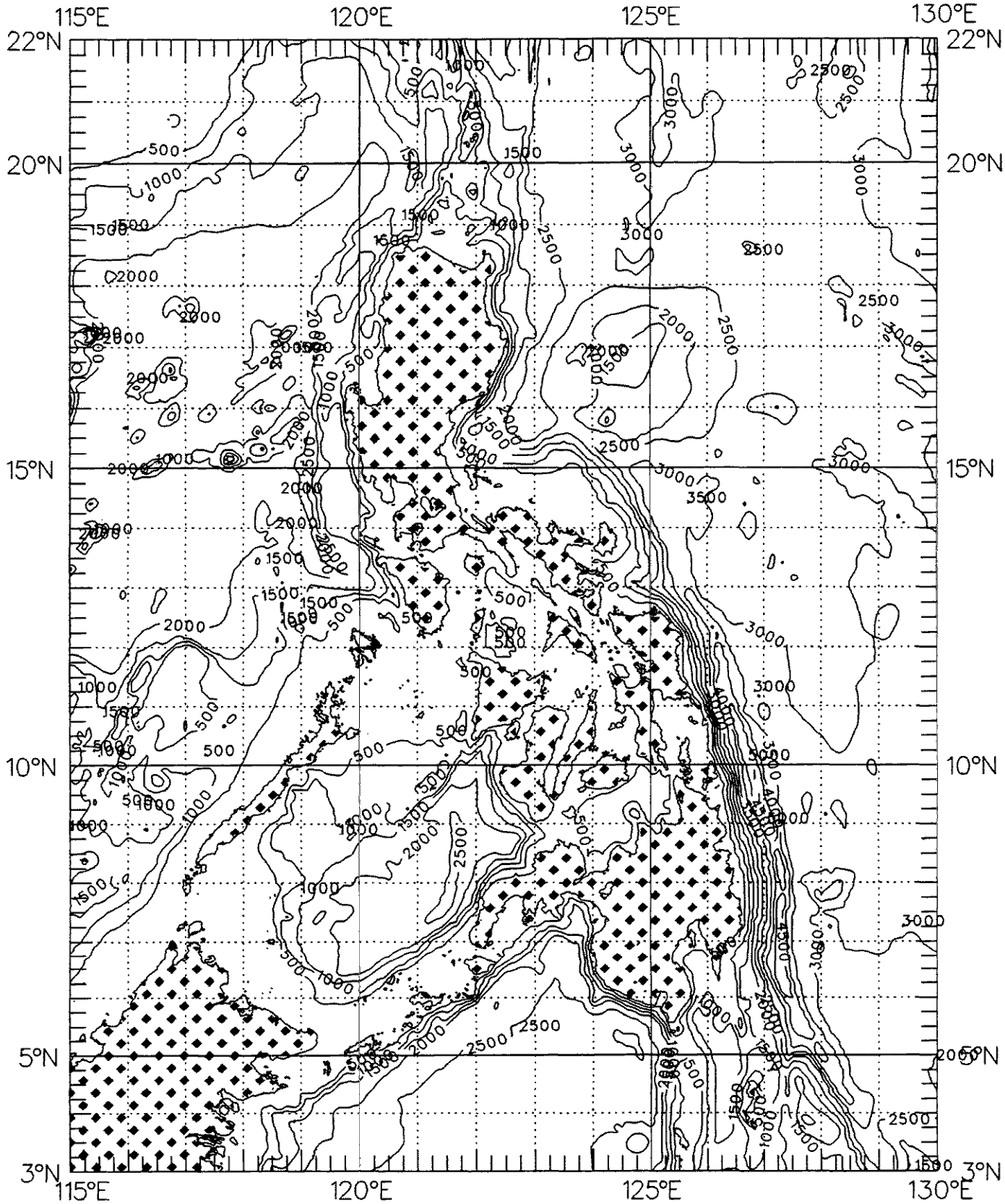

Figure 4.7: Bathymetry surrounding the Philippine Islands with depths in fathoms (The Naval Oceanographic Office).

Tides and ocean currents are constrained by narrow island passages and by the island chains that surround the various marginal seas. Restrictions to water exchange between the open ocean and the marginal seas greatly influence the temperatures and salinities observed along the Philippine Islands coastlines. These restrictions affect the ocean response to influences such as long- and short-wave radiation reaching the water surface, or the advection by ocean currents of temperature and salinity differences into a marginal sea.

Thus the oceanography along the Philippine Islands coastlines and within adjacent marginal seas is quite complicated. It is helpful to focus this discussion on several different regions in turn, to better describe the resulting oceanography.

The following regions will be treated: (1) the western portion of the Philippine Sea (the open ocean region to the east of the Philippine Islands); (2) the northern portion of the South China Sea (west of the major Philippine Islands, separating them from the Vietnam and China coasts of the Asian mainland); (3) the Sulu Sea (which separates the southern Philippine Islands from Palawan Island and the South China Sea; and (4) one of the two major straits which are to the north and south of the Philippines chain, separating the Philippine Sea from the marginal seas, and through which much of the water exchange occurs: Luzon Strait and Bashi Channel (on the north between Luzon and Taiwan); Balabac and Sibutu Straits (on the south, separating Palawan and the Sulu Archipelago from North Borneo) are regions with few, if any, published oceanography studies.

4.2 Ocean Parameters

4.2.1 Introduction

The following is a description of ocean factors which can affect weather occurring in the Philippines and the adjacent ocean areas.

1. Some ocean factors directly affect the overlying atmosphere:

   (a) Sea surface temperature provides a modifying influence on the atmosphere above, so that air temperatures that differ initially from those on the ocean surface beneath are quickly modified, through radiative and sensible heat exchange across the air/sea boundary, toward the more slowly-changing temperatures of the ocean water surface. In the tropical latitudes of the Philippines, the sea surface remains warm, varying relatively little throughout the year.

   (b) Moisture is also provided to the air by the sea surface, so the warm air can become saturated with substantial amounts of water vapor in layers adjacent to the surface.

2. Ocean factors that contribute indirectly to the atmospheric weather above include:

   (a) Ocean Currents which act to advect ocean water into a region; this advected water tends to retain the temperature and salinity of the source region, although these may be modified somewhat as the water moves along into another region.

   (b) The Vertical Distribution of Temperature and Salinity in the near-surface ocean layers affect the exchange of heat across the ocean surface; that heat exchange, in turn, helps determine the convective character and vertical stability of the overlying atmosphere.

3. Several ocean factors may influence naval operations in an area:

   (a) Nearshore Bathymetry affects tides, tidal currents, acoustic propagation (reflection, absorption and scattering of underwater sound), and determines shoreline accessibility.

   (b) Coastal Type and Configuration can also limit access for particular types of naval vessels and operations.

   (c) Waves.

   (d) Tides.

   (e) Internal Waves may affect both surface and subsurface operations.

   (f) Bottom Sediment Type and Character influence the performance of submarine detection systems.

   (g) Underwater Visibility affects nearshore diving and photography operations.

4.2.2 Ocean Parameters by Region

A. Western Philippine Sea (open ocean to the east of the Philippine Islands)

This region is more subject to influences from remote ocean areas than the other regions to be discussed later.

1. Ocean Circulation Patterns here are determined by forces acting on the broad North Pacific Ocean. As the North Pacific Equatorial Current moves westward, it encounters the land barrier of the Philippine Islands. Part of the water carried by this current is directed southward past Mindanao Island to make up the Mindanao Current; this Current carries a significant portion of the North Pacific Equatorial Current water along the Philippine Islands between 10° and 5° North Latitude before it turns eastward; there, it merges with other water to form the narrow North Equatorial Counter-Current that returns eastward, centered at about 5°N (see Fig. 4.8; & Fig. 4.9).

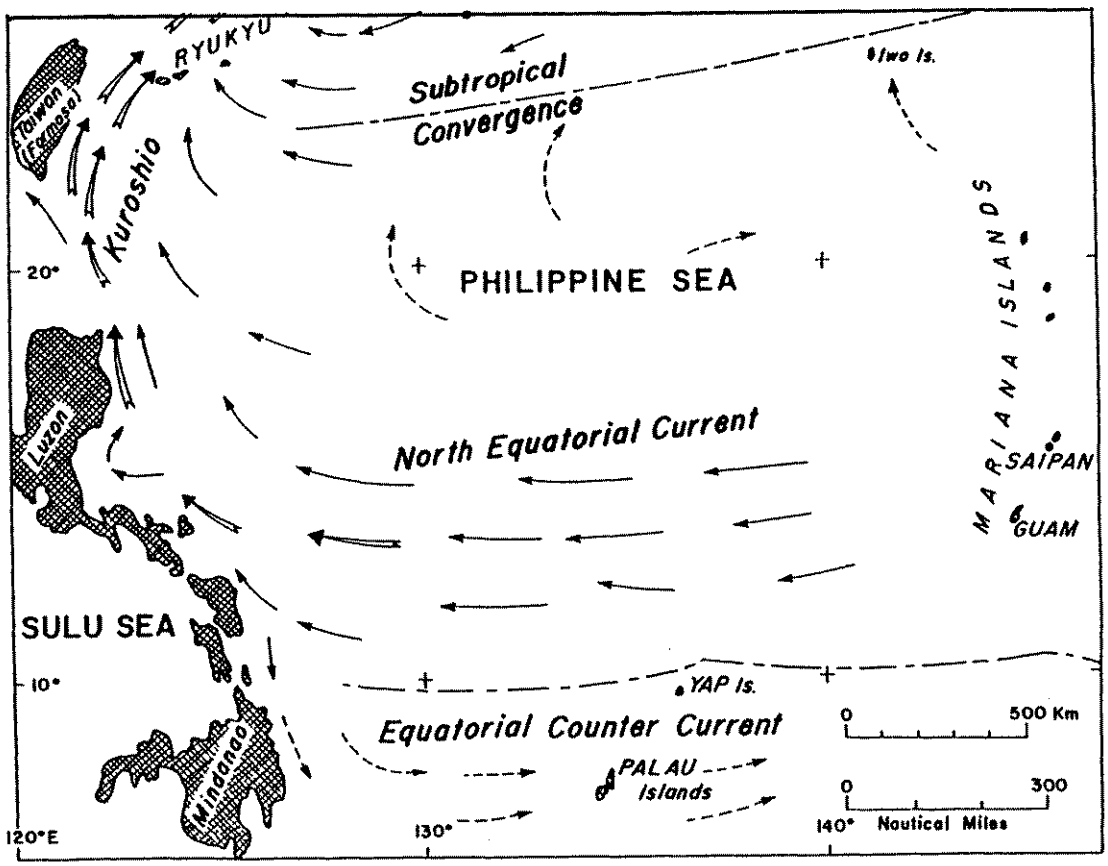

Figure 4.8: Major Currents in the Philippine Sea and Waters South of Japan (adapted from Uda (1966)).

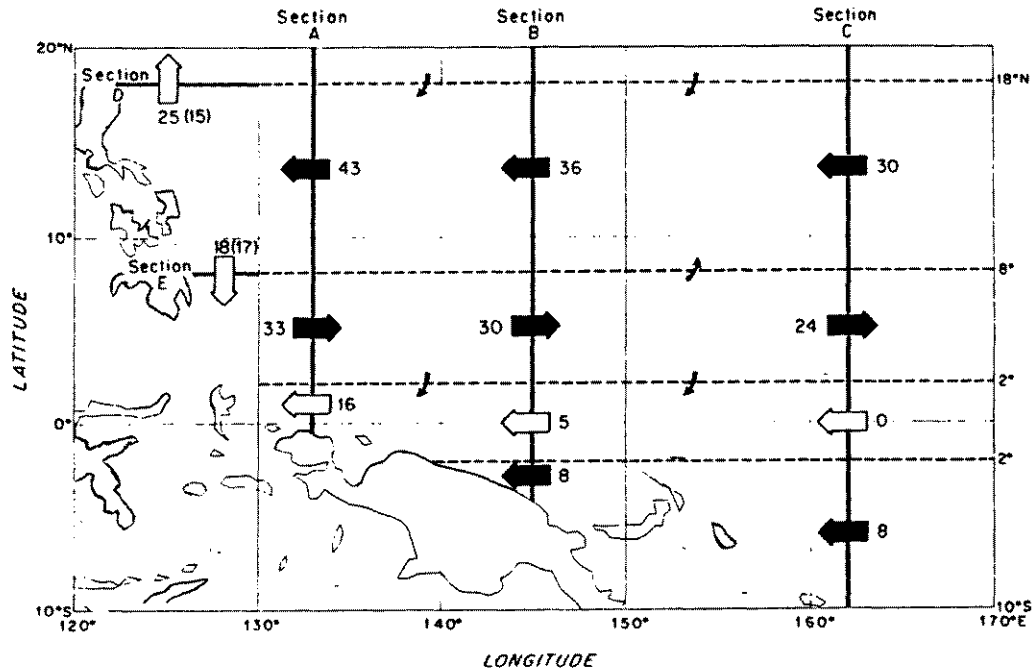

Figure 4.9: A Circulation Diagram for the Water Warmer than 12°C deduced from Annual Mean Hydrographic Sections and Water Budgets (transports in Sv, $10^6 m^3 sec^{-1}$). Bold typeface arrows represent directly calculated transports. Open-faced arrows are transport values inferred from water mass budgets. Shown in parentheses are the transports computed directly for these sections with the available data (adapted from Toole et al. (1988)).

A somewhat larger amount of the North Pacific Equatorial Current water is directed northward past Luzon, when it reaches the Philippine Islands, to make up part of the Kuroshio Current, the major western boundary current of the North Pacific Ocean. The Kuroshio becomes fully developed further to the north, along the Japanese Islands.

There are seasonal variations in the location and strength of the different currents, especially in the boundary between the opposing North Pacific Equatorial Current and Counter-currents. See the variation between summer and winter current patterns from 7° to 10°N to the east of Mindanao (see Figs. 4.10a & 4.10b). The boundary becomes confused and widens during summer; also, the Counter-current receives a large volume of water from the southern hemisphere as it dominates the weaker Mindanao Current outflow.

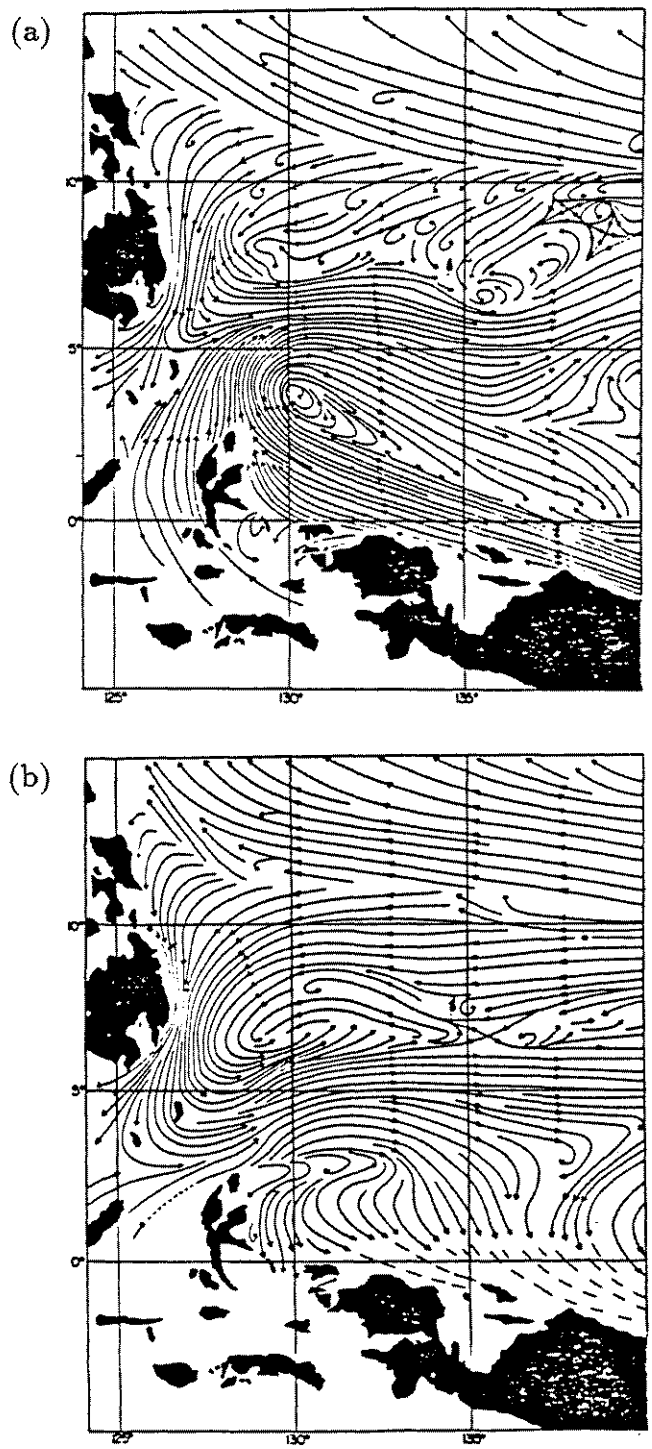

Figure 4.10: The Equatorial Currents of the Western Pacific Ocean in the Northern Hemisphere during (a) Summer and (b) Winter (adapted from Kendall (1969)).

In July, three Lagrangian drifters were launched in the Mindanao Current; the launch point and date, the length of record and failure mode for Buoys 52, 53 and 55 are indicated in Table 4.1 below, taken from Carpenter (1989).

Table 4.1:

BUOY	Date of launch	Location of launch	Record length	Failure Mode
Buoy 52	16 July 88	6.944°N 126.619°E	53 days	Lost drogue
Buoy 53	22 July 88	7.983°N 127.958°E	220 days	Grounded
Buoy 55	16 July 88	6.861°N 126.861°E	63 days	Grounded

Trajectories of these buoys are plotted in three figures (see Carpenter (1989), Figs. 4.11(a), 4.11(b) & 4.12); squares are placed as markers for buoy locations at 12Z each second day, and the beginning and ending Julian dates are indicated on each trajectory. Although Buoys 52 and 55 were launched on the same date (16 July 88, Julian day 198), and very close together, the paths traced after the third square (sixth day) are entirely different. Buoy 52 is caught in the North Pacific Equatorial Counter-current and is carried rapidly eastward; it describes one counter-clockwise loop in a 2-week period during its trajectory. Buoy 55 moves to the southwest, describes a counter-clockwise loop of almost 3 weeks duration, and continues northwestward through the Celebes (Sulawesi) Sea toward Borneo; there the coastline directed the buoy trajectory southward into the Southern Hemisphere.

Buoy 53 was launched 6 days later and at about one degree further to the north and to the east from the launch point for Buoys 52 and 55. After a very slow start for the first 53 days, Buoy 53 moved eastward in the Equatorial counter-current; it then describes half a loop (counter-clockwise) northward, where it was caught in the westward and relatively slow drift of the North Pacific Equatorial Current. It finally grounded along the southeast coast of Luzon.

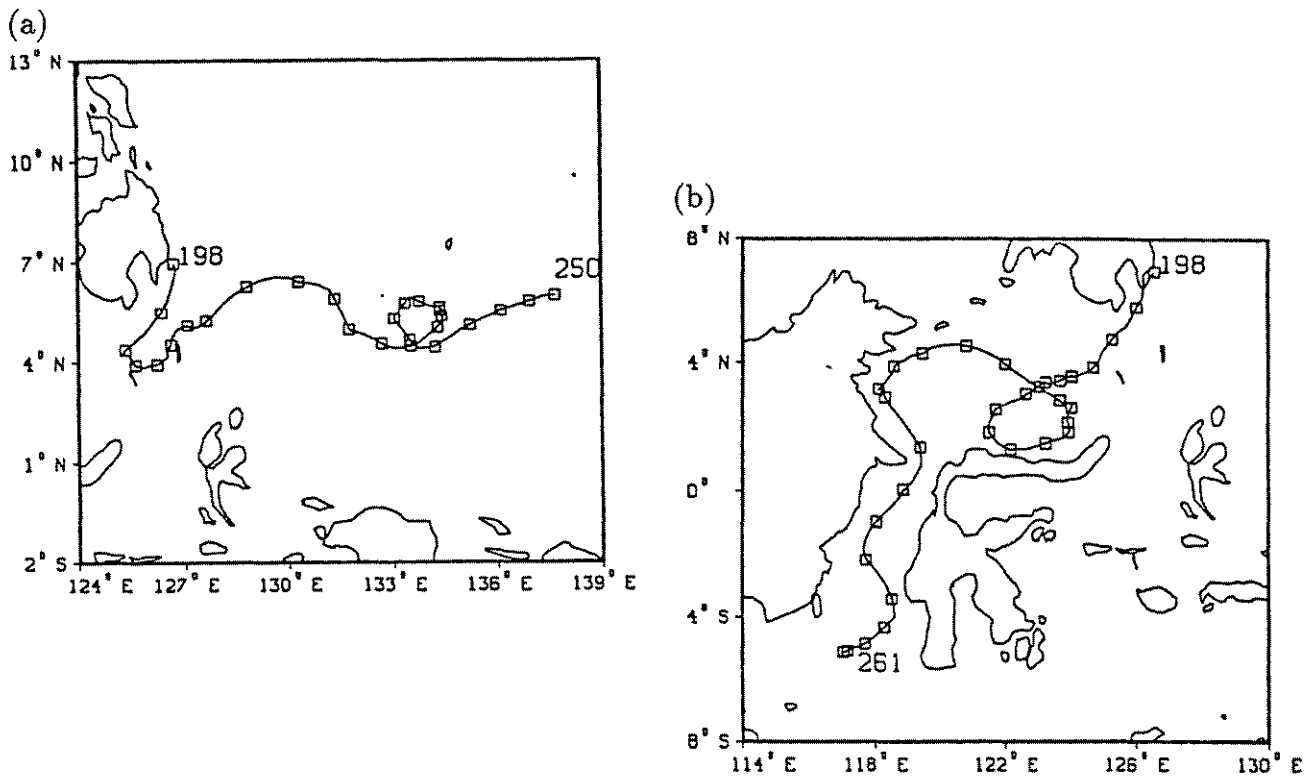

Figure 4.11: Lagragian Trajectories of (a) Buoy 52 and (b) Buoy 55. Julian dates mark the beginning and end of each record and a square is placed as a marker for 12Z every second day (adapted from Carpenter (1989)).

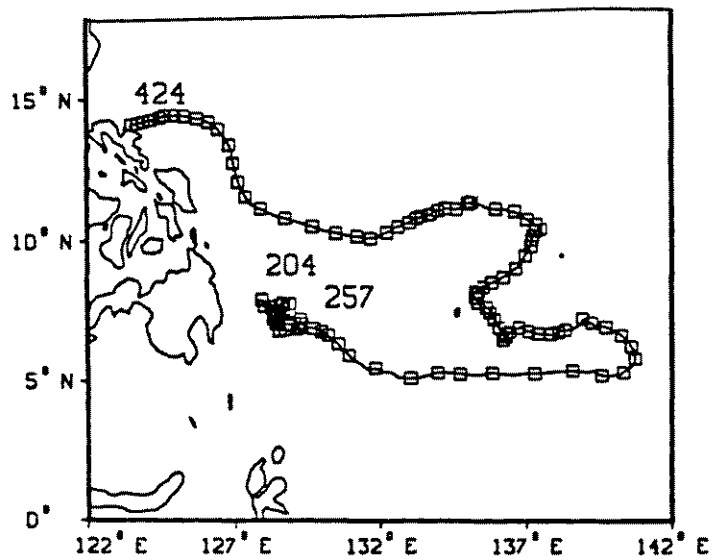

Figure 4.12: Lagragian Trajectory of Buoy 53. Julian dates mark the beginning and end of each record and a square is placed as a marker for 12Z every second day (adapted from Carpenter (1989)).

Current speeds calculated in the Mindanao Current during winter are shown in Fig. 4.13. These vary from 0.6 to 2.0 knots in the strongest part of the current.

The vertical variation in speed is shown in Fig. 4.14 for three stations in the Mindanao Current during winter 1968 along 7°30' N (see Fig. 4.15 for station locations). Stations RY 3234 and RY 3235 show a pronounced maximum speed at about 50 meters depth (1.25 to 1.60 $m \cdot s^{-1}$); a minimum speed occurs at about 10 meters depth (about 0.9 and 1.05 $m \cdot s^{-1}$). Below the maximum, an almost-steady decline in speed with depth occurs, approaching zero at about 380 and 510 meters depth.

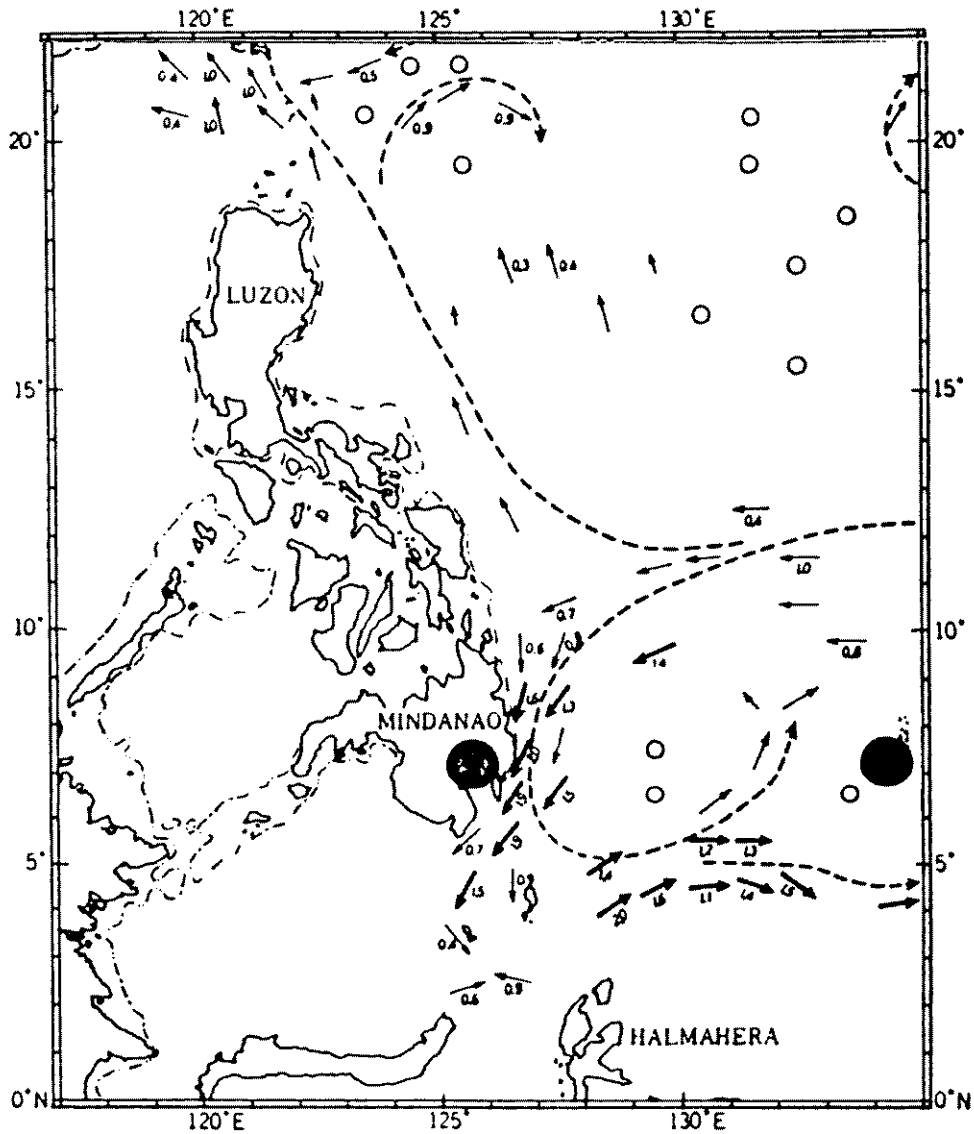

Figure 4.13: Currents (in knots; 1 knot equals 0.51 m s^{-1}) for Northern Hemisphere Winter. Solid circles are locations of two tide guage stations (adapted from Lukas (1988)).

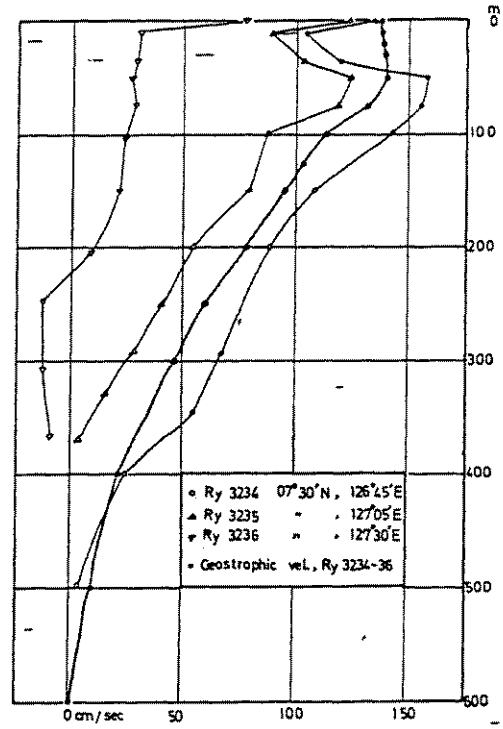

Figure 4.14: Vertical Distributions of the Measured and Computed Speed Relative to 600 db in the Mindanao Current at 7°30'N (adapted from Matsuzawa (1968)).

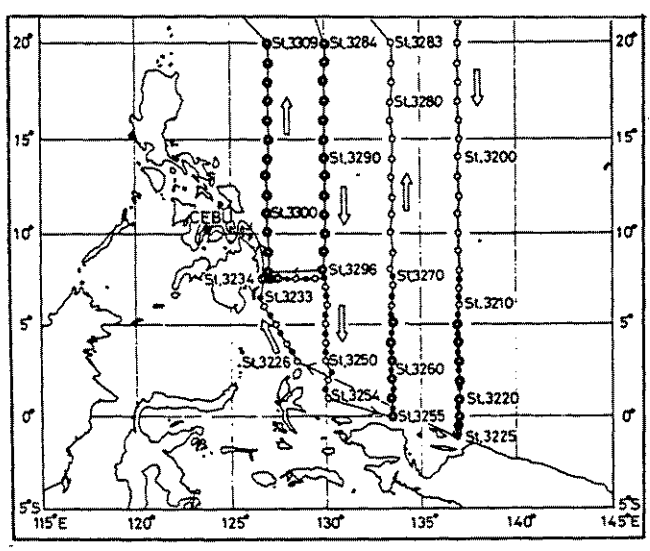

Figure 4.15: Track Chart of the Second Cruise for the Cooperative Study of the Kuroshio made by the *Ryofu Maru* of the JMA in January to March 1968. The open circle, double circle and dot indicate the deep station, current measurement station and shallow station (adapted from Matsuzawa (1968)).

2. Sea Surface Temperature. During August, the western North Pacific Ocean shows maximum values between about 5°S and 30°N along its western boundaries. The Philippine coastlines experience these high temperatures, with a value of 29°C along the western coast of Luzon; Fig. 4.16(a). By February, the region of temperature maximum has moved into the southern hemisphere, from the equator to about 20°S; see Fig. 4.16(b). Then there is a weak temperature gradient along both east and west coasts of the Philippines; the temperature ranges from 27°C off Mindanao to 25°C in Luzon Strait.

Monthly charts prepared from Comprehensive Ocean-Atmosphere Data Set (Sadler et al. 1987) are included as part of Appendix A. These charts represent averages of 80 years of data for 2-degree latitude/longitude areas from 5° to 26°N and from 110° to 140°E; the Philippine Islands are centered in this region. Charts for August, November, February and May are reproduced here in Figs. 4.17 & 4.18. Details of the seasonal changes in temperature are provided in Figs. 4.17 & 4.18 as they change between the extreme values shown earlier. Sea surface temperatures reach maximum value (>29°C) in the South China Sea in May, while coldest temperatures in the area (<15°C) occur adjacent to China in Taiwan Strait in February. Thus the marginal seas experience a greater annual range in surface temperature than do regions in the open ocean to the east of the Philippine Islands.

Somewhat north of the Philippines, off Taiwan, sea surface temperatures measured in winter (December '62 – January '63) and summer (June '63) are shown in Figs. 4.19(a) & 4.19(b). About 4°C seasonal variation occurs nearshore and in Luzon Strait, but it lessens to 2.5 to 3°C further offshore, south of 22°N in the Philippine Sea. Figure 4.19(a) shows the location of two coastal stations on the eastern coast of Taiwan from which vertical sections are made of temperature that are shown later: Ho Peng (Ho stations) and Shi Ti (ST stations); those sections of temperature versus depth extend offshore from these locations about 4 and 5 km.

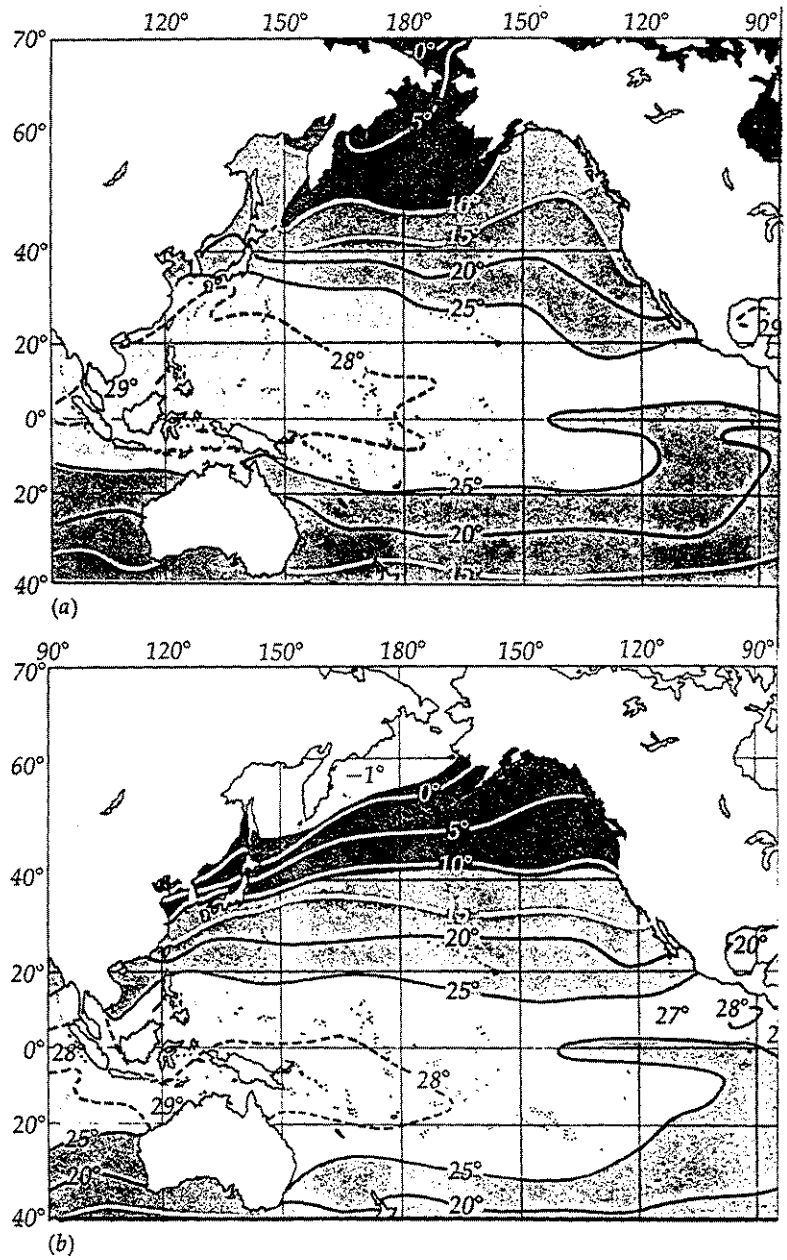

Figure 4.16: Surface Temperature of the Oceans (a) in August and (b) in February (adapted from Ingmanson and Wallace (1973)).

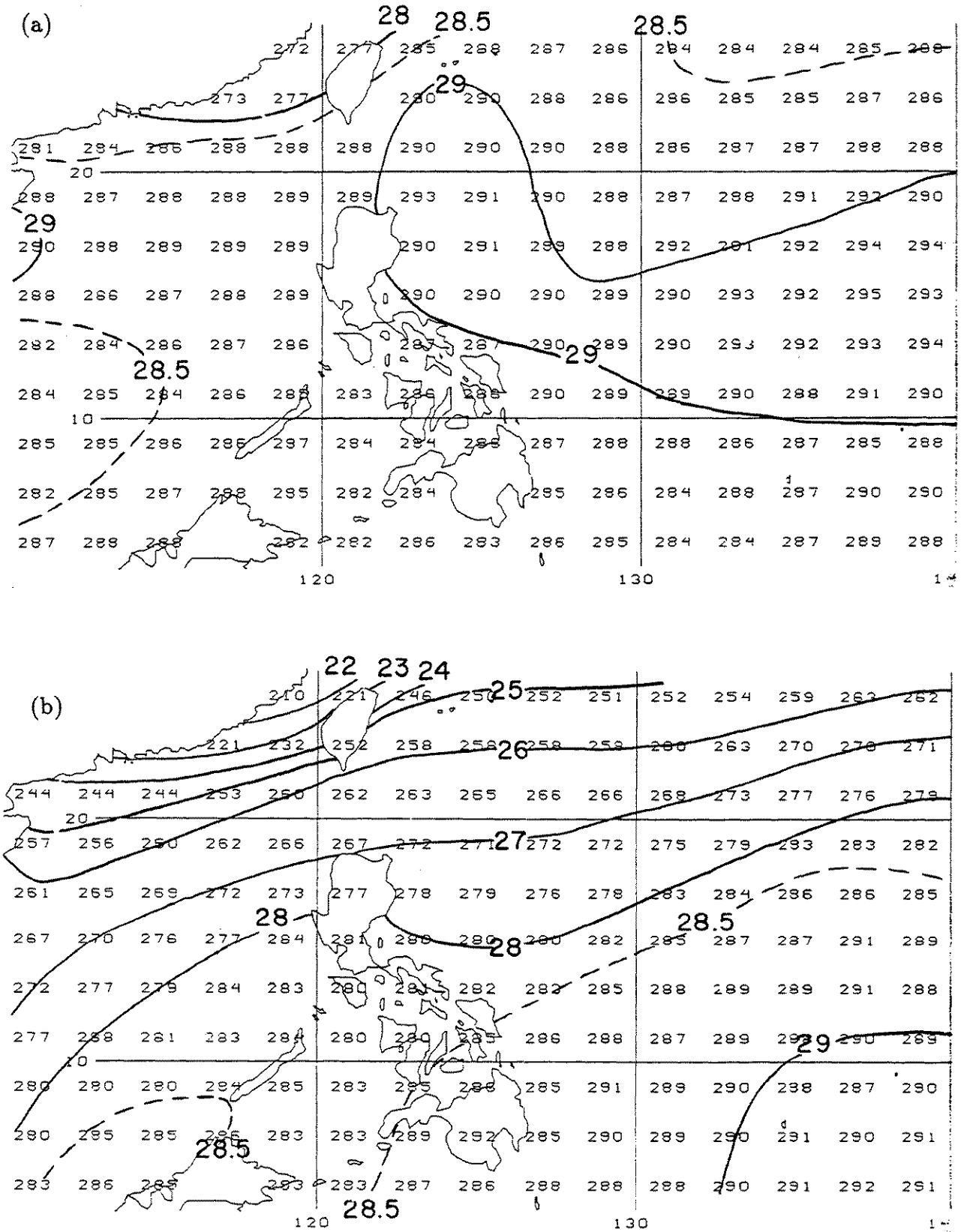

Figure 4.17: Monthly Sea-Surface Temperature; August (a), November (b). (Adapted from Sadler et al. (1987). See Appendix A for details.)

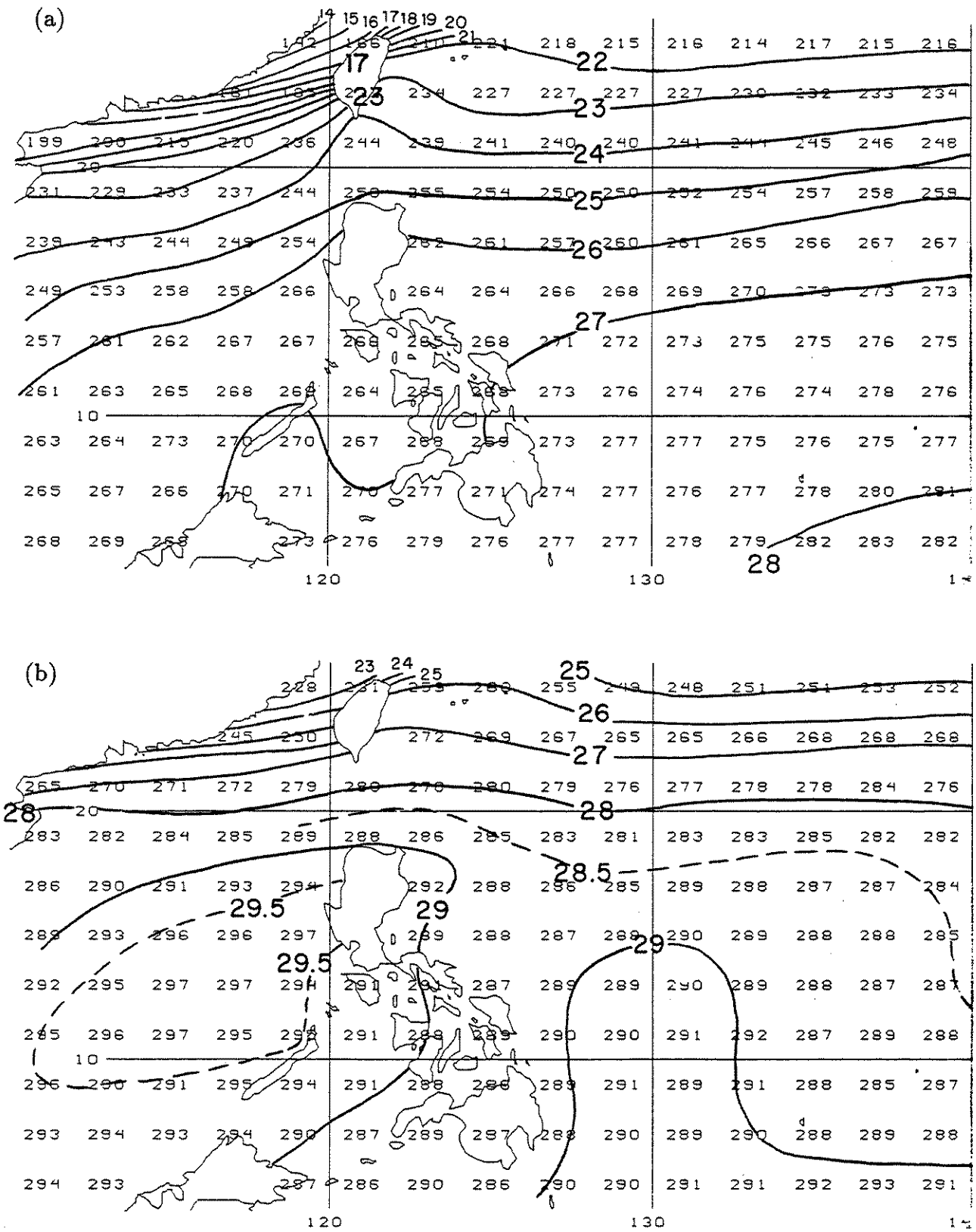

Figure 4.18: Monthly Sea-Surface Temperature; February (a), May (b). (Adapted from Sadler et al. (1987). See Appendix A for details.)

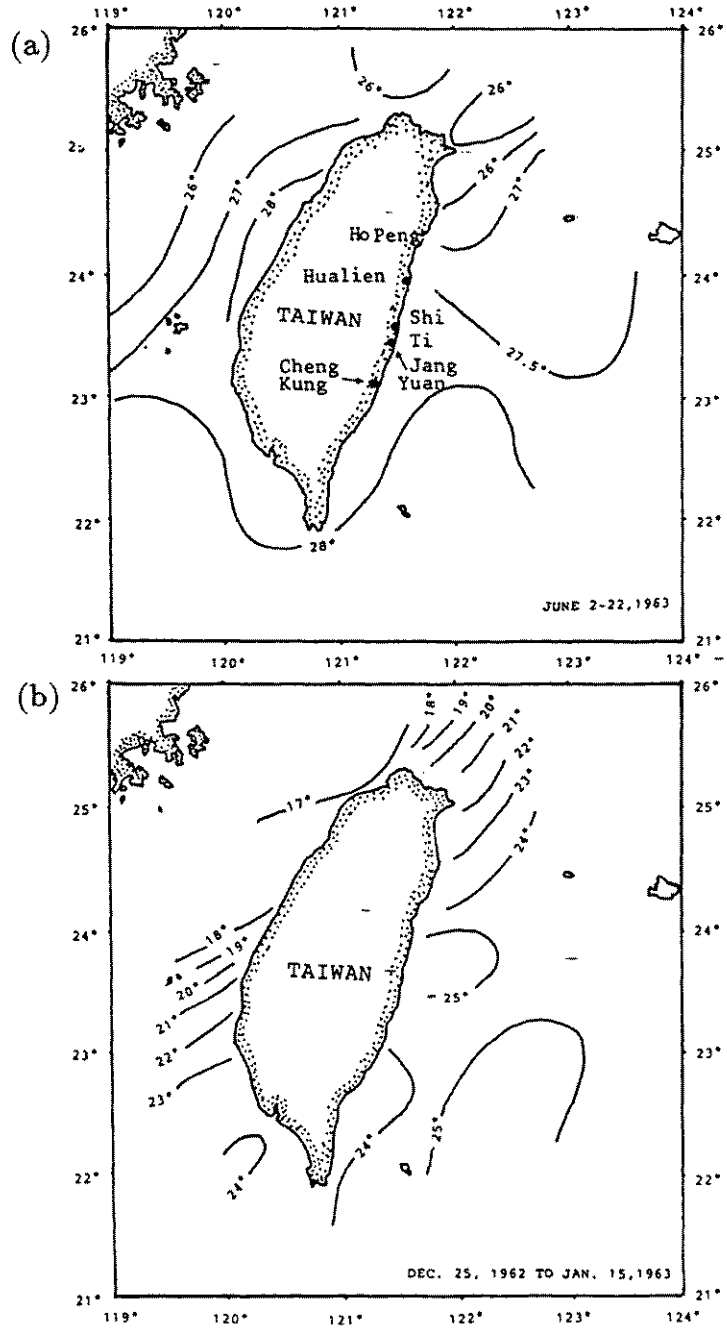

Figure 4.19: Sea Surface Temperature (°C) around Taiwan in Summer (a) and Winter (b) (adapted from Yin (1988)).

3. Vertical Variation of Temperature. At the nearshore locations off Taiwan (H_o stations are at 24°20' N; ST stations are at 23°30' N), the cross-sections for winter and summer are shown in Figs. 4.20(a), 4.20(b), 4.21(a) & 4.21(b). Pronounced mixed layers of uniform temperature adjacent to the surface extend to about 100 m depth in winter, with a thermocline that shows a pronounced gradient immediately below the mixed layer. Winter surface temperatures of 23 to 25°C are replaced in summer by temperatures of 26 to 29°C. In summer, the strong thermocline begins at the sea surface, and becomes less strong below 100 to 150 meters in depth.

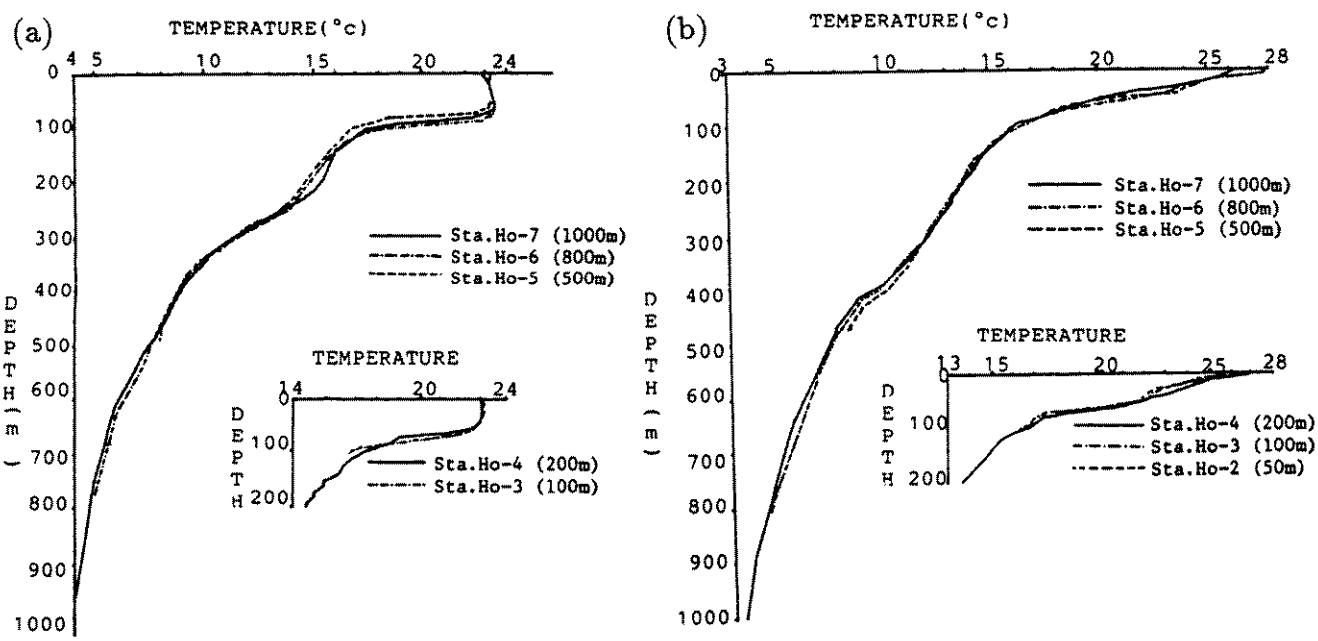

Figure 4.20: Temperature Distribution at Stations Ho-1 to 7 in (a) December 1984 and (b) May 1985 (adapted from Yin (1988)). Lowermost thermometer depth in parentheses.

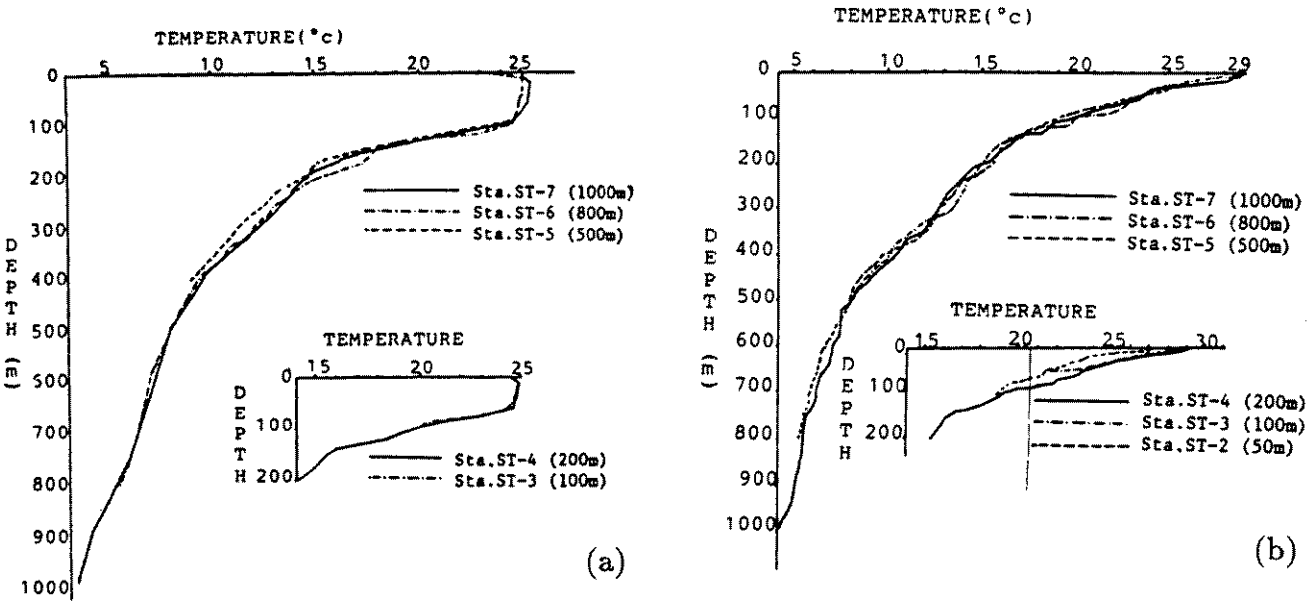

Figure 4.21: Temperature Distribution at Stations ST-1 to 7 in (a) November 1984 and (b) July 1984 (adapted from Yin (1984)). Lowermost thermometer depth in parentheses.

Further south, at the latitudes of the Philippines and along 130°E. Longitude, vertical sections are shown drawn from stations observed on two cruises of the US/PRC (People's Republic of China) cooperative program of 1987; the first cruise occurred in January-February 1987; the second cruise was in November-December 1987. Both cruises thus represent winter conditions (station locations are shown in Fig. 4.22 along 130°E. Longitude). Figure 4.23(a) of Toole et al. (1988) shows the temperature section from the surface to 1000 meters depth for the first cruise; Fig. 4.23(b) shows similar results for the second cruise. In both sections, a strong thermocline is present in the region from 50 to 150 meters, extending from low latitudes northward to about 10°N. Further north, the thermocline gradient weakens somewhat, deepening and extending much deeper; the gradient occurs between 100 and 400 meters depth at 18°N.

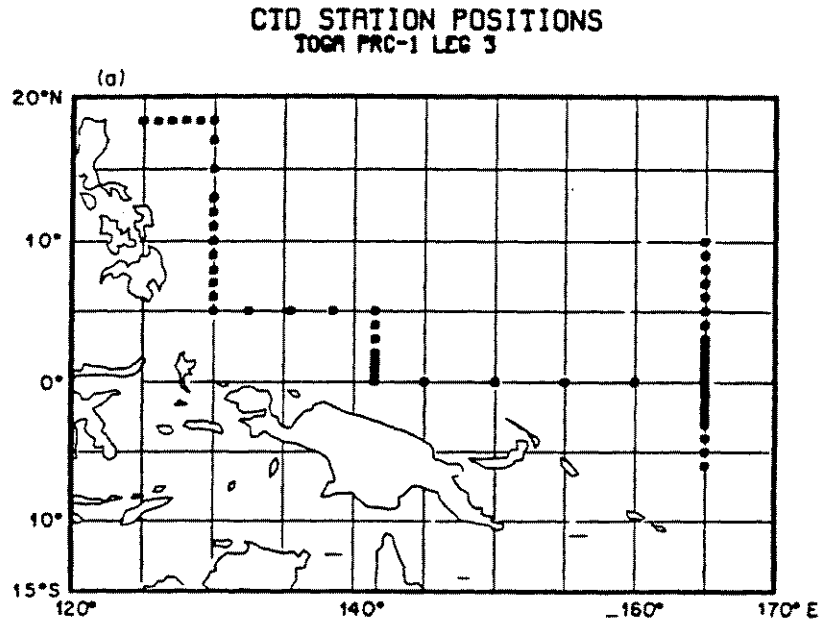

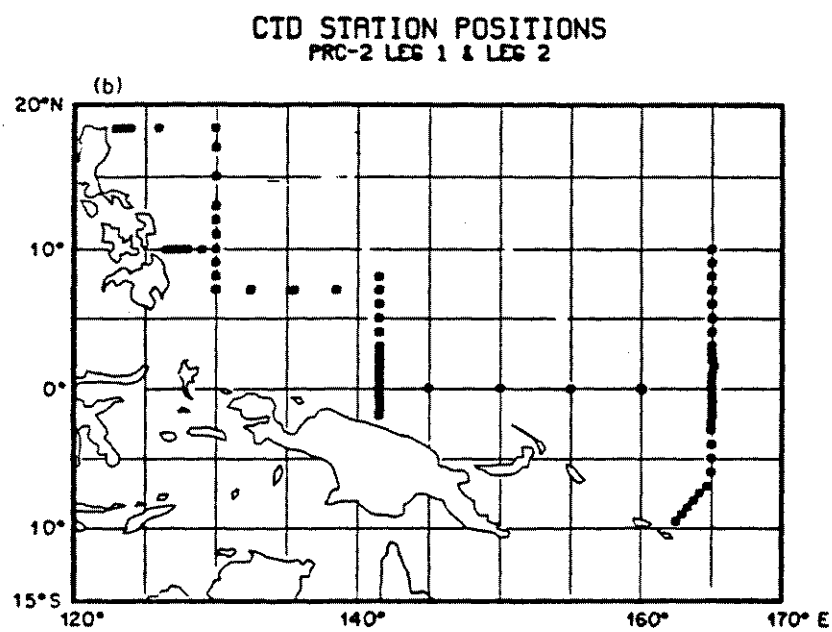

Figure 4.22: Section Maps for the CTD Observations obtained during the First Two Cruises of the US/PRC Cooperative Program. (a) The first cruise observations: 30 January to 18 February 1987. (b) The second cruise observations: 18 November to 16 December 1987 (after Toole et al. (1988)).

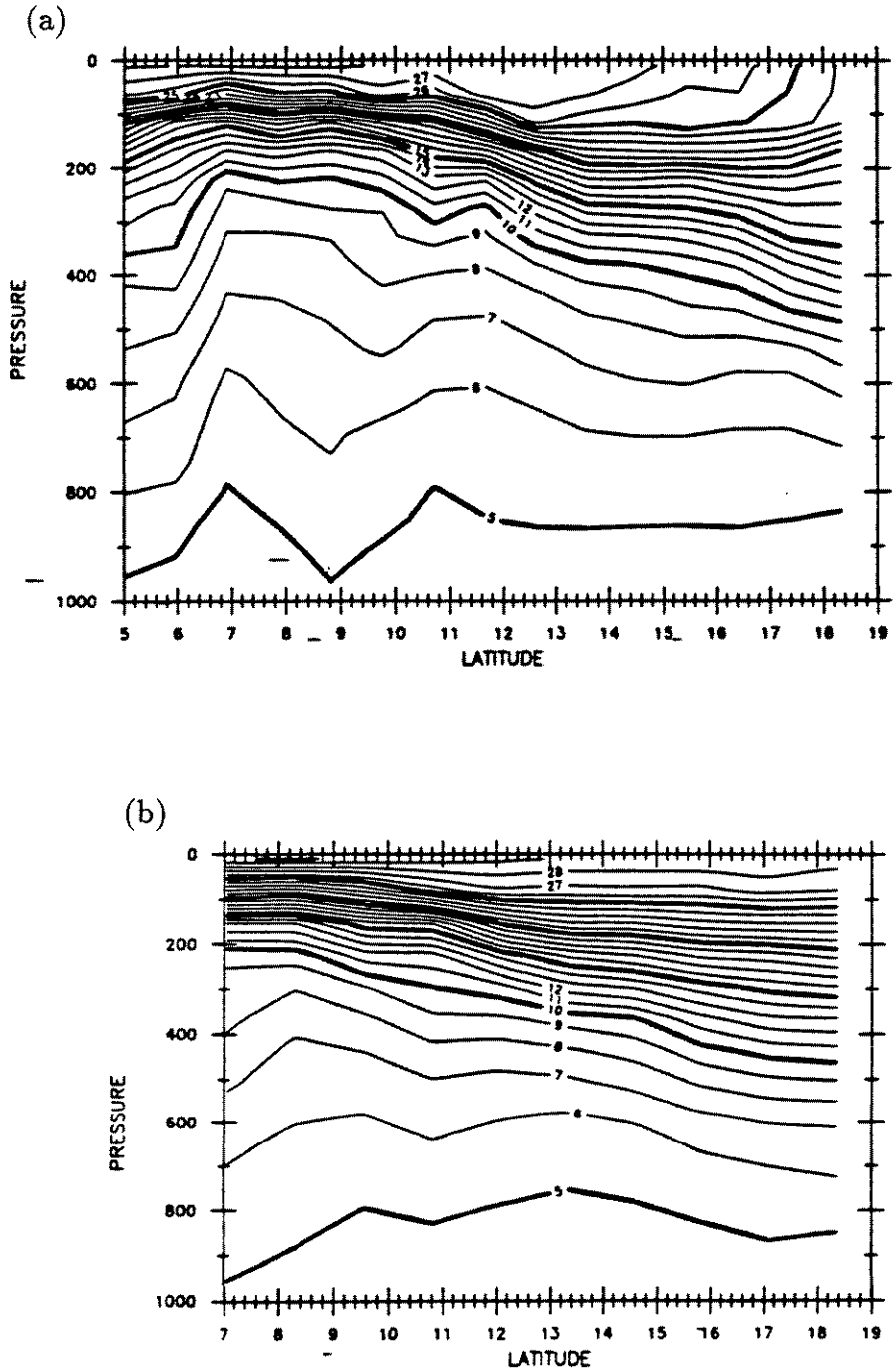

Figure 4.23: Sections of Temperature in °C, constructed along 130°E during the (a) first cruise and (b) second cruise of the US/PRC cooperative program (adapted from Toole et al. (1988)).

Along 129°E. Longitude, and further south (from 1.5° to 5.5°N) in the Philippine Sea, a cross-section of temperature to 300 db (read "300 meters") depth during July 1988 is provided in Fig. 4.24, a study of the Mindanao Eddy (Carpenter 1989). This section was produced from airborne expendable bathythermograph (AXBT) observations. Two of the observations are shown in Fig. 4.25(a) (at about 1°15′N) and in Fig. 4.25(b) (at about 7°24′N), both near 129°E. Longitude; note the change in thermocline character between these two latitudes. Further north, the thermocline gradient becomes steeper and less irregular.

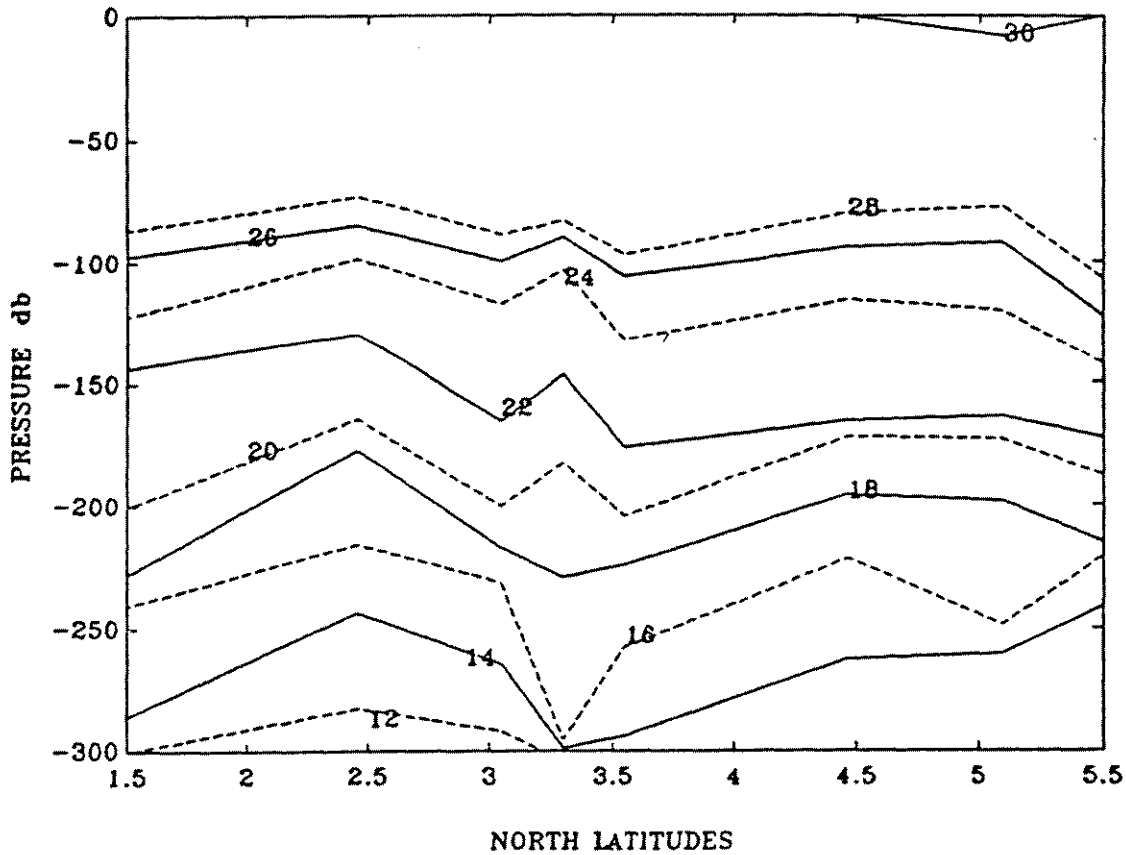

Figure 4.24: Vertical Temperature Cross-section B: Located along 129°E (adapted from Carpenter (1989)).

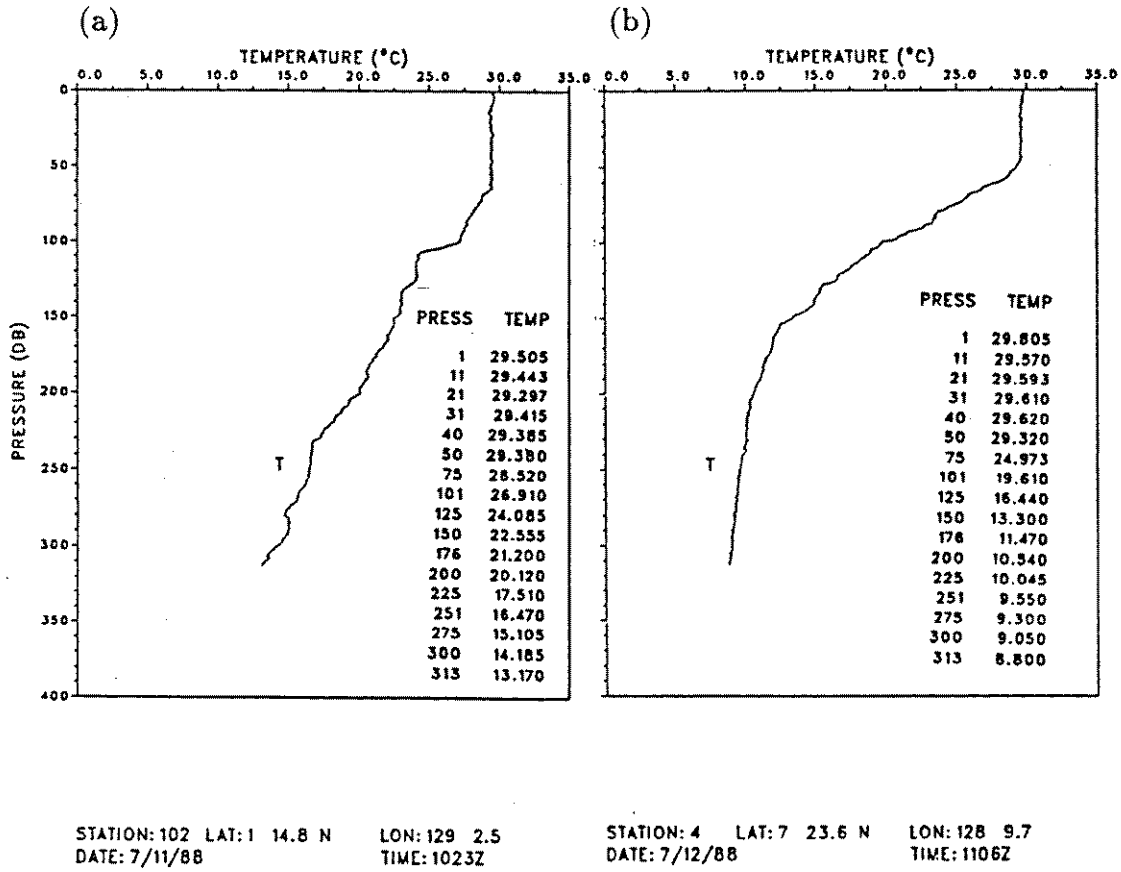

Figure 4.25: Vertical Temperature Distribution at two locations in the Mindanao Current region, measured by Airborne Expendable Bathythermograph (AXBT) Observations in July 1988 (adapted from Carpenter (1989)).

A conductivity-temperature-depth (CTD) measurement for a nearby location (6.95°N; 126.71°E) shows characteristics intermediate between these AXBT observations. There is a definite mixed layer in all three examples, extending from the surface to 40-60 meters depth. This mixed layer probably is maintained by the North Pacific Equatorial Counter-current flowing in this region.

A study (Schramm 1979) describes temperature changes in the ocean caused by Typhoon Phyllis as it passed across the Philippine Sea during August 14–17, 1975 (see Fig. 4.26). The measurements were made by calibrated AXBT's dropped from Navy P-3 aircraft during three flights across the area: 14 hours ahead of the storm passage, 10 hours after storm passage; and two days later. The region studied was 20° to 26°N; 133° to 140°E within dashed lines on Fig. 4.26. During this interval, Typhoon Phyllis moved northward along 137°E. Vertical sections of temperature are shown later below the line A–B along 24°N; point A is at 24°N, 133°E, while point B is at 24°N, 140°E. Sea surface temperature prior to the Typhoon passage ranges from 27.7° to 29°C, with a very weak horizontal gradient (see Fig. 4.27(a)).

After the Typhoon passage on the 15th (see Fig.4.27(b)) pronounced cooling has occurred, especially adjacent and to the right of the storm track along 137°E.

The vertical distribution of sea temperatures along line A–B is shown for 14 August (see Fig. 4.28); for 15 August (see Fig. 4.29); and for 17 August (see Fig. 4.30) between the surface and about 350 meters depth. The initial mixed layer at about 35 meters on the 14th is interrupted extensively adjacent to the storm path; it is destroyed immediately to the right, with deep, colder water brought to the surface; and it is deepened considerably to the left of the storm path, to about 50 meters. Temperatures are affected to depths greater than 300 meters; these effects persist for at least two additional days (see Fig. 4.30). Temperature change at various depths on the section are shown in Fig. 4.31; they exceed 5°C decrease just to the right of the storm path at about 45 meters depth; about 2°C change occurs at points about 2 degrees of longitude to the left (negative) and to the right (positive) at about 50 meters depth. The negative temperature changes represent upwelling of deeper water into a region (see Figs. 4.32 and 4.33).

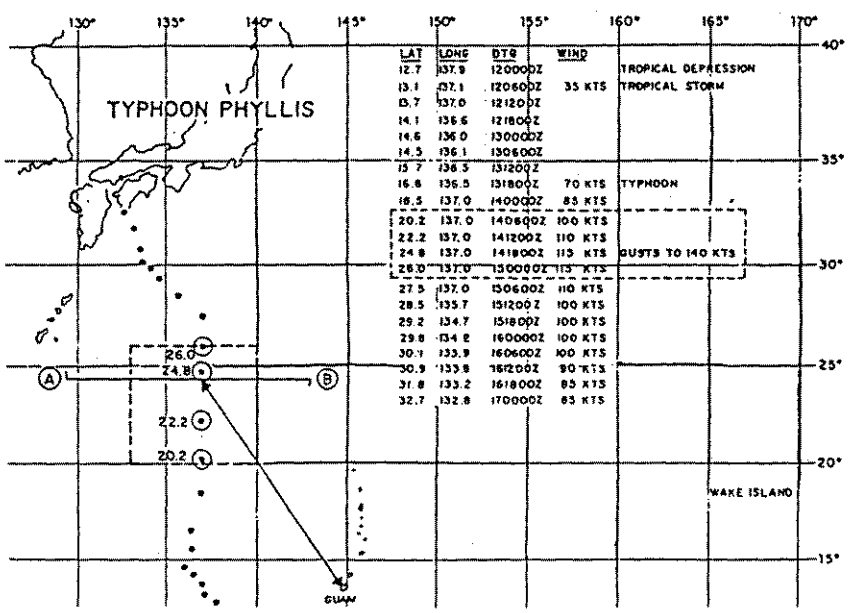

Figure 4.26: Track of Typhoon Phyllis (adapted from Schramm (1979)).

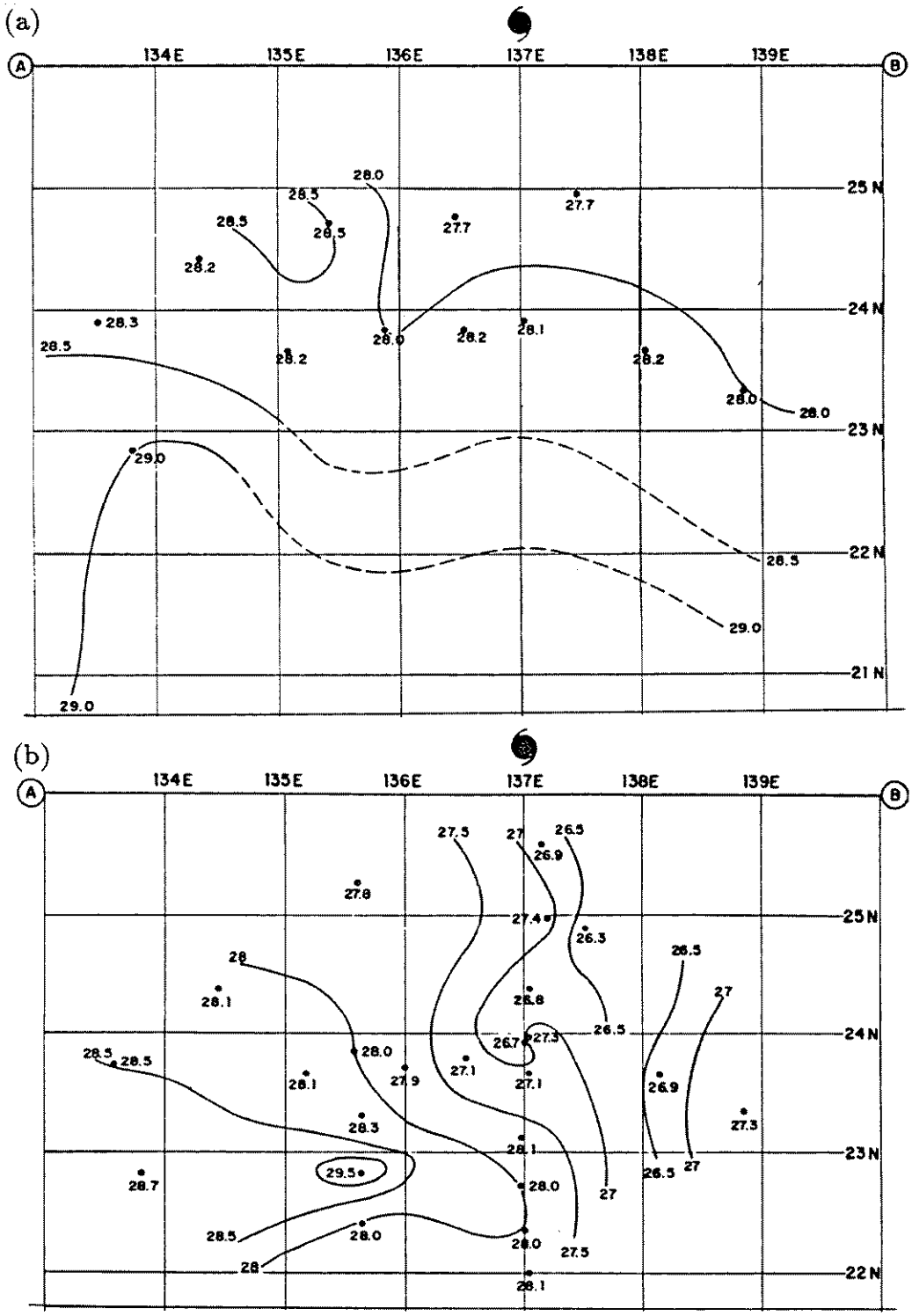

Figure 4.27: Sea Surface Temperature on (a) 14th and (b) 15th (adapted from Schramm (1979)). Isotherms in degrees C.

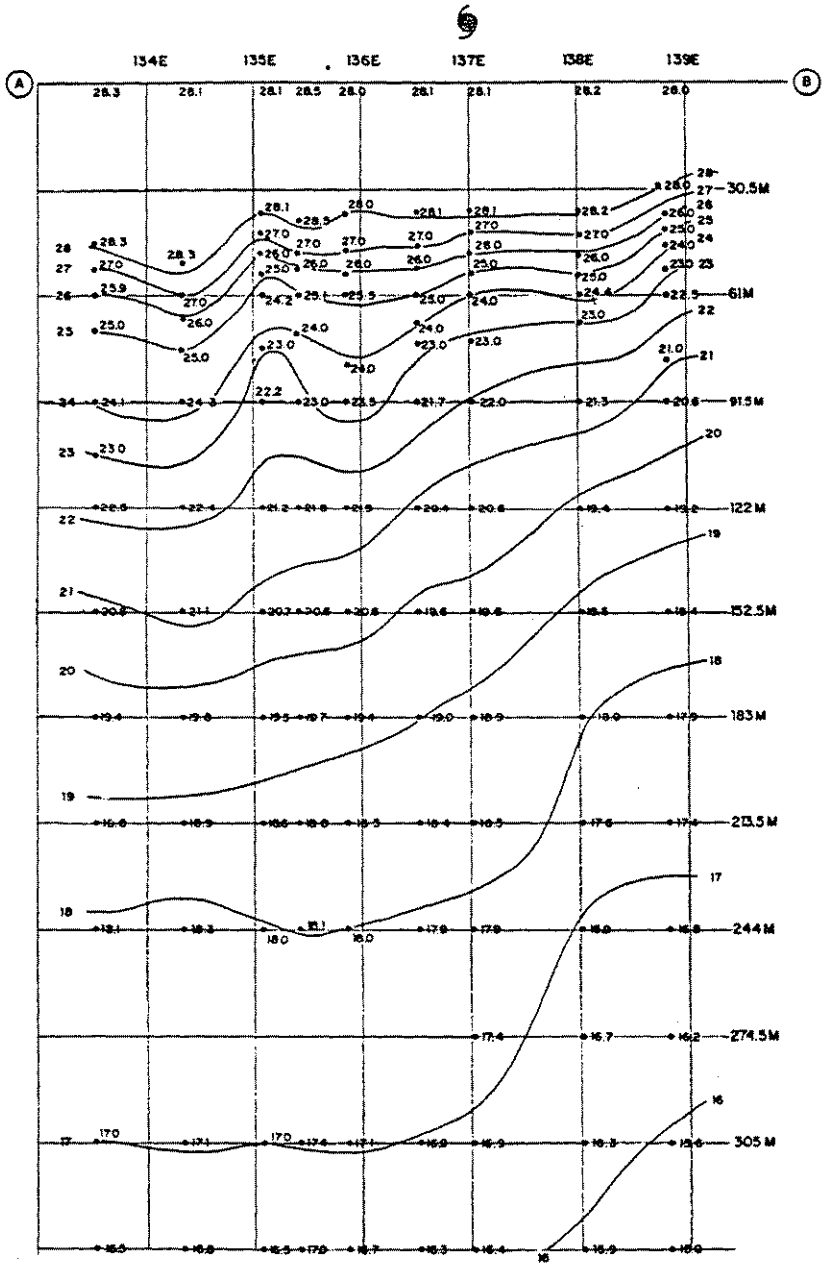

Figure 4.28: West to East Vertical Cross-section, along 24°N, perpendicular to Track of Typhoon Phyllis, on 14 August (adapted from Schramm (1979)). Isotherms in degrees C.

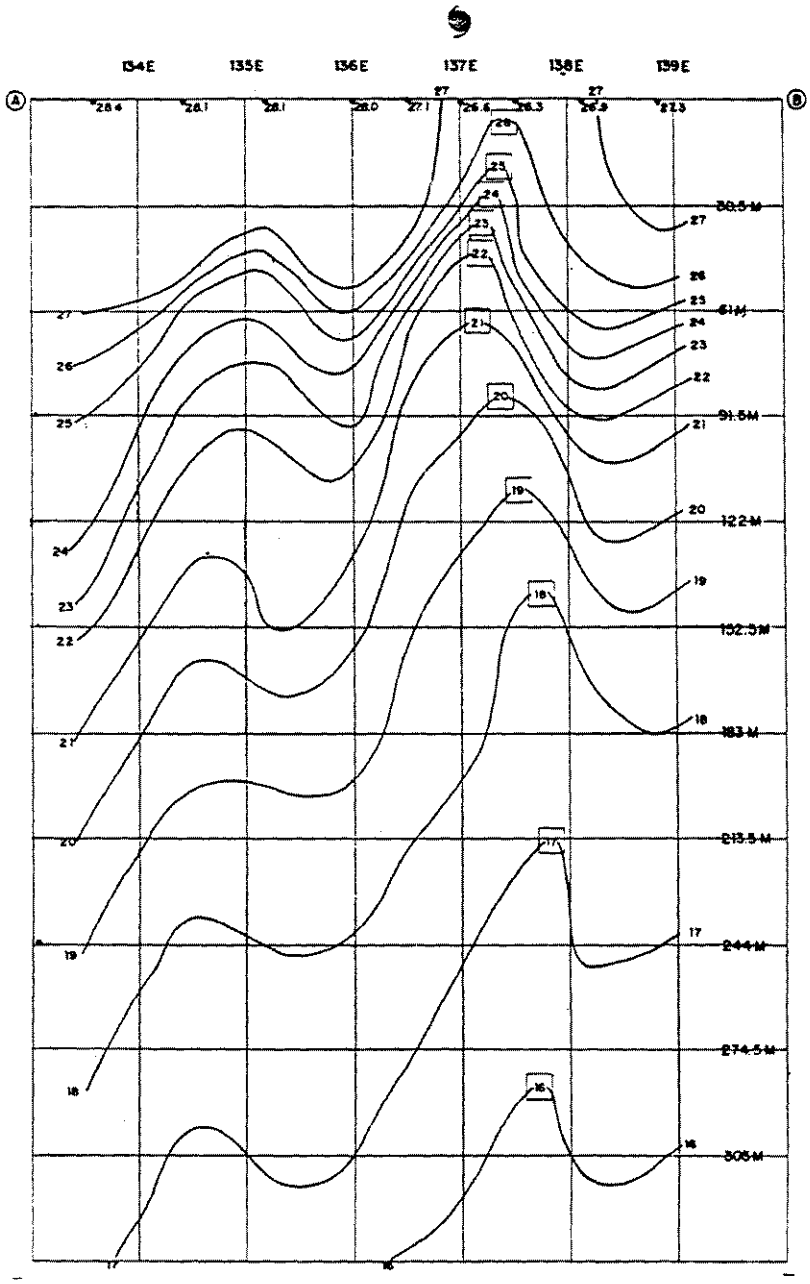

Figure 4.29: West to East Vertical Cross-section,along 24°N, perpendicular to Track of Typhoon Phyllis, on 15 August (adapted from Schramm (1979)). Isotherms in degrees C.

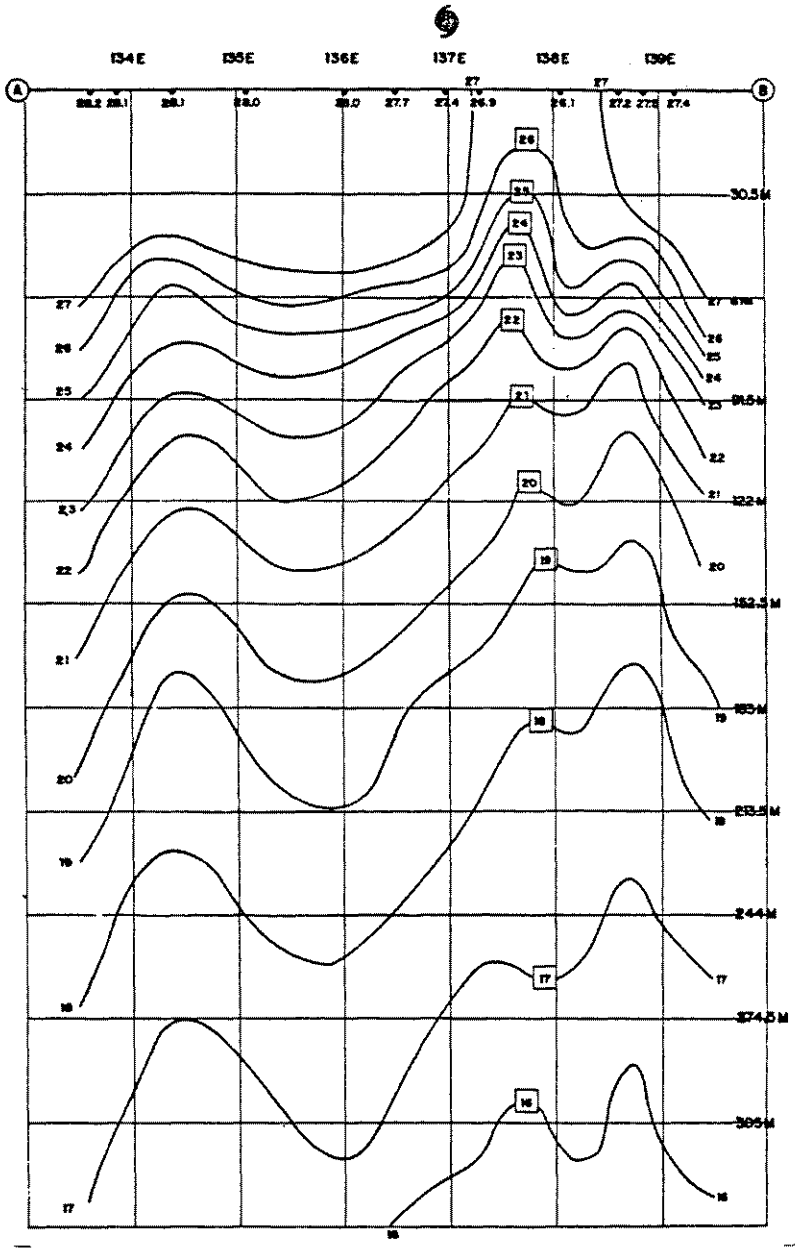

Figure 4.30: West to East Vertical Cross-section along 24°N, perpendicular to Track of Typhoon Phyllis, on 17 August (adapted from Schramm (1979)). Isotherms in degrees C.

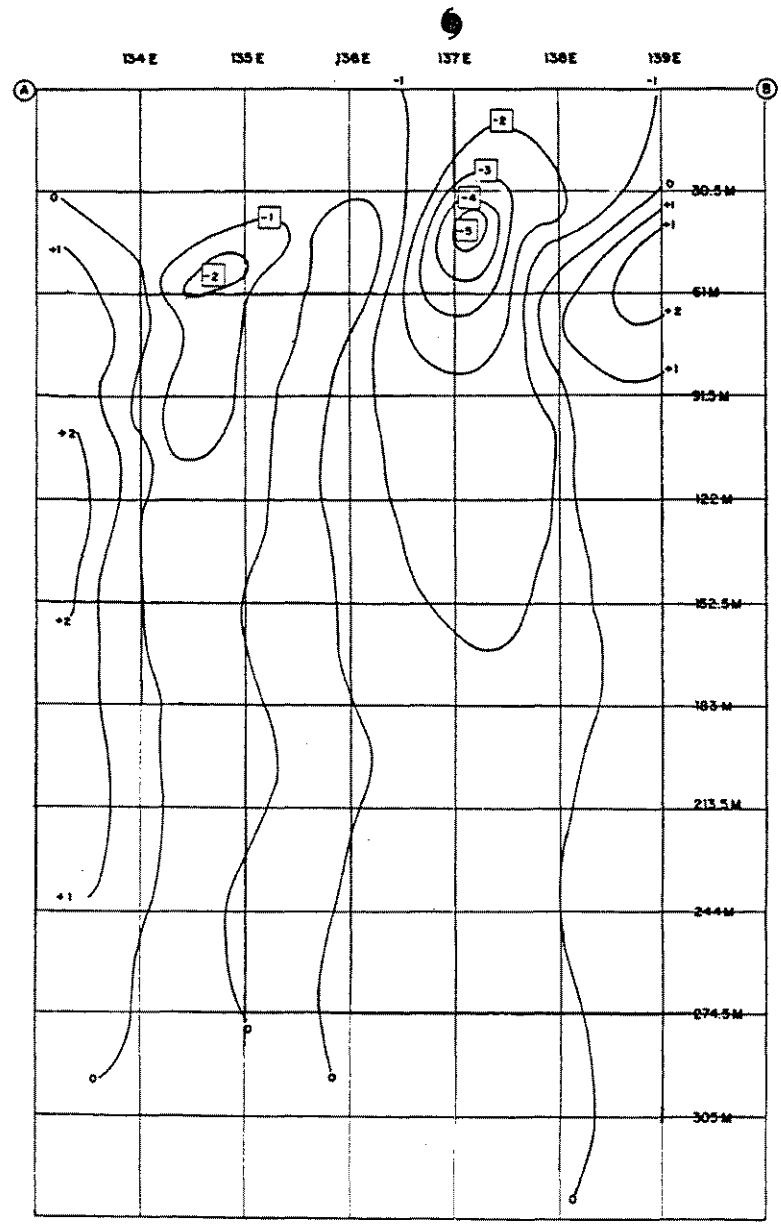

Figure 4.31: Vertical Cross-section depicting Changes in Temperature from the 14th to the 15th (adapted from Schramm (1979)).

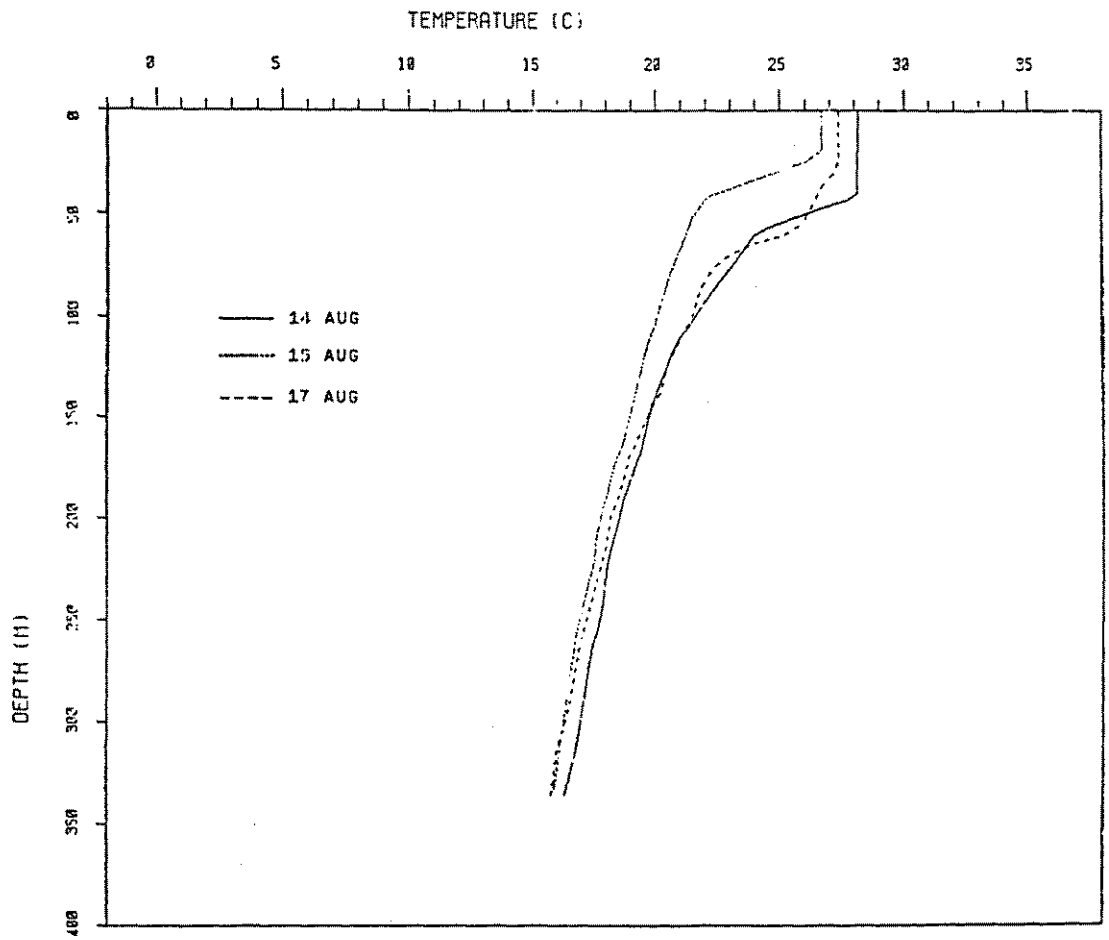

Figure 4.32: Under Eye of Track of Typhoon Phyllis: Profiles 3 (14th), 35 (15th) and 51 (17th) (adapted from Schramm (1979)).

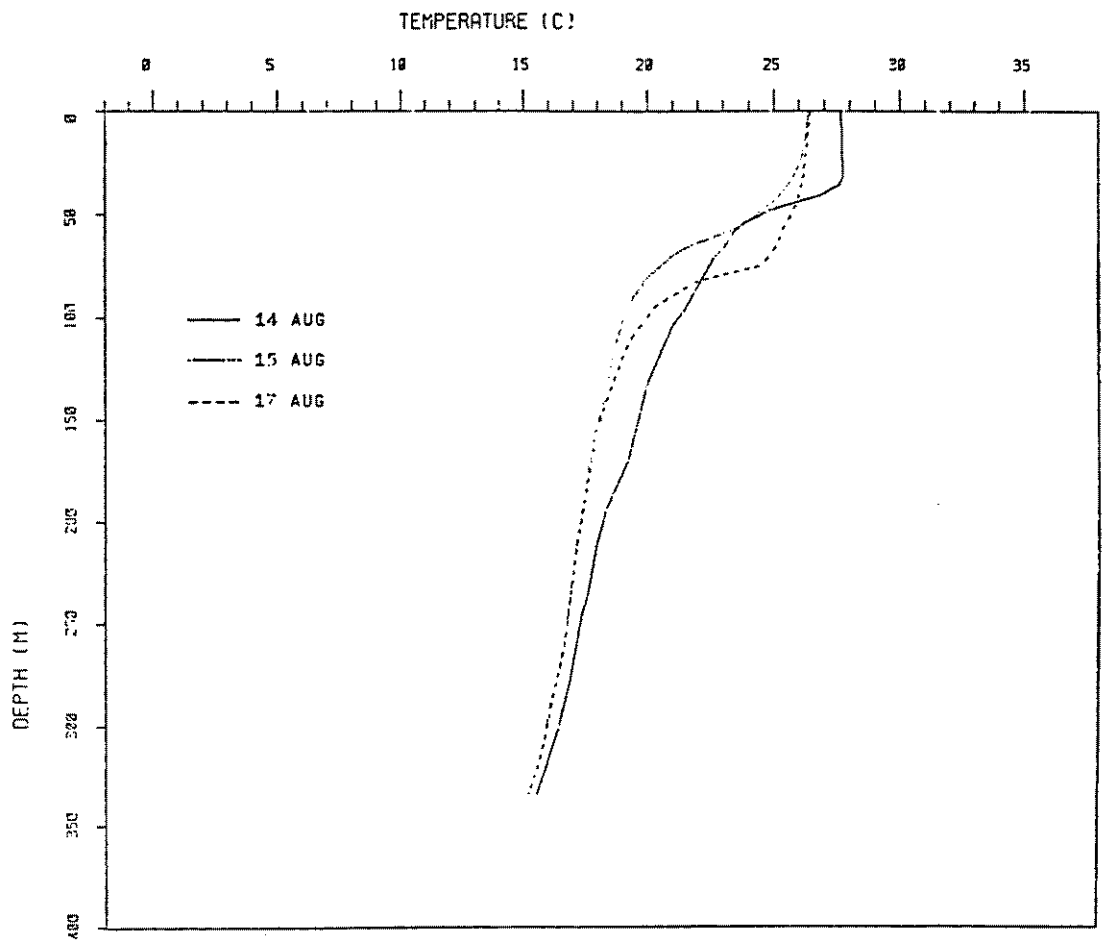

Figure 4.33: 30 n mi to Right of Track of Typhoon Phyllis: Profiles 22 (14th), 32 (15th) and 53 (17th) (adapted from Schramm (1979)).

4. Salinity. The mean annual salinity at the sea surface for the western North Pacific Ocean and the region surrounding the Philippine Islands is shown in Fig. 4.34. More detailed seasonal charts of surface salinity for February and August are shown by Figs. 4.35(a) & (b) for the regions immediately adjacent to the Philippines.

To the east of the Philippines, salinities occur that are higher than 34.0 ppm (parts per thousand). Salinity values higher than this extend through the Bashi Channel to the north of Luzon into the South China Sea, and bring 34.4 ppm values close to the shore north of 12°N during February. In August 34.4 ppm values are pushed offshore and are replaced by lower salinity values adjacent to the philippines. Then, the 34.0 ppm value stretches from Luzon to Taiwan, in the north; and 34.0 ppm value is in the Basilan Strait southward from Mindanao. In the Celebes (Sulawesi) Sea southwest of Mindanao, salinity values are from 34.0 to 33.0 ppm in February; in August, values there are greater than 34.0 ppm.

In the Bashi Channel north of Luzon, the Northeast Monsoon in February brings higher salinity values westward into the extreme northern part of the South China Sea.

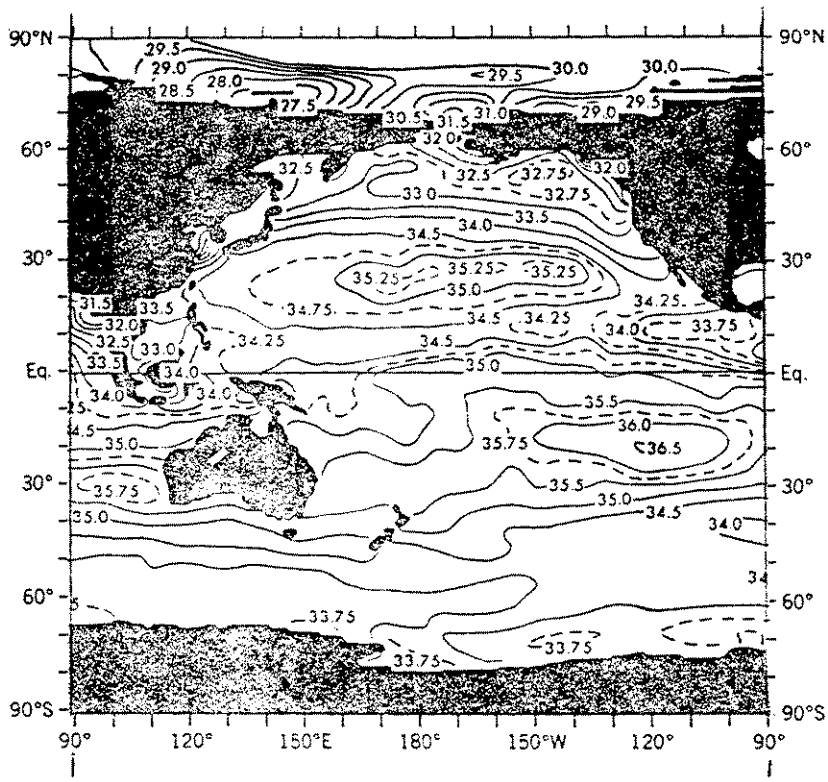

Figure 4.34: Annual Mean Salinity (ppm) at the Sea Surface (adapted from Levitus (1982)).

(a)

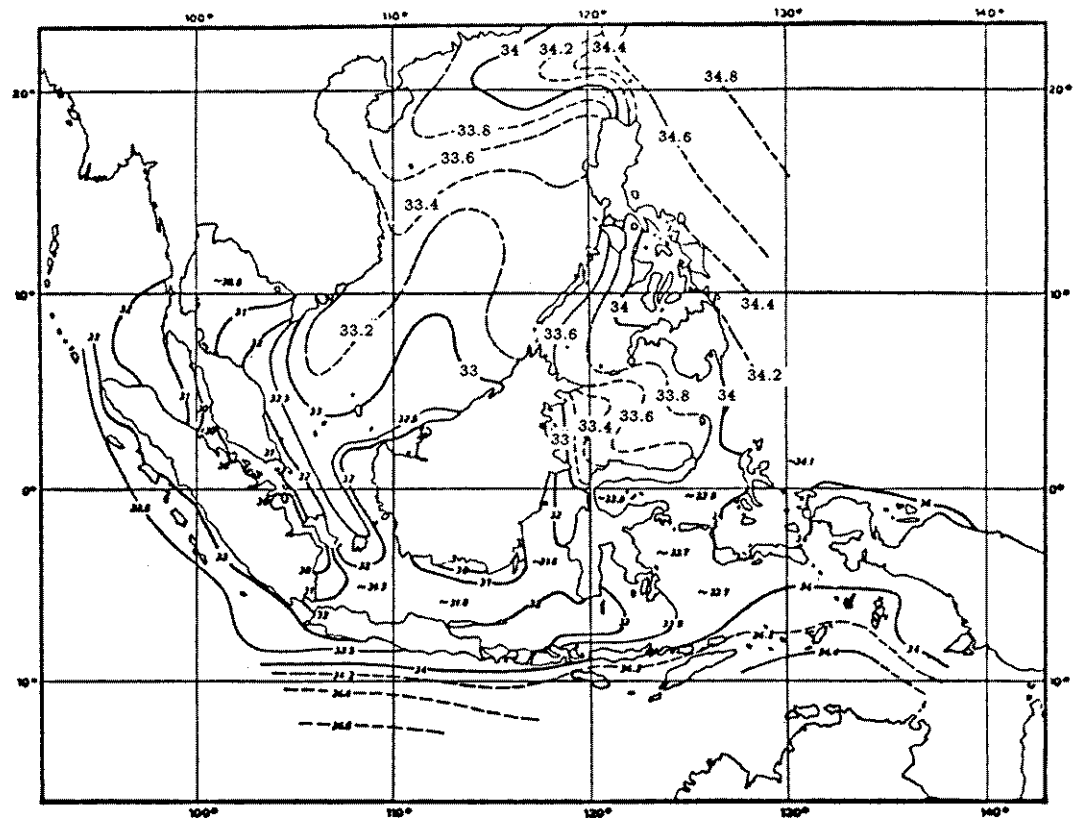

(b)

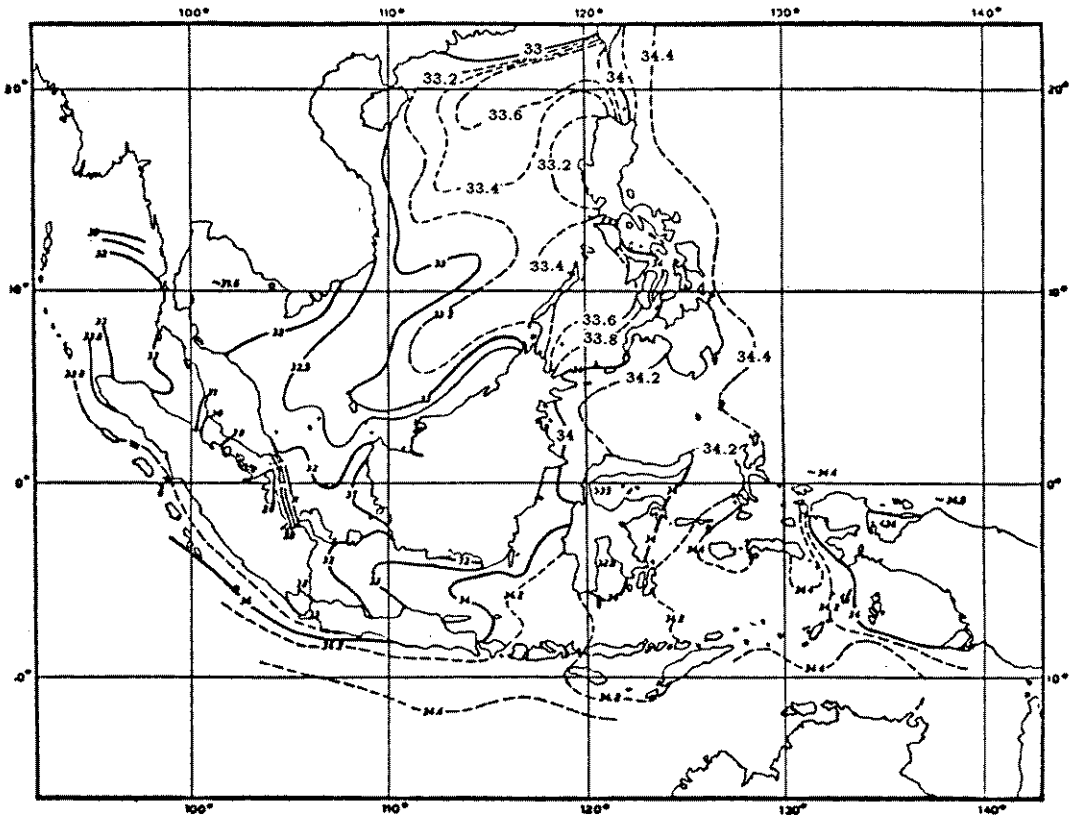

Figure 4.35: Average Surface Salinity (ppm) in Southeast Asian Waters in (a) February and (b) August (adapted from LaFond (1966)).

5. Salinity Variation with Depth. A schematic cross-section in the Philippine Sea from the equator to Taiwan (Formosa) shows the different salinity features in the upper 1200 meters of ocean (see Fig. 4.36). The uppermost layer features a salinity maximum that varies from 80 to 200 meters depth. Sections prepared from observations show the complexity of salinity distribution in these upper layers; the vertical section across the Mindanao Current at 7°30'N (eastward from Station 3234 through Station 3240, as shown by Fig. 4.37(a)) shows this maximum (>34.8 ppm) occurring at about 100 meters depth. Further south, in a section extending to the northwest from Halmahera toward Mindanao (stations 3226 through 3233 in Fig. 4.37(b)), this maximum appears also at about 100 meters. In both cases, there is a pronounced salinity gradient, with values increasing with depth, northward from 5°N; this gradient region starts at about 50 meters, associated with the strong thermocline also present. This maximum salinity feature also is displayed along 130°E taken by US/PRC Cruises 1 and 2 (see Fig. 4.22 for station locations and time).

A salinity minimum occurs below the maximum region; it is centered at about 400 meters depth at 5°N, and then deepens toward the north to 650 meters at 20°N (see Fig. 4.36). This feature is especially pronounced in the US/PRC sections along 130°E, reaching values at the core below 34.3 ppm north of about 15°N (see Figs. 4.38(a) and 4.38(b)).

These salinity features are illustrated also on a section made across the northern Philippine Sea region by Cruise CHIPS-1 of the Institute of Oceanography, National Taiwan University in May–June 1985, eastward from Taiwan along about 21°45′N (Fig. 4.39). The large section extends from the surface to 5000 db (read "5000 meters depth"); the upper 1000 db (1000 meters) is shown with an enlarged vertical scale in the upper part of the figure. A salinity maximum of about 34.9 ppm occurs centered at about 200 meters, while the salinity minimum, at or below 34.3 ppm, appears at 600–700 meters.

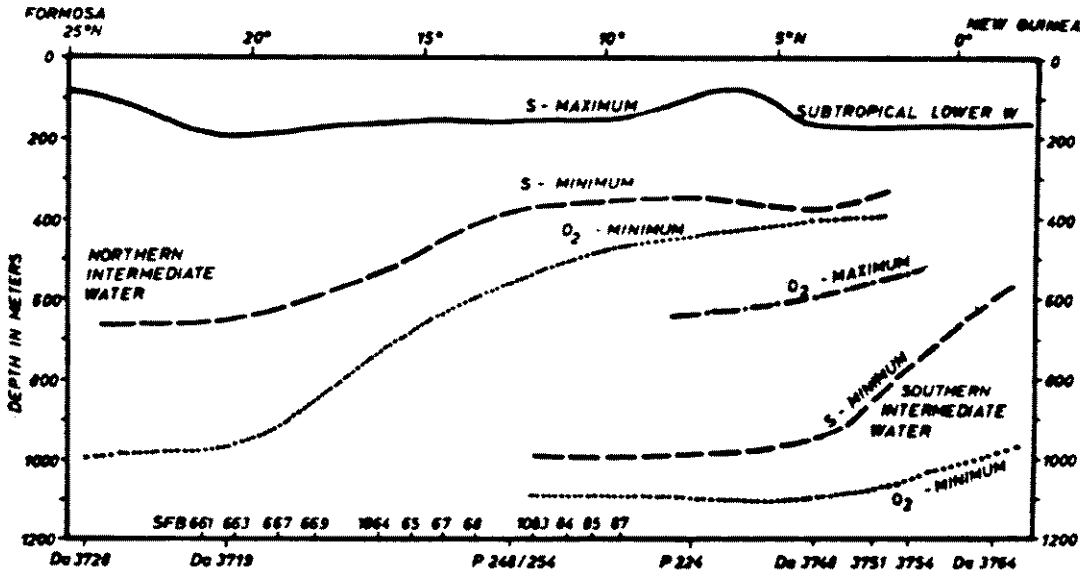

Figure 4.36: Schematic Representation of the Position of the Core Layers of the Different Water Masses in the Philippine Sea in a Section from Taiwan (Formosa) to New Guinea (adapted from Uda (1966)).

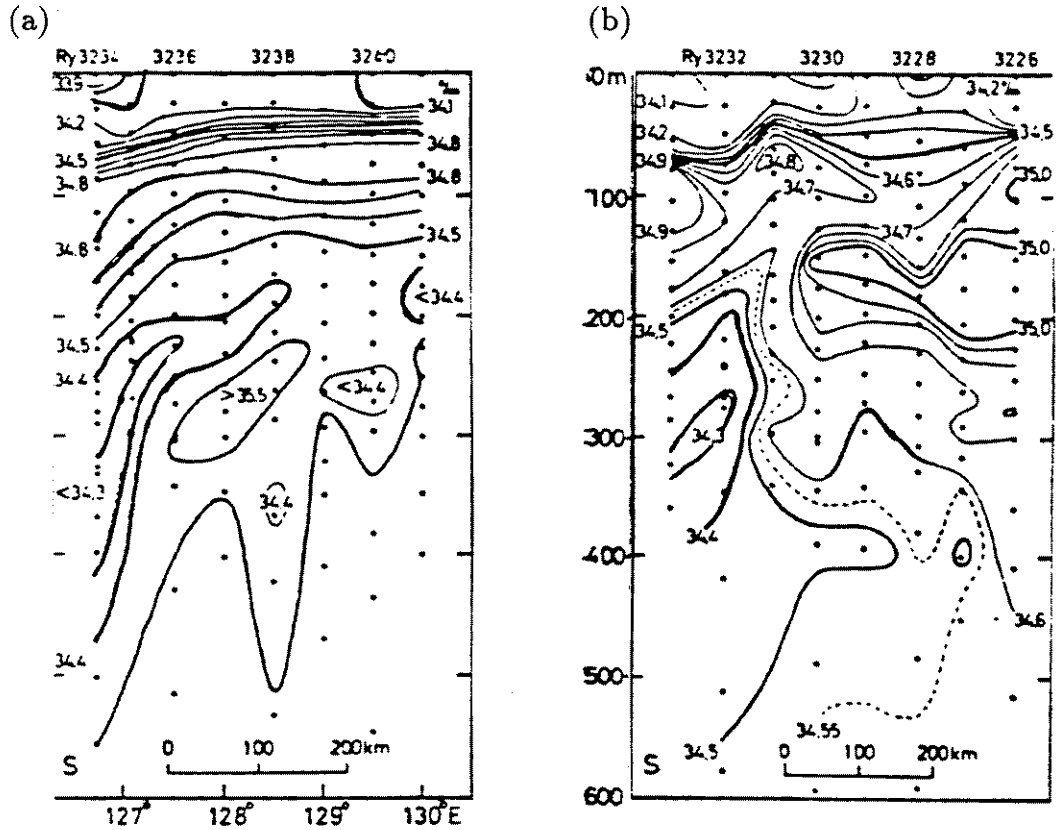

Figure 4.37: Vertical Sectionof Salinity (a) across the Mindanao Current at 7°30′N and (b) between Mindanao and Halmahera (adapted from Matsuzawa (1968)).

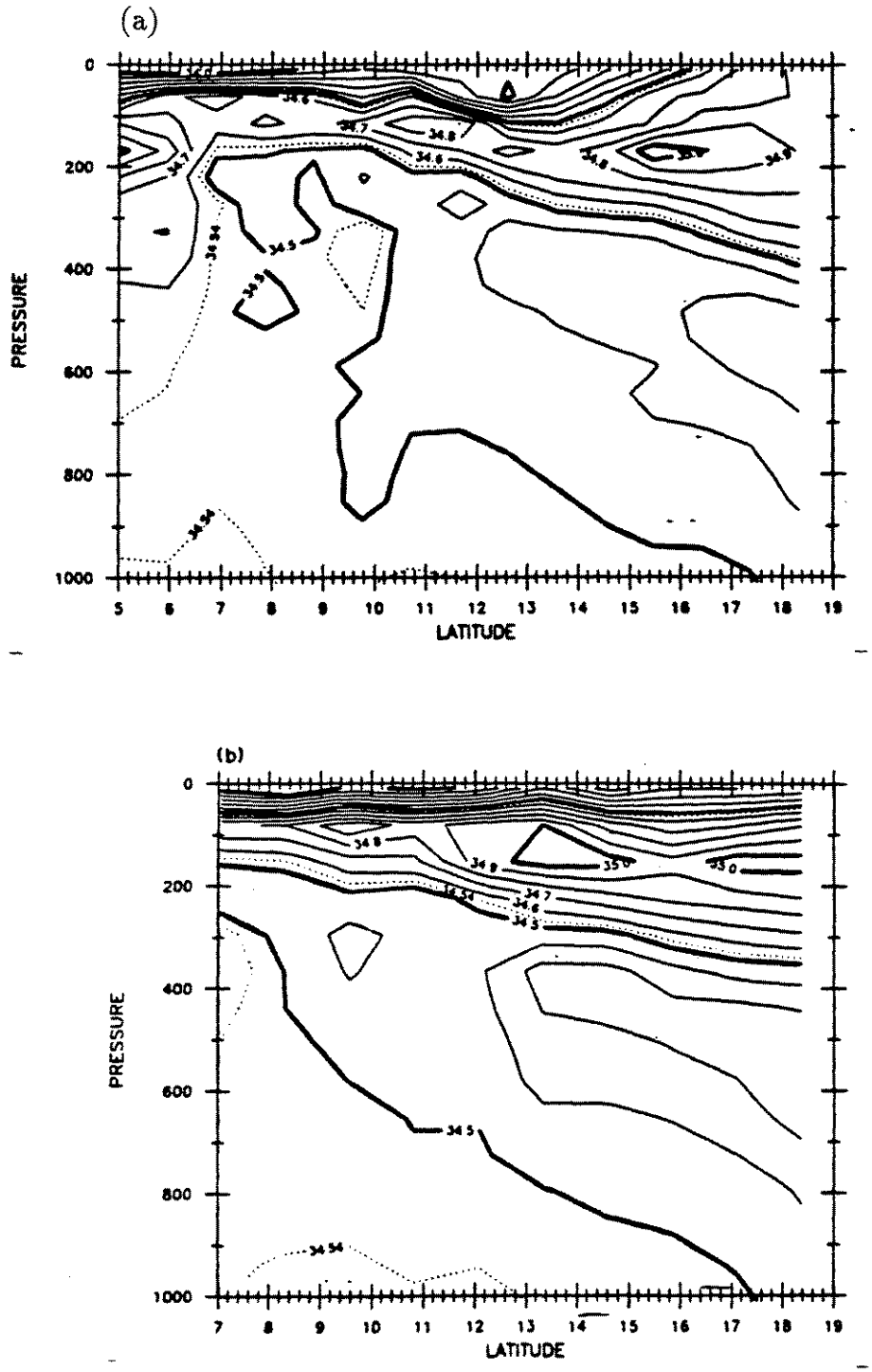

Figure 4.38: Sections of Salinity in psu (read ppm) Constructed from data obtained along 130°E during the (a) First and (b) Second Cruises of the US/PRC Cooperative Program; Station Locations are shown in Fig. 4.22 (adapted from Toole et al. (1988)).

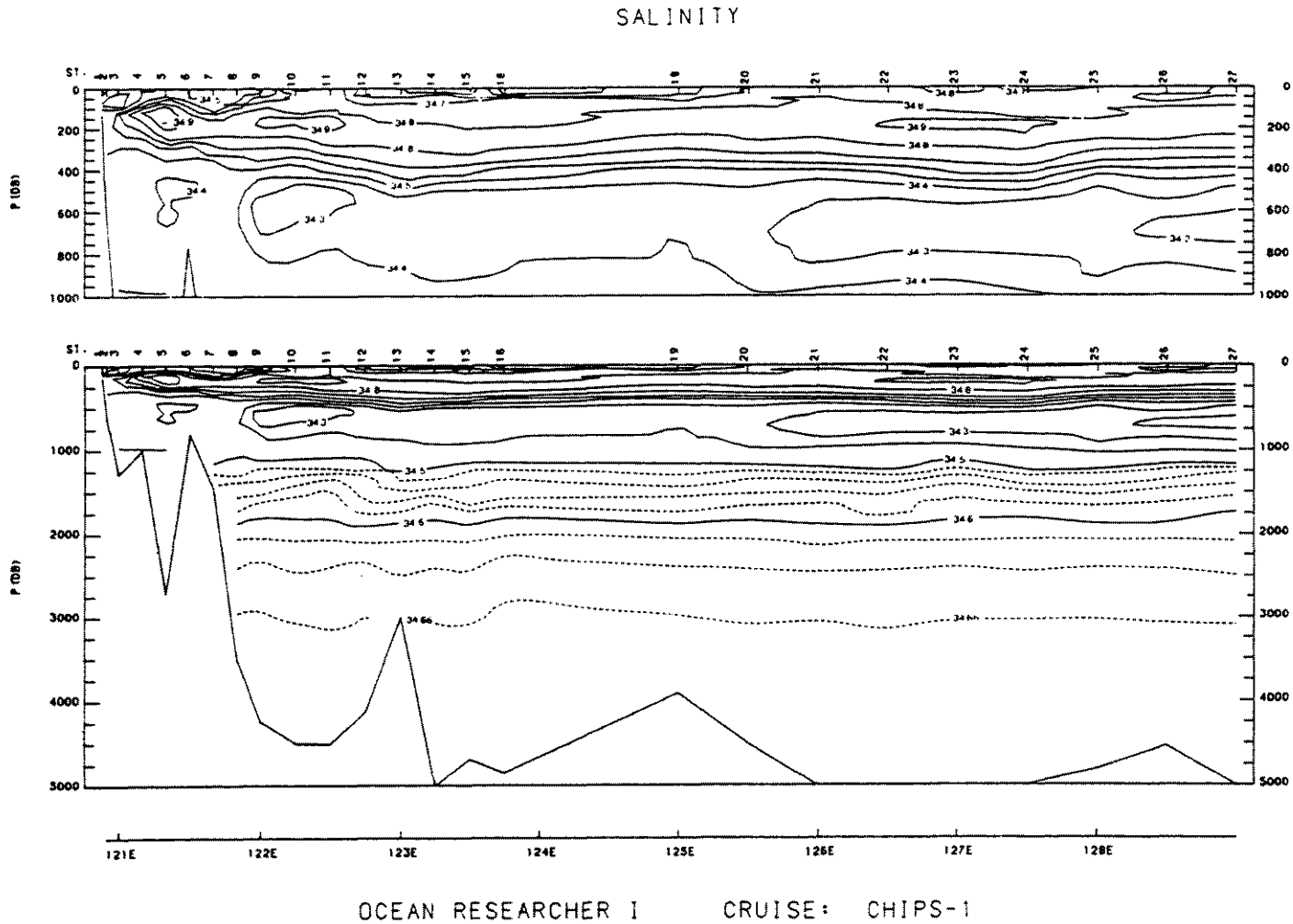

Figure 4.39: Section Plot of Salinity (adapted from Liu et al. (1986)).

6. Temperature versus Salinity. A plot of these variables is used to identify water masses in the oceans. Along the CHIPS-1 section (see Salinity-Depth discussion above) observations of potential temperature (θ) were plotted against salinity (S) for the water flowing northward across the section, and for the water flowing southward (see Figs. 4.40(a) and 4.40(b)). The envelopes of values that identify the open ocean watermasses are shown for the western North Pacific Ocean on those diagrams for Western North Pacific Water(WNPW) and for Equatorial Pacific Water (EPW). WNPW originates in the subtropics while EPW originates along the equator. When observed θ-S (or T-S) curves fall within the envelope which defines a watermass, it indicates no modifying influences (such as mixing with other waters having different characteristics) have been experienced as the water is carried away from its source region by ocean circulation. The results along 21°45′N CHIPS-1 section in the western Philippine Sea indicate some slight modification has occurred from WNPW toward EPW as the water has been carried along the western boundary of the North Pacific Ocean. There appears to be little or no difference between the northward and southward flowing water.

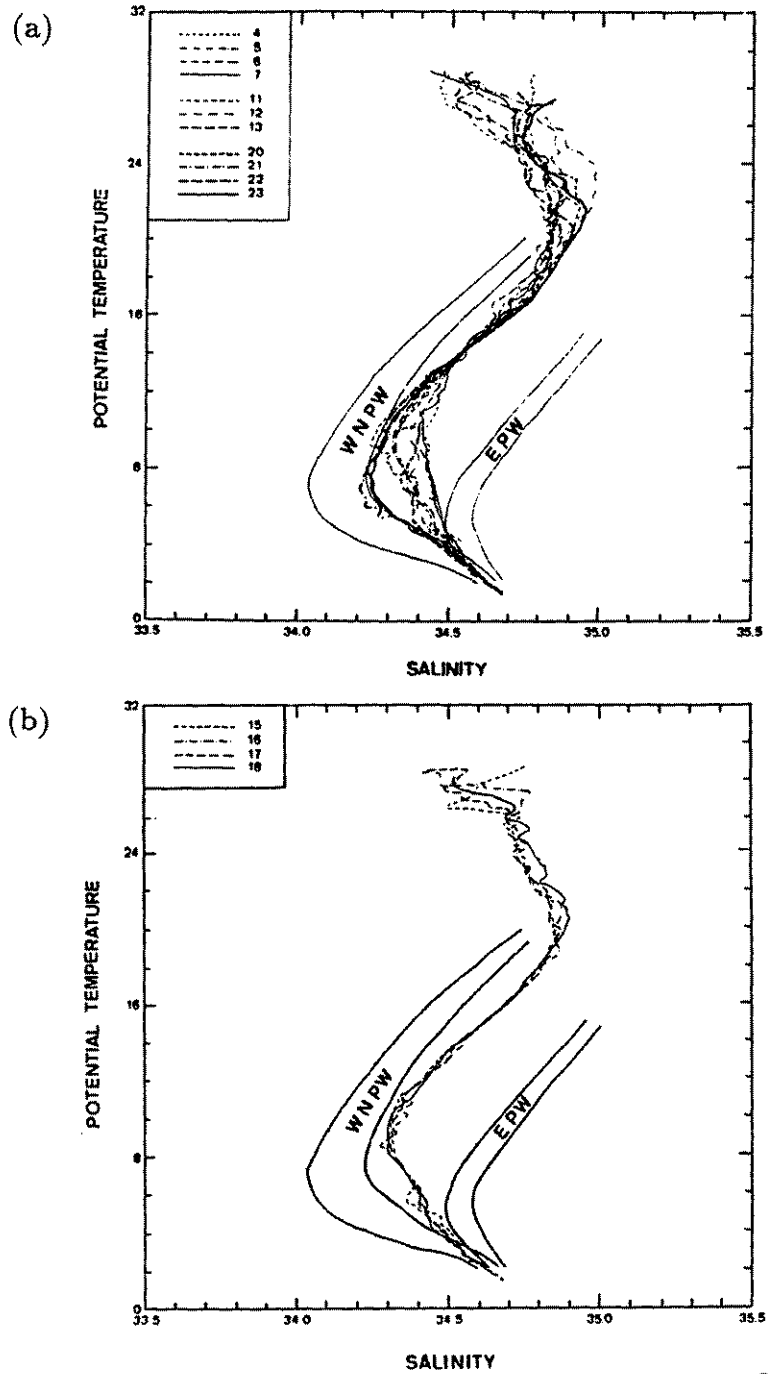

Figure 4.40: (a) θ-S Diagram for Stations that have Northward-flowing Water along 21.75°N. WNPW means the western North Pacific water type and EPW means the equatorial Pacific water type. Station numbers are indicated in the upper left corner, extending eastward from Taiwan from 121°E to 129°E. Longitude. (b) θ-S Diagram for ST. 15-18 for Southward-flowing Water (adapted from Liu et al. (1986)).

7. Mixed Layer Depth versus Wave Height. For the region just offshore from Taiwan, as described above in the temperature-depth section, Yin (1988) plotted the value of the highest 1/10 of the observed waves ($H_{1/10}$) against mixed layer depth (MLD) for the stations along the Ho and ST sections and obtained a linear best-fit correlation curve. The monthly variation of MLD at Station Ho-1 is shown in Fig. 4.41. The effects of the strong Northeast Monsoon winds are clear from November–January.

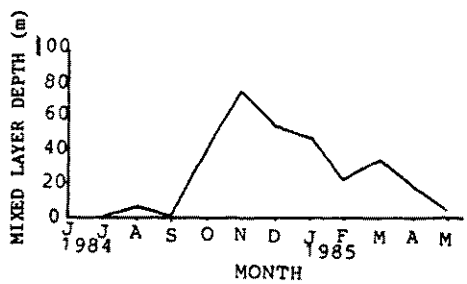

Figure 4.41: Variation of the Mixed Layer Thickness at Station Ho-1 (adapted from Yin (1988)).

8. Wave Height. Detailed statistics of wave heights have been analyzed over this region from ship data compiled between 1854–1987, with most observations taken from 1948–1987. Charts from the Naval Oceanography Command Detachment, Asheville (1989) are included in Appendix D. Wave heights are influenced strongly by surface winds; thus the greatest percentage of high waves occur during the wintertime periods of strong winds. In other seasons, approaching typhoons provide high waves in the region, especially on the right-hand side of the typhoon forward-motion vector. These storm waves are forecasted routinely along with the path of the typhoon and expected windspeed, as described in the case studies included in the handbook.

9. Visibility. The visibility underwater has been measured traditionally by observing the depth at which a white disc of standard size can no longer be seen from the sea surface: the Secchi Depth[1]. A chart of this value, in meters, is shown for the Philippine Sea in Fig. 4.42. The values vary considerably, but generally occur in the range of 20 to 40 meters. Items which might reduce this value are plankton blooms or suspended sediment in nearshore regions.

[1]Modern instruments and definitions for visibility have serious questions regarding the Secchi Depth observation technique. However, the mass of measurements by this technique still provide a means of comparison for this elusive underwater parameter that may be significant for the Navy diver or photographic operations.

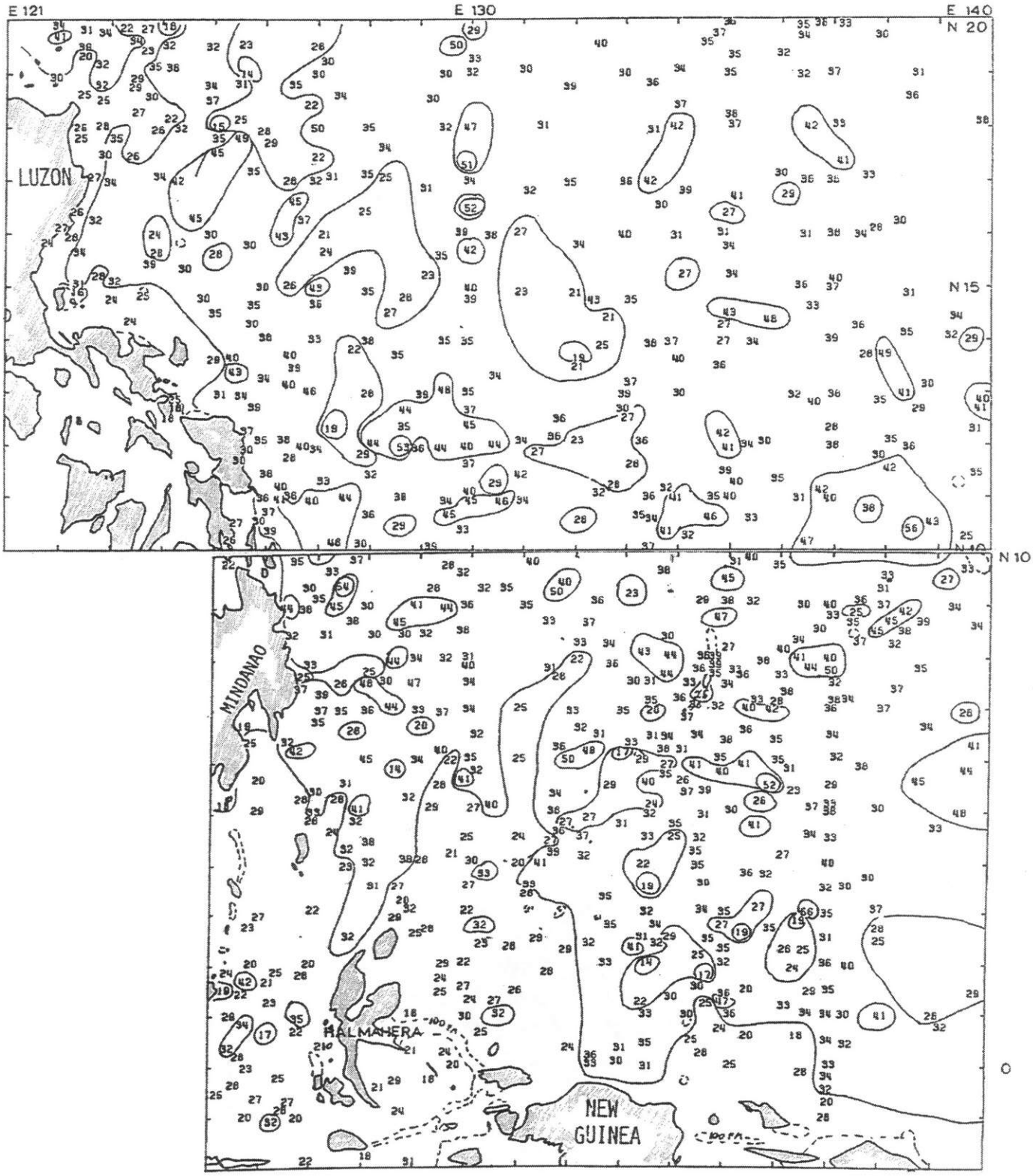

Figure 4.42: Entire Year, Secchi Depths, Philippine Sea and Pacific Ocean (2°S–20°N) (adapted from Murdock (1980)).

10. Sediments. Sediment covering the sea floor can affect several types of naval operations in an ocean region. The Philippine Sea adjacent to the Philippines is covered with lithogenous sediment (see Fig. 4.43). A preponderance of terrigenous and pelagic clay nearshore occurs there (Fig. 4.44(a)); some calcareous ooze occurs in Luzon Strait and off the southeastern coast of Luzon. Further seaward, south of 20°N, are regions of biosilicious ooze and mud; while north of 20°N, calcareous ooze and marl occur. A substantial area of pelagic "red" clay is shown near the Philippines in fig. 4.44(b), which further distinguishes the various sediment categories.

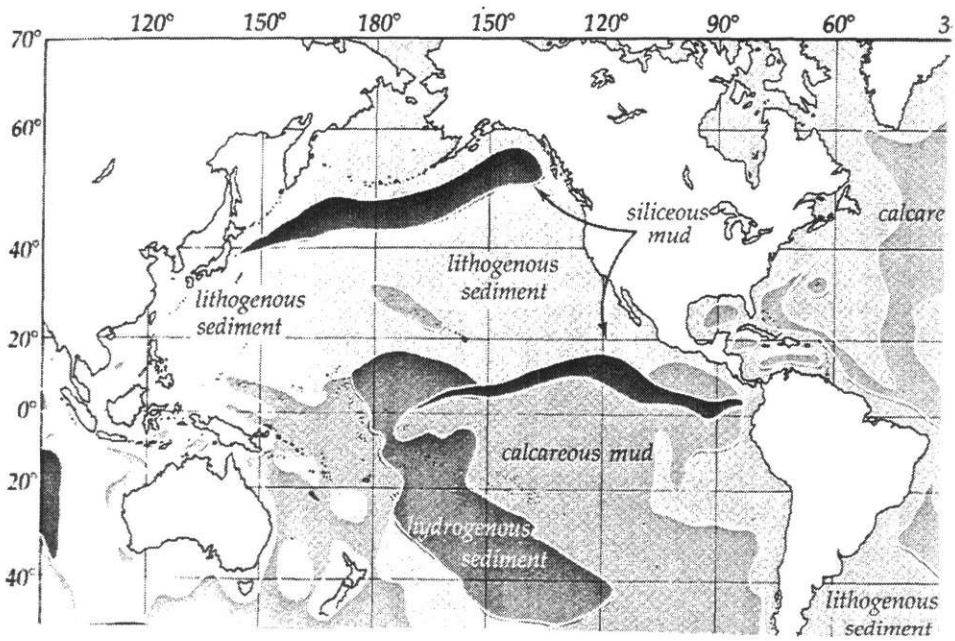

Figure 4.43: Distribution of Ocean Bottom Sediments (adapted from Ingmanson and Wallace (1973)).

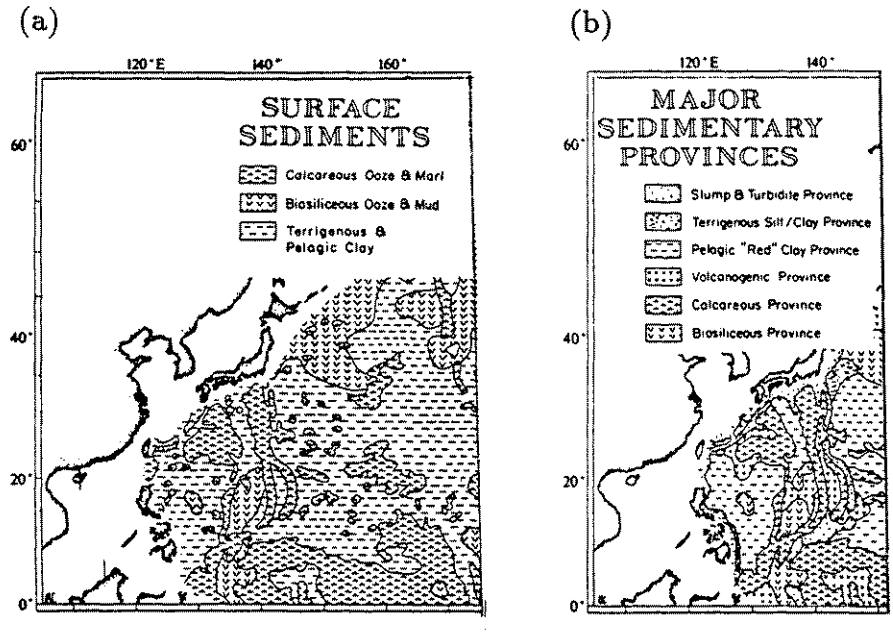

Figure 4.44: (a) Distribution of Surficial Sediments on the Seafloor of the North Pacific Ocean in Terms of the Three Major Types of Pelagic Sediments: Terrigenous and Pelagic Clays, Calcareous Oozes and Marls, and Biosiliceous Oozes and Muds. (b) Pelagic Sedimentary Provinces of the North Pacific Ocean (adapted from McCoy and Sancetta (1985)).

11. Sound Backscattering. A Russian study (Shevtosov et al. 1985) has presented results of backscattering of sound measurements for the western tropical Pacific Ocean (see Figs. 4.45(a) & (b) and 4.46). In Fig. 4.45(b) averages for night conditions are shown for 30 kHz sound (line 1); for 12-kHz sound (line 2), and the sound velocity profile (line 3). At night, the backscattering signal level for both frequencies is low at the sea surface, but increases through the mixed layer and thermocline layer (at 100–150 meters depth). The 30-kHz scattering decreases abruptly below that depth, while the 12-kHz scattering decreases erratically and much more gradually. The 12-hKz values are considerably larger at and below the maximum value, through all depths to 750 meters.

The maximum backscattering values for daytime conditions in Fig. 4.45(a) are much smaller than for night, never approaching the minimum values shown for night. The daytime values are much more consistent with depth, but indicate some layering which is not at the same depth for both frequencies.

In Fig. 4.46, the indicated migrating sound scattering layer (1) in the upper levels is consistent with the contrasting scattering levels between day and night shown in Table 4.2 and in Fig. 4.46. The deeper layering "of a physical nature" also shows that consistency.

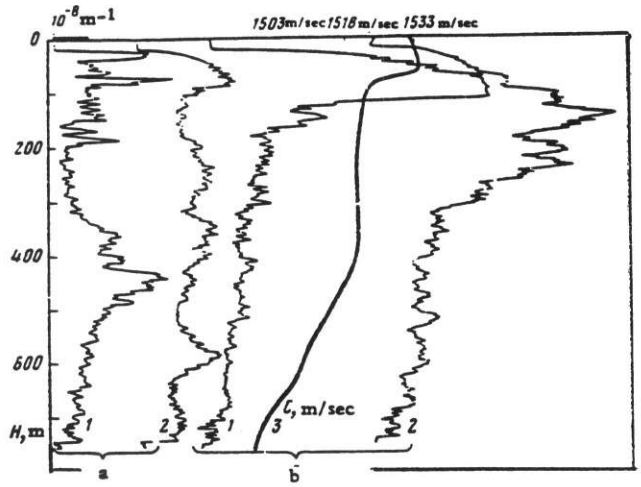

Figure 4.45: Profiles of the Backscattering Signal Level, averaged over 100 Pulses at 2.5-sec Intervals, for 12- and 30-kHz Frequency Sound, obtained during the Day (a) and Night (b) in the Tropical Zone of the Pacific Ocean: 1) 30-kHz frequency; 2) 12-kHz frequency; and 3) Vertical Profile of the Sound Velocity (adapted from Shevtosov et al. (1985)).

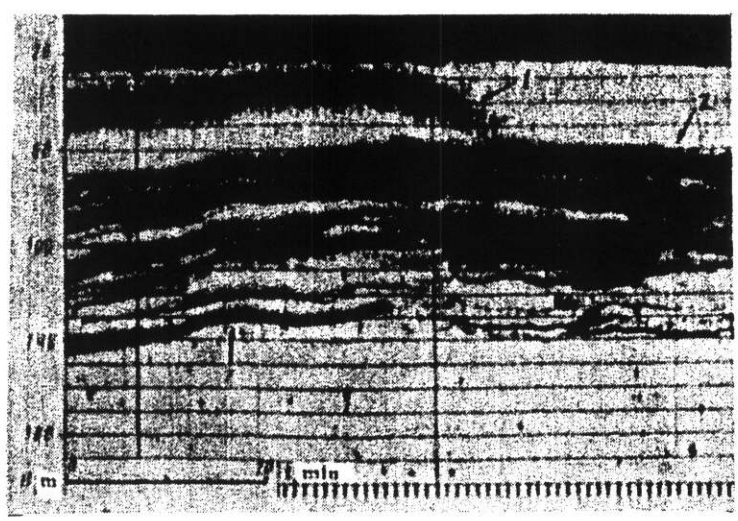

Figure 4.46: Comparative Trace of Acoustic Inhomogeneities of a Physical Nature and a Migrating Sound-scattering layer (SSL): 1) Migrating SSL; 2) Acoustic Inhomogeneities of a Physical Nature (adapted from Shevtosov et al. (1985)).

Table 4.2: Layer-Averaged Values of the Backscattering Intensity for 30-kHz Frequency Sound from the Results of Measurements at Stations Typical of the Southern and Northern Regions of the Northwest Pacific Ocean (Shevtosov et al. 1985)

Depth, m	Backscattering intensity dB per 1 m^{-1}				Noise
	Northern region		Southern region		
	Day	Night	Day	Night	
20-75	–90	–85	–76	–70	–125
75-150	–100	–90	–70	–62	–118
150-225	–95	–95	–73	–65	–113
225-300	–96	–97	–74	–74	–109
300-450	–	–	–65	–70	–103
450-600	–	–	–68	–76	–98
600-750	–	–	–70	–72	–93

12. Tides. Tide reference stations in the Philippine Islands are located at Cebu, on Cebu Island; at Davao, on Davao Gulf on Mindanao; at Jolo, on Jolo Island in the Sulu Archipelago; at Legaspi Port on Albay Gulf, southeastern Luzon; at Manila on Manila Bay, Luzon; and at San Fernando Harbor on Lingayen Gulf, Luzon (see Tide Tables for 1990, U. S. Dept. of Commerce National Ocean Service, 1989). The time and height of high and low waters is given daily through the year for these reference stations. Current year tide tables may be purchased from National Oceanic and Atmospheric Administration (NOAA) Distribution Branch, 6501 Lafayette Ave., Riverdale, MD 20737, telephone (301) 436-6990.

B. South China Sea (northern portion)

The major northern islands of the Philippines (especially Luzon and Mindoro) and Palawan are bounded to the west by the northern portion of the South China Sea (see Fig. 4.47). This Sea fills a broad, deep central basin of >4000 meters depth that extends eastward into the Manila Trench (>4000 meters) and into the Palawan Trough (>3000 meters) as shown in Fig. 4.47. To the northwest there are very broad and shallow shelf regions, less than 200 meters in depth, along the Vietnamese and Chinese coasts and extending into the Formosa (Taiwan) Strait.

1. Current Circulation Patterns. Since the South China Sea is a marginal basin along the Asian continent, it is influenced greatly by the monsoon circulations in the atmosphere there, which reverse direction between winter and summer.

The strong Northeast Monsoon in February is shown by the inset diagram (upper right) in Fig. 4.48(a). The resultant ocean currents have a counter-clockwise circulation. Much of the South China Sea is occupied by currents directed generally toward the west or southwest; a narrow strong current flows to the south along the western boundary (Asian coastline); eventually this water flows toward the southeast between Borneo and Sumatra into the Southern Hemisphere.

By August, the Southwest Monsoon is blowing strongly (see inset diagram on Figure 4.48(b)) over this region. The resulting currents have also reversed direction, moving toward the northeast over most of the South China Sea. Water enters the Sea from the Southern Hemisphere between Sumatra and Borneo and it exits through both Formosa and Luzon Straits at the northern end.

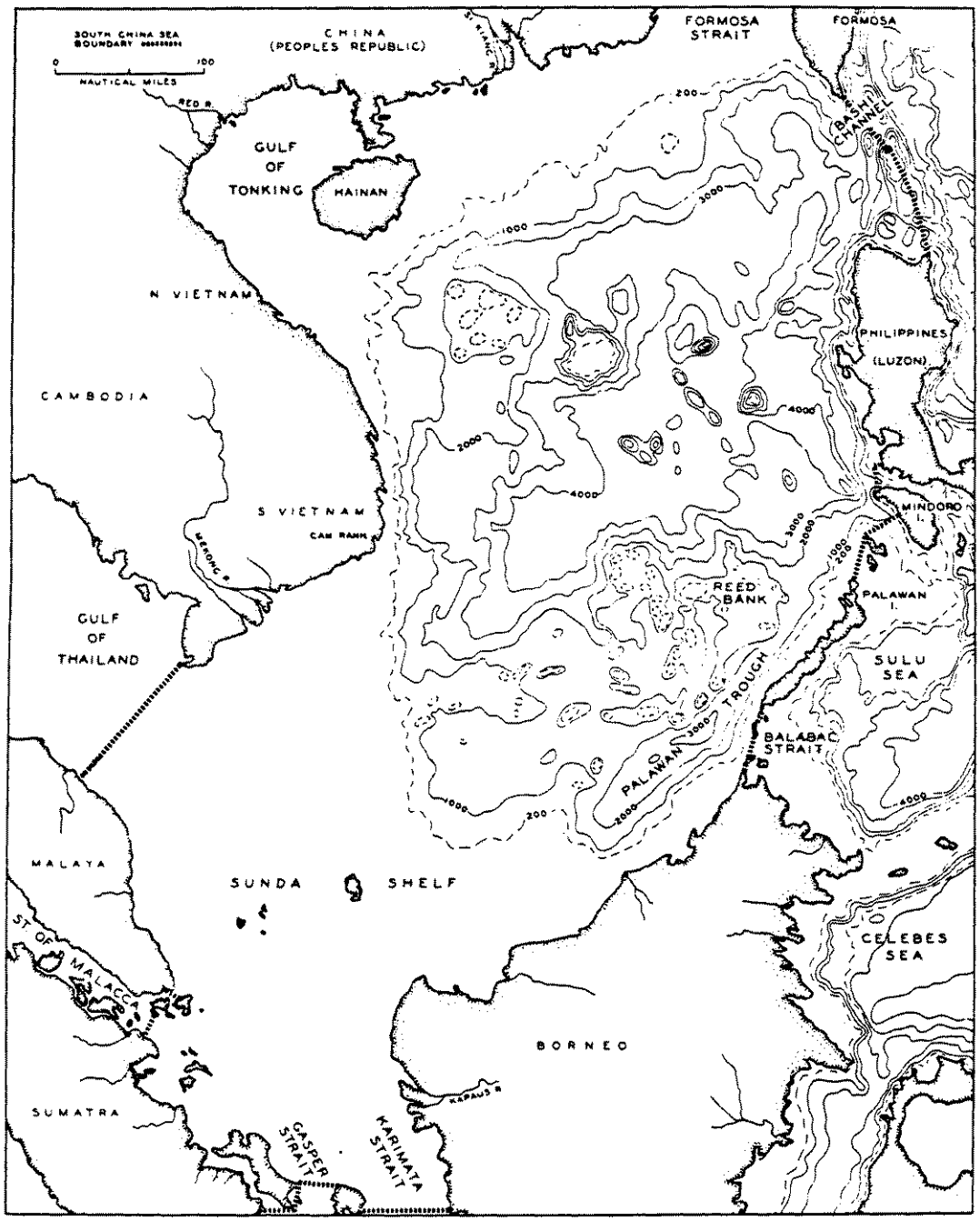

Figure 4.47: General Topography and Boundary Features of South China Sea (contours in meters) (adapted from LaFond (1966)).

(a)

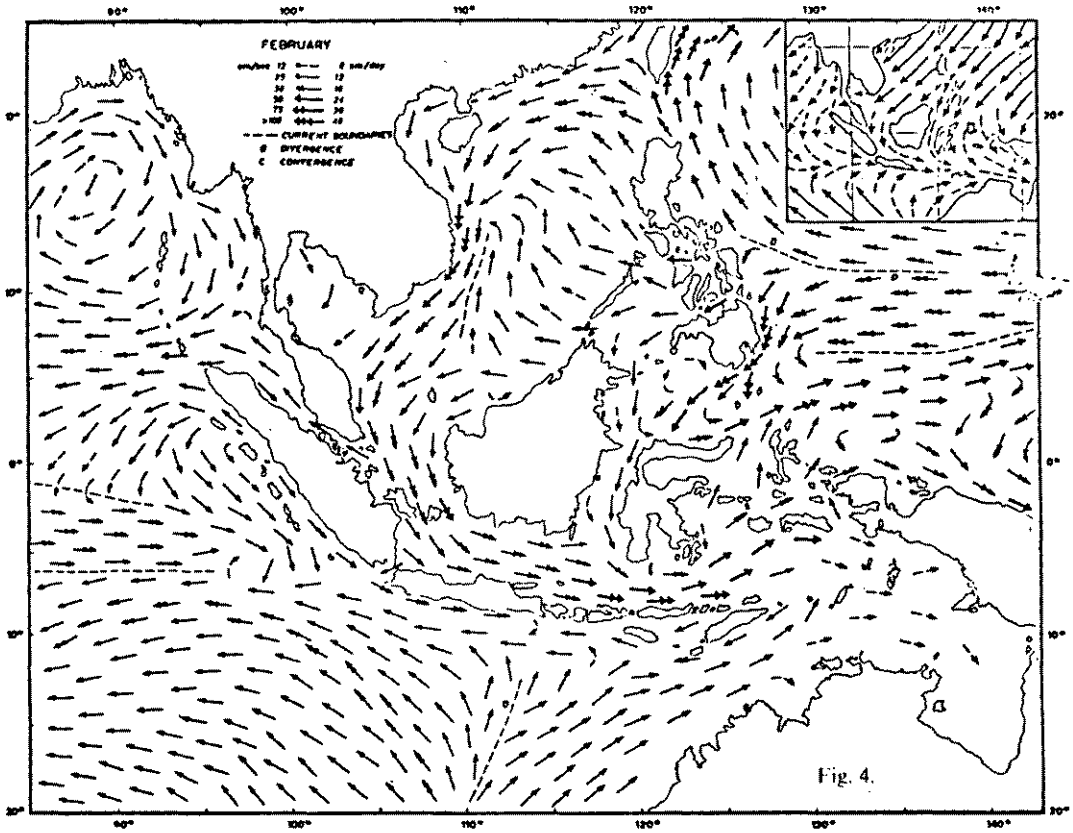

(b)

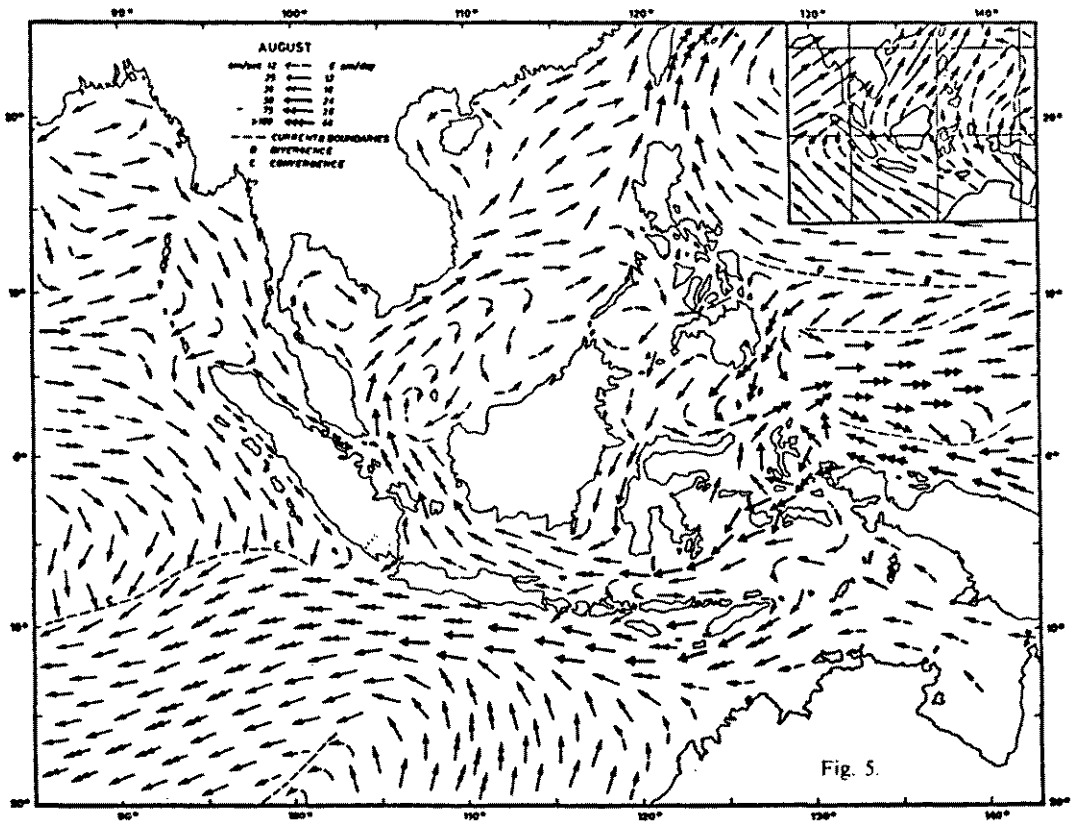

Figure 4.48: Sea Surface Current Distribution for South China Sea: (a) February and (b) August. Inset diagrams show surface winds that reverse seasonally (Monsoon Winds) (adapted from LaFond (1966)).

In a study in 1985–1986, a number of stations were sampled off the southwestern coast of Taiwan, in the northernmost part of the south China Sea (see Fig. 4.49(a)). The bottom topography is shown in Fig. 4.49(b); the depths vary considerably in this slope region, from less than 100 meters in Taiwan Strait to over 2000 meters further south. Figure 4.50 illustrates the current pattern reversal between July (Southwest Monsoon) and October (Northeast Monsoon).

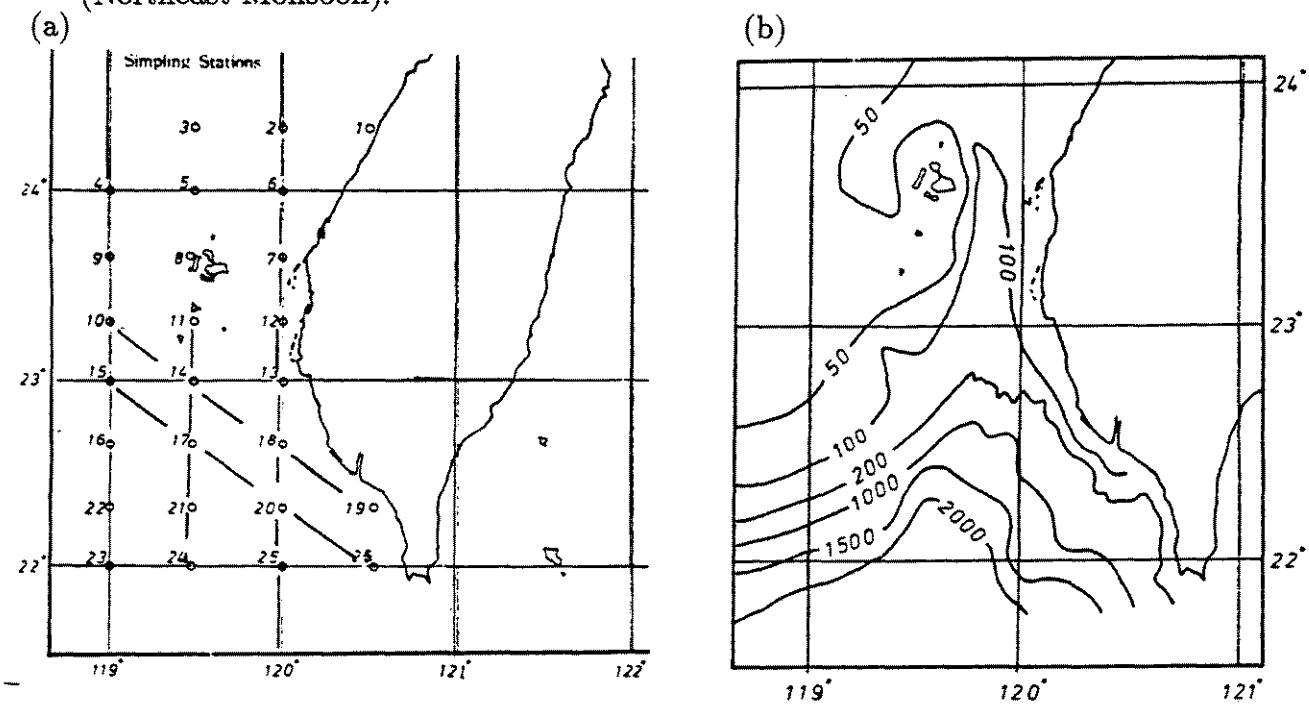

Figure 4.49: (a) Sampling Locations along the Southwestern Coast of Taiwan. (b) Bottom Topography of Southwestern Coast of Taiwan (adapted from Hung et al. (1986)).

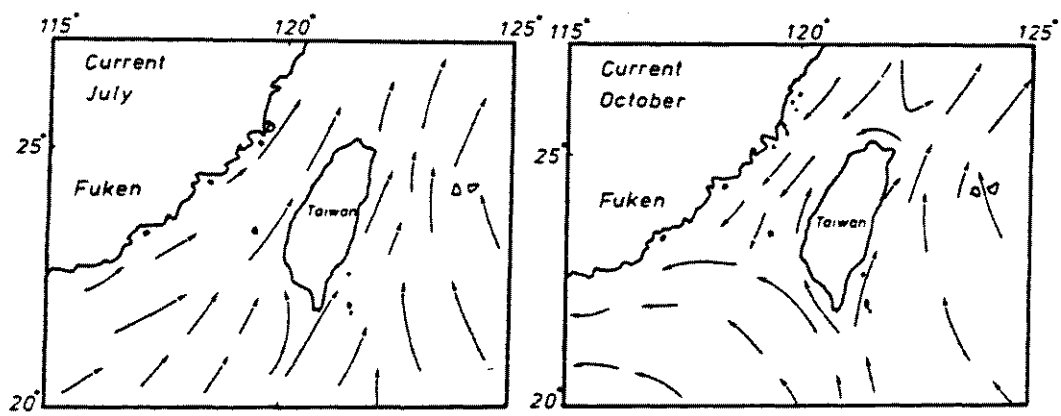

Figure 4.50: Currents Patterns surrounding Taiwan (adapted from Hung et al. (1968)).

2. Sea Surface Temperature. The charts shown in Figs. 4.17 and 4.18 indicate the seasonal changes that occur, while sea surface temperatures for each month are included in Appendix A. In February there is a broad region of the Philippines which show temperatures of 26° to 27°C. Extending to the southwest of northern Luzon, the 26° isotherm marks the southeastern limit of a sea surface temperature gradient that occupies the region to the northwest. The 22° isotherm that extends west-southwestward from Taiwan marks the southern boundary of a very strong temperature gradient that occupies the Taiwan Strait region and the China coastal area. The temperature drops to 14°C in Taiwan Strait.

By May, effects of the spring warming have developed temperatures over 29°C (the seasonal maximum value for this region) over a broad area of the eastern South China Sea. Toward the north, a weak temperature gradient occurs, with temperatures below 23°C in Taiwan Strait.

In August, temperatures lie between 27 and 29°C over the region, with most areas showing 28.5 to 29°C. By November, cooling has established temperatures as low as 21°C in Taiwan Strait, and temperature gradients are increasing over the region; most areas show temperatures from 28.5 to 26°C.

3. Temperature Variation with Depth. Observations were made in a series of studies to the southwest of Taiwan at locations shown in Fig. 4.49(a). These stations were sampled 9 August and 11 October 1985; and on 2 March and 25 May 1986 (see Fig. 4.51). Sections of temperature from the sea surface to the bottom, or to a maximum depth of 200 meters, are shown along the lines of stations drawn in this figure: line 10–19; line 15–26; line 11–24; and line 12–25. The first two lines are oriented NW–SE at two different distances offshore. The other two lines are oriented N–S, also at two different distances offshore. The four sections are arranged in the figure so the seasonal variation can be traced easily from left to right (Summer, Fall, Winter (lower right) and Spring (upper right)); the sections are arranged vertically with those oriented NW–SE above the N–S sections. The temperature distributions display the usual seasonal variation; the seasonal thermocline reaches the sea surface in summer, and then descends below a cooler mixed layer that forms during the fall and winter (especially evident in water over the greater depths. The thermocline gradient increases as the seasonal cooling and deepening proceeds.

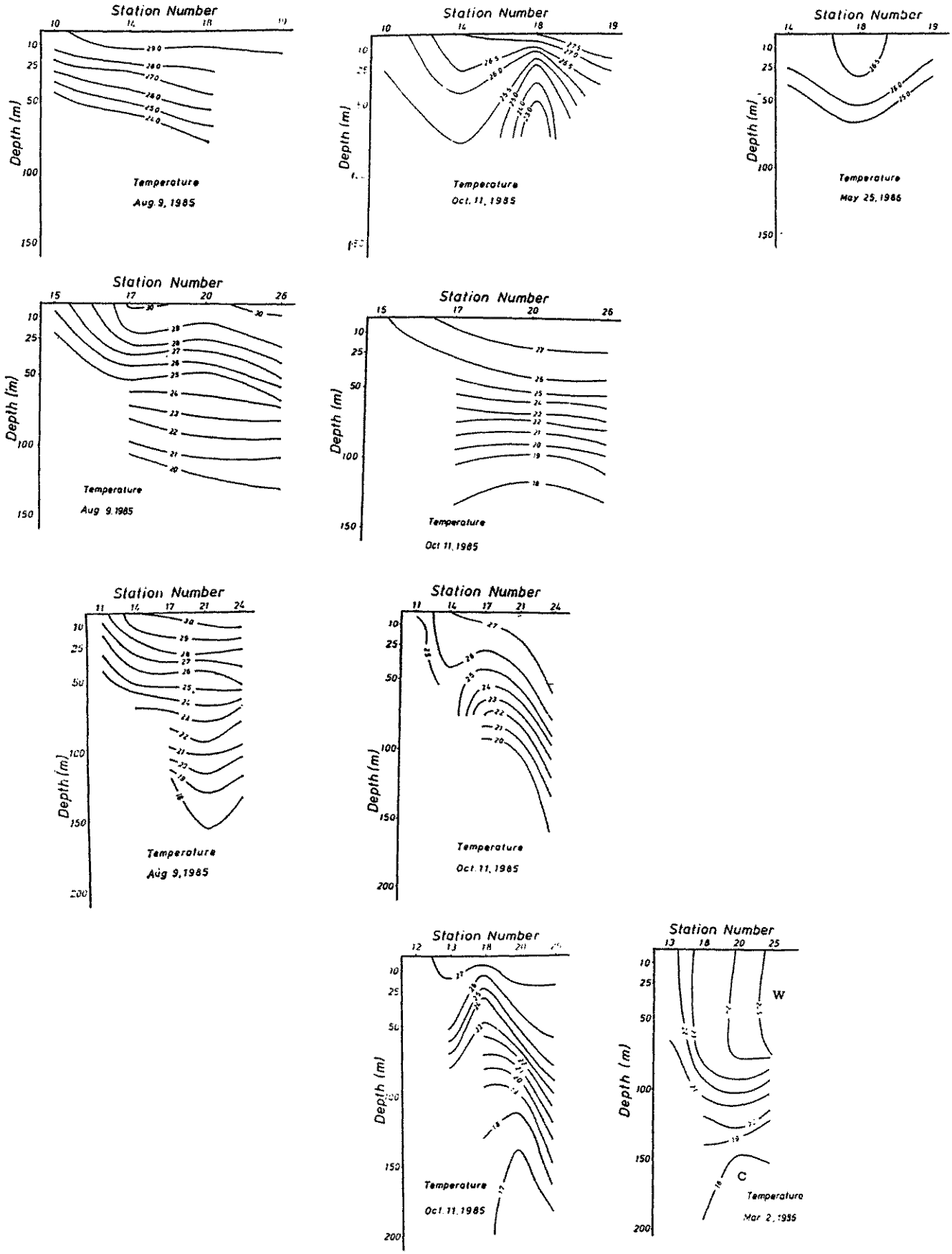

Figure 4.51: Temperature (°C) versus Depth (meters) along the Various Sampling Lines in Fig. 4.49(a) (adapted from Hung et al. (1986)).

4. Salinity. The winter (February) salinity distribution at the sea surface shows effects of the counterclockwise circulation during the Northeast Monsoon (see Fig. 4.35(a)). Water with salinity values in excess of 34.0 ppm enters through the Luzon Strait from the Philippine Sea, and gradually becomes modified to lower values (to 33.3 ppm) as it is carried to the southwest along the Chinese and Vietnamese coasts. Water with lower salinity (33.0 ppm) moves to the north along the eastern half of the South China Sea; it gradually is increased during its movement northward. Salinity values along Palawan and the west coasts of the northern Philippines range from 33.2 to 34.0 ppm. The summer (August) salinity distribution shows the influence of the southwest Monsoon (see Fig. 4.35(b)). The strong currents from the southwest along the western boundary carry water with lower salinity (33.0 ppm) into the western South China Sea. This forces the tongue of higher salinity water offshore into the middle of the Sea. The lower salinity tongue cuts across from SW–NE from Vietnam to northern Luzon and forces the higher salinities to the region northward from about15°N.

5. Salinity Variation with Depth. The sections with the observations taken to the southwest of Taiwan are shown in Fig. 4.52, similar to those shown earlier for temperature. These seasonal salinity changes closely follow those of temperature. In August, the salinity values increase from the low values (33.0 to 33.7 ppm) at the surface toward a layer of maximum salinity (34.5 to 34.7 ppm) that occurs at about 100 meters depth. The salinity gradient is strongest at the top of the (temperature) thermocline region, weakening somewhat at greater depths.

In October, surface salinity values are higher (33.8 to 33.9 ppm), and the gradient increases with depth through the observed water column to values of 34.7 or 34.8 ppm at the greatest depths observed (no evidence of the salinity maximum layer shows at these depths). Strong salinity gradients occur associated with the deeper thermocline.

In March, the one section observed shows no evidence of strong salinity gradients anywhere in the 150-meter layer adjacent to the surface. The salinity values there are as high (34.65 to 34.8 ppm) as the maximum values observed at any depth in other seasons.

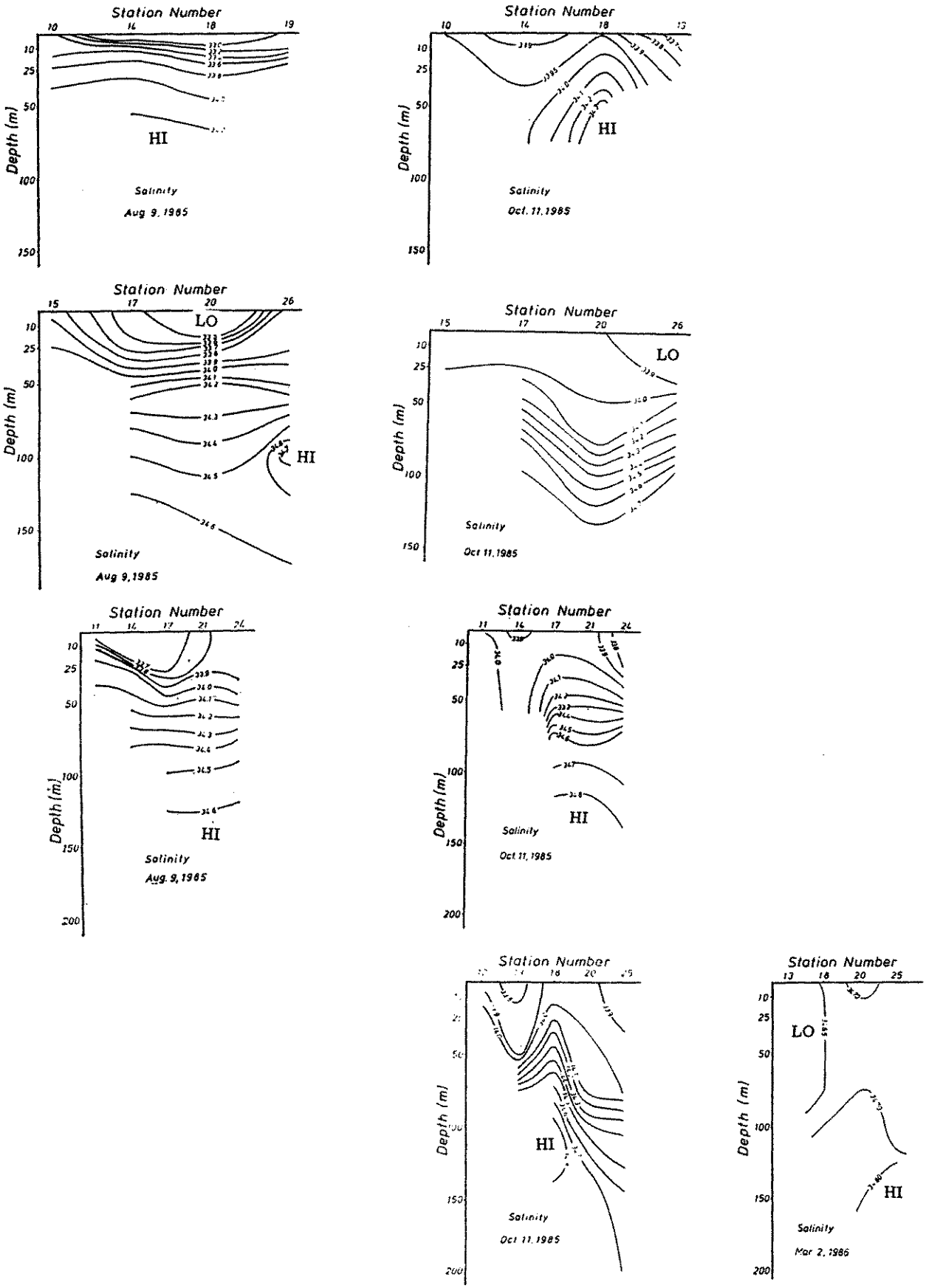

Figure 4.52: Salinity in ppm versus Depth (meters) along the Various Sampling Lines in Fig. 4.49(a) (adapted from Hung et al. (1986)).

6. Temperature versus Salinity Relation. Summer cruise observations (August–September 1970) are plotted from locations shown by Fig. 4.53(a) in the northern South China Sea and are shown in Fig. 4.53(b). Most of the values are in the upper 150 meters. The low surface salinities increase abruptly at the top of the thermocline and then generally increase gradually as temperatures decrease down to near 150 meters depth.

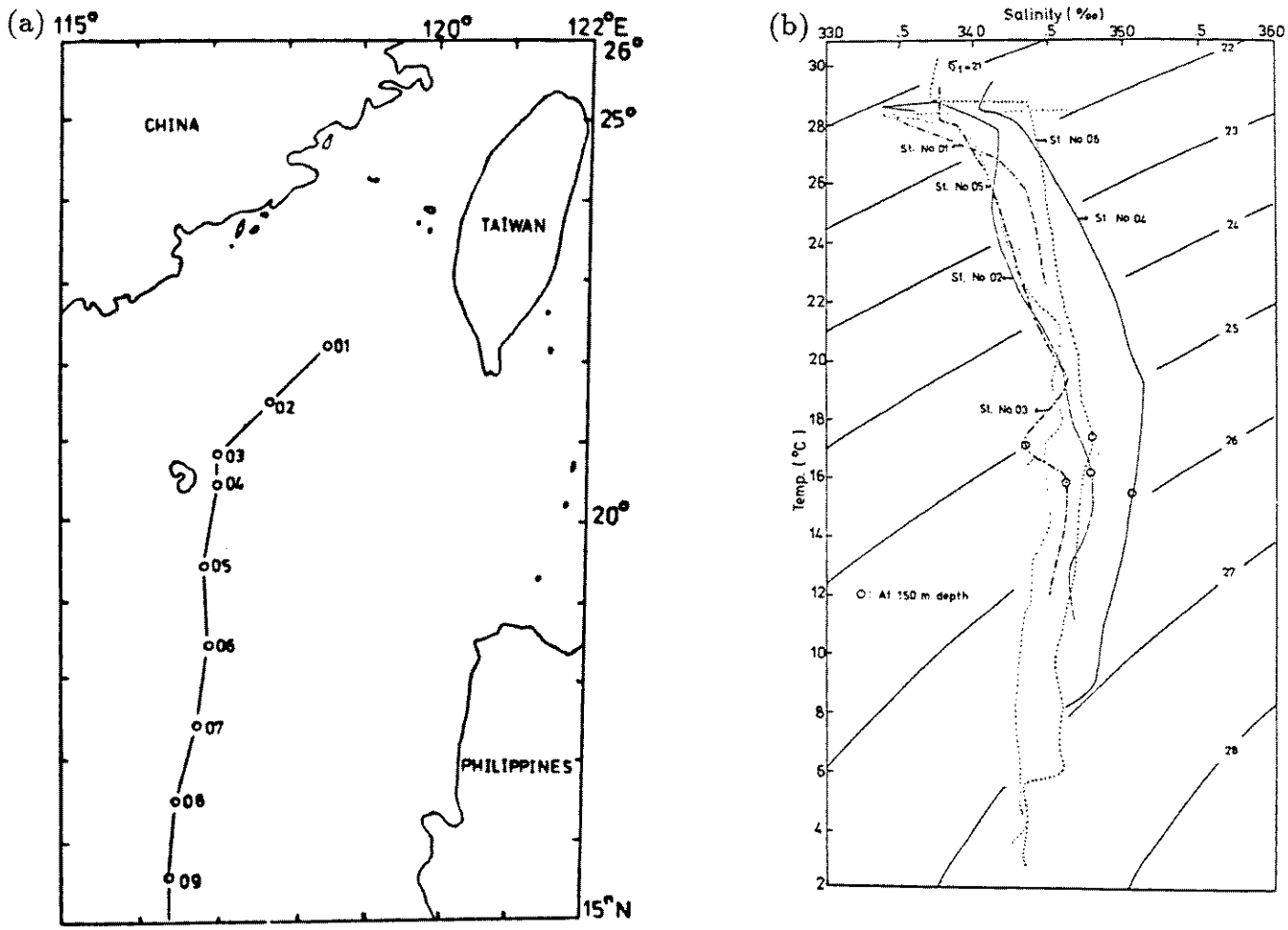

Figure 4.53: (a) Some of the Stations in the South China Sea Cruise in 1970. (b) TS-diagrams for the Six Selected Stations from South China Sea Cruise in August-September 1970 (adapted from Fan and Yu (1981)).

7. Upwelling. Seasonal upwelling is supported by the study from which the salinity and temperature observations with depth were reported above (see Fig. 4.51); other nutrient and chemical observations were made which support seasonal upwelling at some stations in the region off southwestern Taiwan, during August and October, 1985; the upwelling appeared to shift to other stations during the Northeast Monsoon (December and March), and then return to the original stations with the onset of the Southwest Monsoon in May. Currents from the South China Sea, northern China coast and the Kuroshio Current appear to influence this upwelling, in addition to effects from bottom topography and the monsoon winds. An extension of this study into an adjacent region (to the north) was reported in Hung et al. (1987), with observations made in September & December, 1986; and in February & May, 1987.

8. Transparency. Values of Secchi Depth are reported for the northern South China Sea for the winter (December–March) and for other seasons (April–November); see Murdock (1980), Figs. 4.54(a) & (b). Values less than 20 meters occur in Taiwan Strait and along the China coastline in both charts; the low values extend further offshore from China during the winter, and a tongue of low value extends southwest from Taiwan and Bashi Strait. Few locations show values greater than 30 meters.

The remainder of the year, however, shows more regions with greater depths; the small values (20 meters or less) occur generally very close to adjacent coastlines.

Figure 4.55 shows the annual values for the central region of the South China Sea. Features here resemble those for the northern section in April–November (see Fig. 4.54(b)).

9. Typhoon Surge Model. A study (Li and Su 1987) has reported the development of a model that calculates sea level changes that combine effects of typhoons approaching Taiwan and the astronomical tide. Typhoon surges during periods of spring tides (during full or new moon phases) have caused coastal lowland flooding. Air pressure gradient and windstress are considered the driving forces for the typhoon surge. The model was tested by use with conditions during Typhoon Wayne, which struck western coastal Taiwan with great resulting damage. The observed sea surface height agrees well with the model computations.

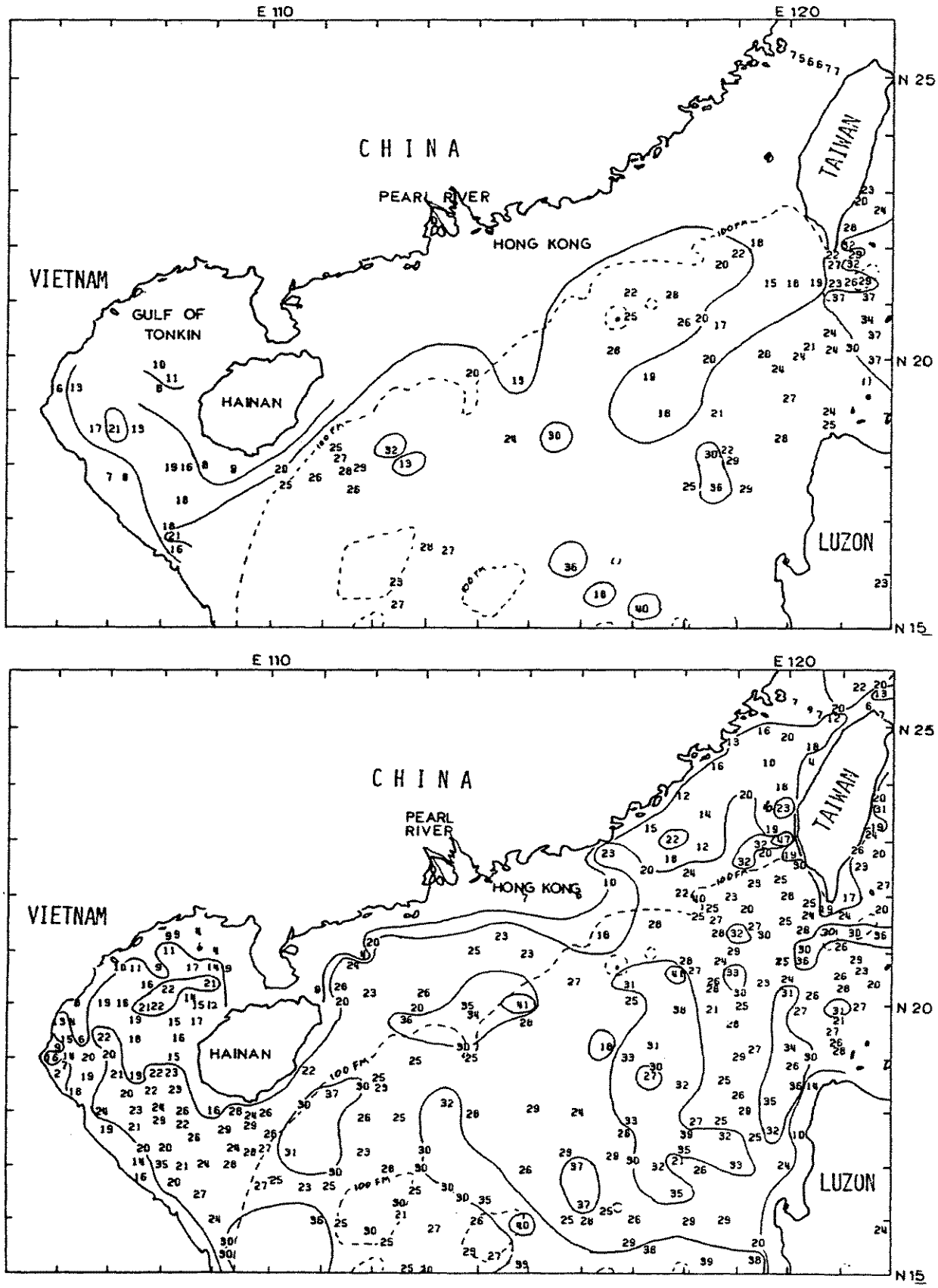

Figure 4.54: Secchi Depths, South China Sea (Northern Section), (a) DEC–MAR & (b) APR–NOV (adapted from Murdock (1980)).

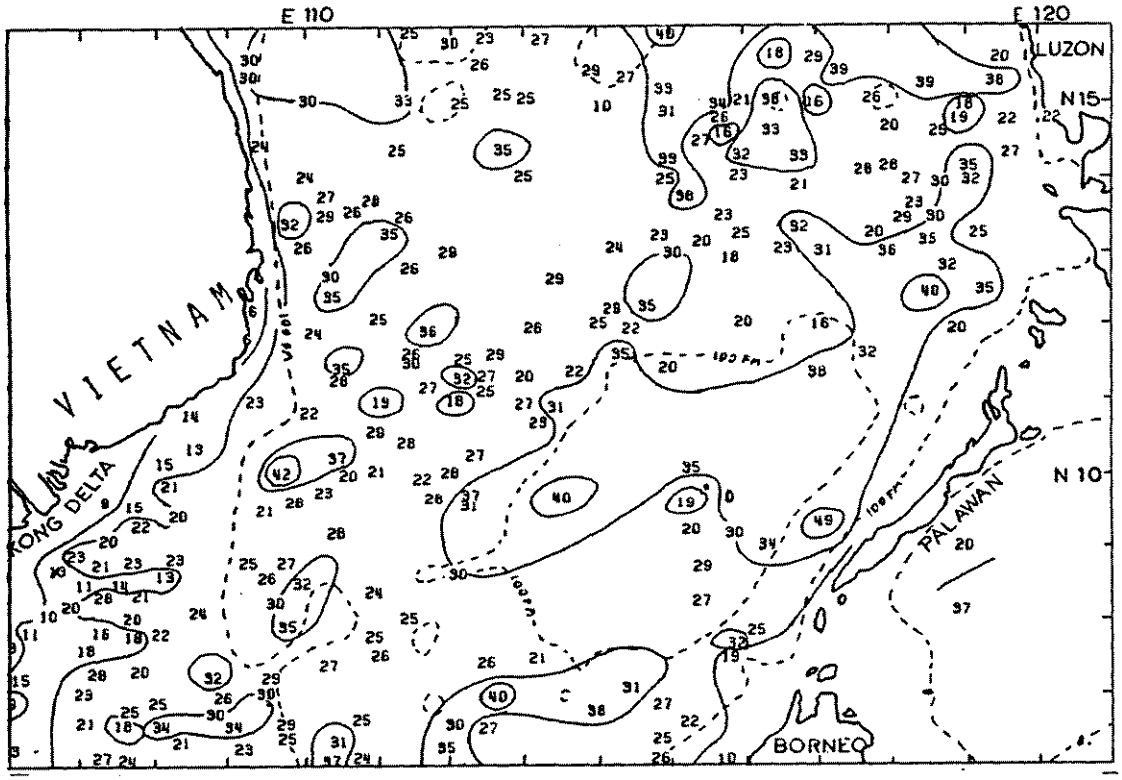

Figure 4.55: Secchi Depths, South China Sea (Central Section), Entire Year (adapted from Murdock (1980)).

10. Turbidity Currents. Current meter records have been made of turbidity currents that flowed in Abra Canyon off the Abra Delta along the northwest coastline of Luzon, during flood conditions (Shepard et al. 1977). Figures 4.56, 4.57, & 4.58 illustrate flow characteristics of such currents along a canyon floor: Fig. 4.56 shows one instance of up-canyon flow, followed by strong down-canyon flow for many minutes before a lull interval. Figure 4.57 indicates this type of alternating flow occurred many times in Abra Canyon (at a depth of 622 meters). The turbidity current extends at least 30 meters above the canyon floor. Figure 4.58 illustrates the assymmetry of the current with time; a rapid build-up occurs to the peak speed, followed by a slow decay, down to zero current.

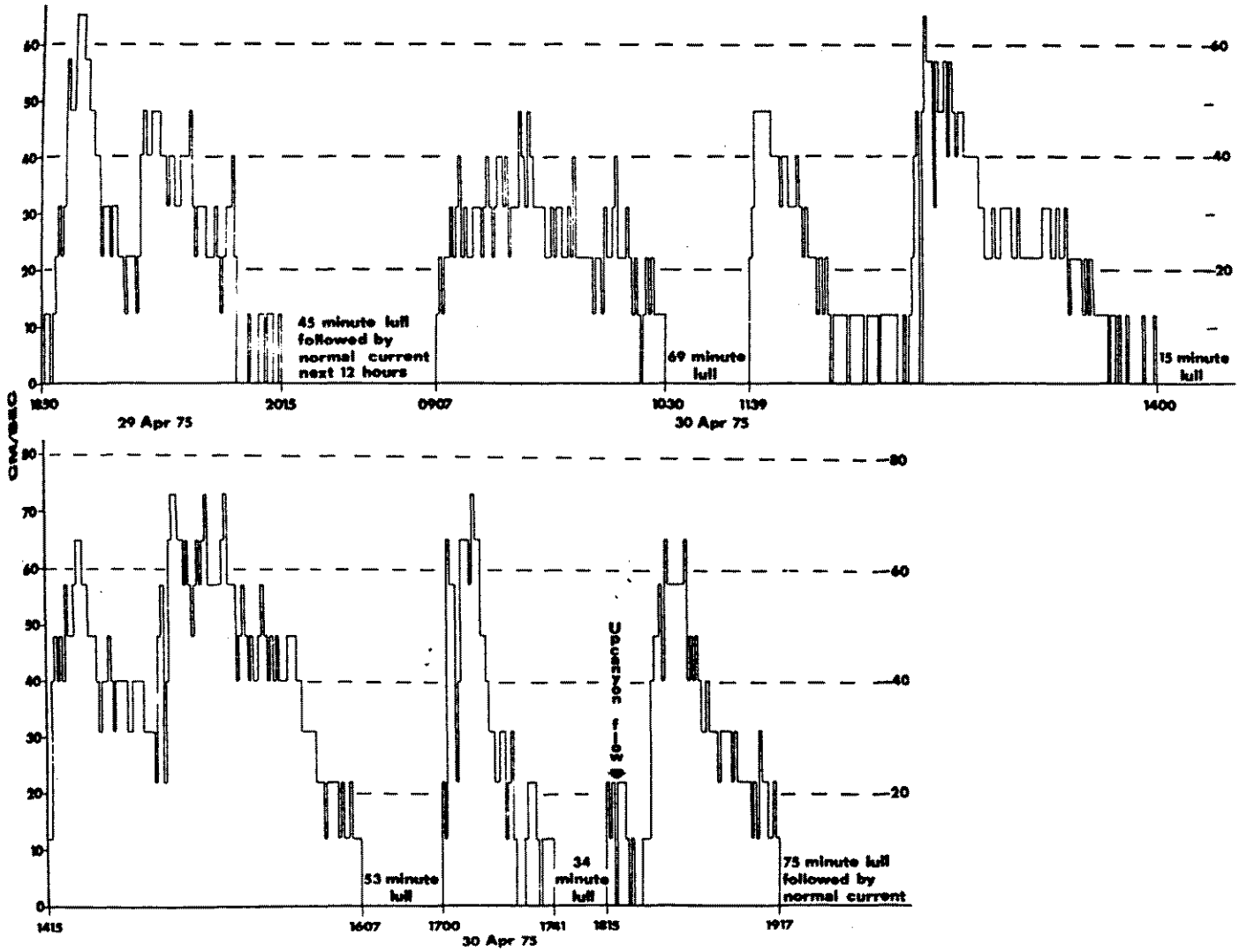

Figure 4.56: One-minute Current Averages during the Strong Downcanyon Surges in Rio Balsas Canyon (depth = 285 m). Note length of time with no measureable current following the flows. Also note that only one period of upcanyon flow was observed (at time = 18:15). The steplike changes are due to nature of recording for 1-min averaging, each step representing one additional mark on the tape during the 1-min period (adapted from Shepard et al. (1977)).

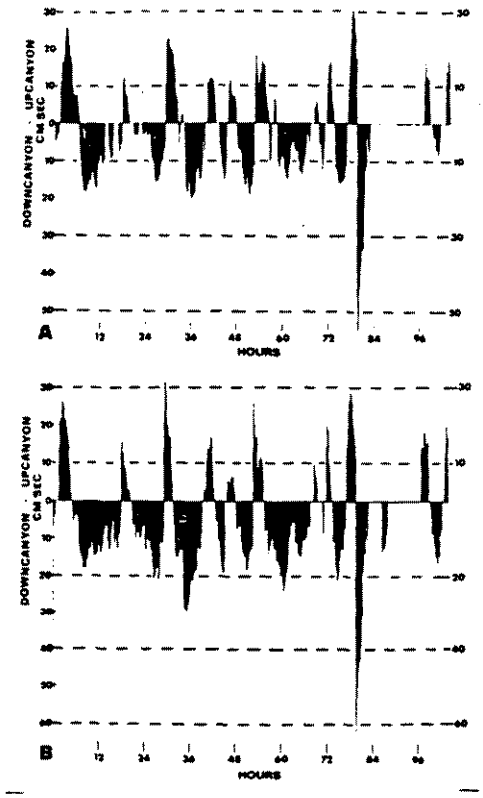

Figure 4.57: Turbidity Current in Abra Canyon off Northwest Luzon (depth = 622 m). The velocity profile shows (A) 5-min averages at 3 m above the bottom and (B) 7.5-min averages for 30 m above the bottom (1 min for peak flow) (adapted from Shepard et al. (1977)).

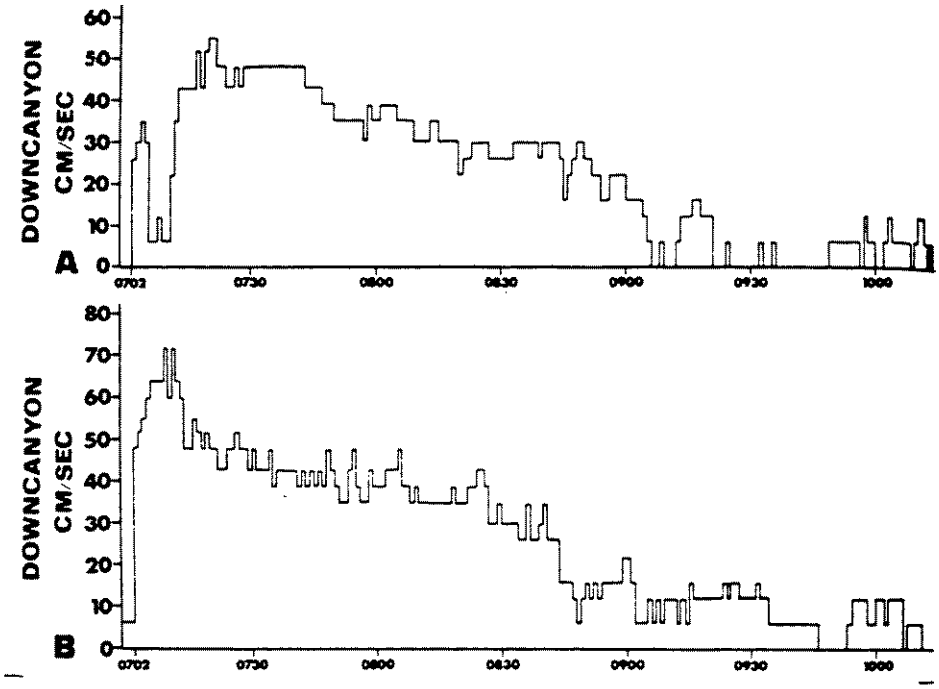

Figure 4.58: One-minute Averages for Current Velocities during the Abra Canyon Turbidity Current (depth = 622 m). Note rapid build-up to the peak and the slow decay to the period of no measureable velocity. A. 30 m above the bottom; downcanyon flow followed by an amazingly long period (14.5 h, **not** shown in the figure) of no velocity. B. 3 m above the bottom; downcanyon flow followed by 3.5-h lull (**not** shown in the figure) (adapted from Shepard et al. (1977)).

C. Sulu Sea

This is a basin that lies to the west of Mindanao; it is bounded on the northwest by Palawan and to the northeast by the Philippine Islands Mindoro, Panay, and Negros (see Fig. 4.1). The Sulu Archipelago and northeastern Borneo provide the southeastern and southwestern boundaries (see Fig. 4.59; and Fig. 4.60). Broad coastal shelves appear along those southern coastlines, as well as to the northeast of Palawan. A few locations reach depths greater than 5000 meters along the eastern perimeter off Mindanao and Negros. Note Basilan Island just south of Mindanao. Between Basilan and Mindanao lies Basilan Strait, which separates the major Philippine Islands from the Sulu Archipelago.

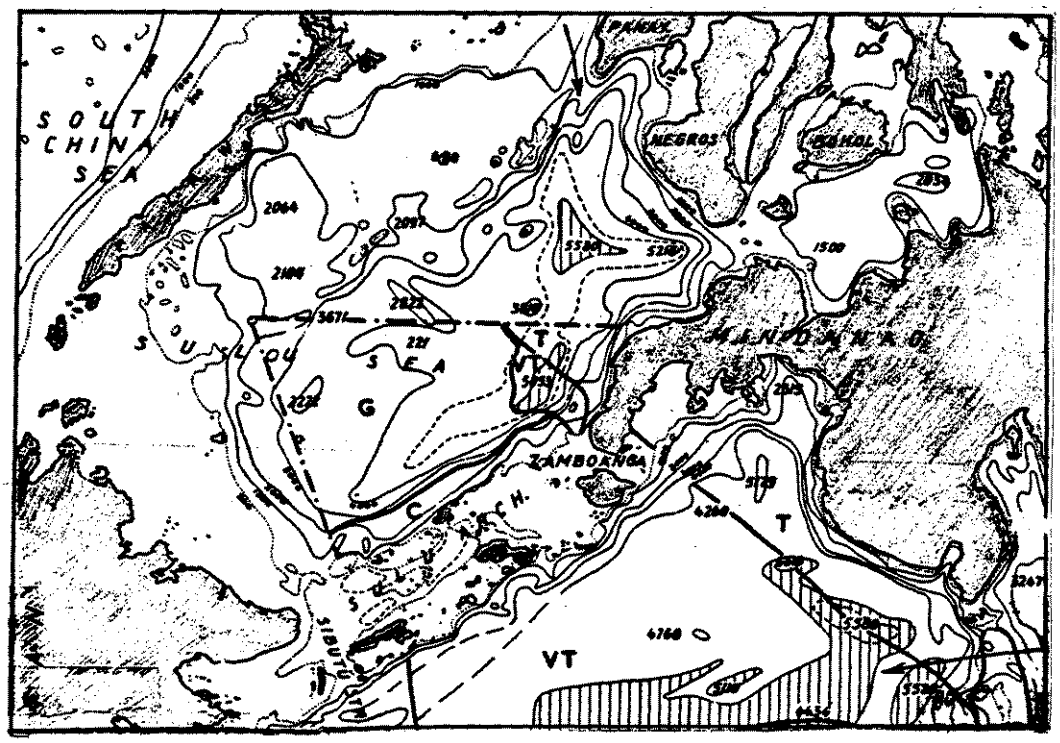

Figure 4.59: Sulu Sea and northern Sulawesi (Celebes) Sea shows bathymetry (depths greater than 5000 m are shaded); flow of bottom water (arrows); and bottom sediments: T = terrigeneous mud; G = globigerina ooze; C = coralline mud and sand; VT = volcanic and terrigeneous mud; V = volcanic mud (adapted from Tjia (1966)).

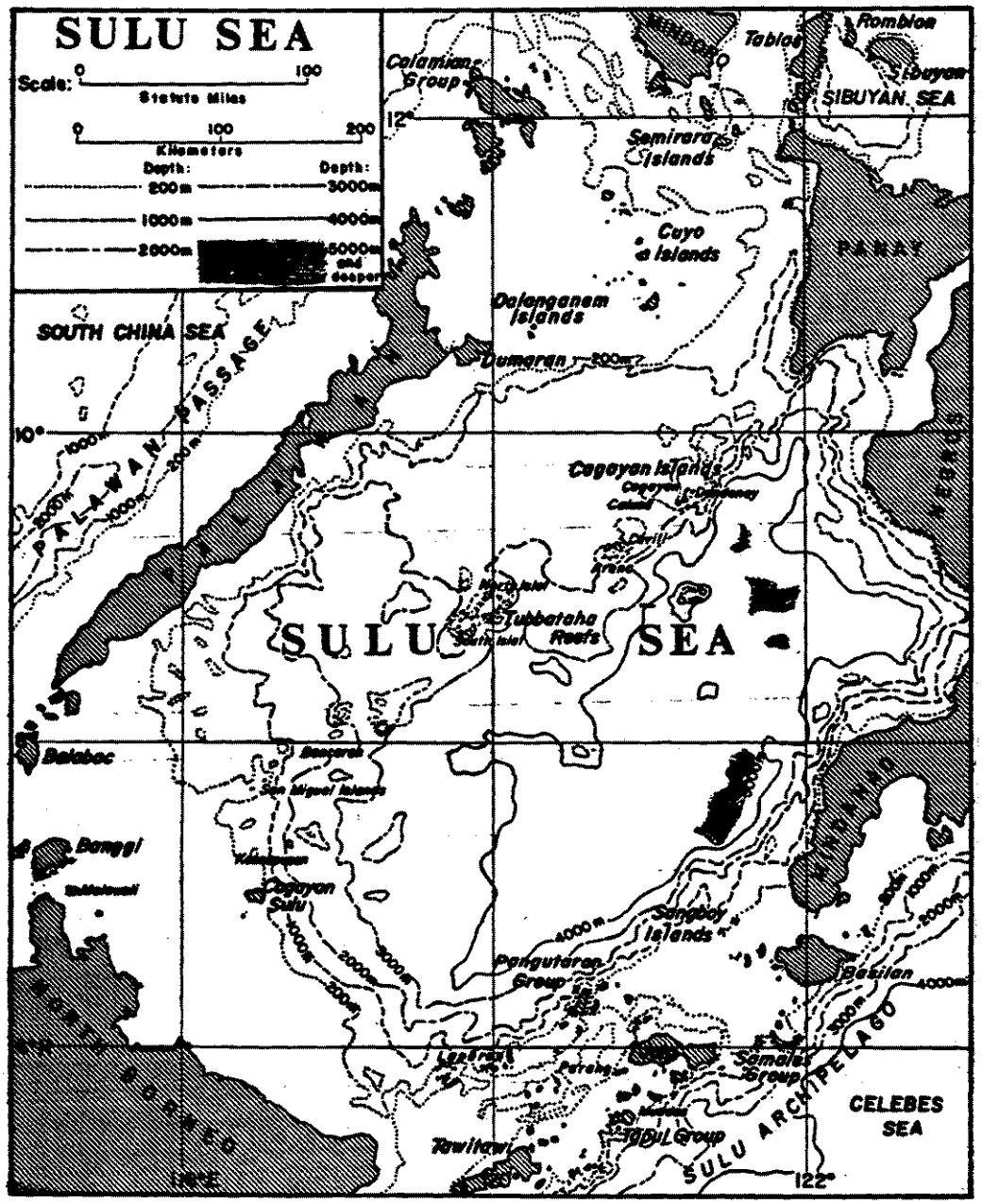

Figure 4.60: Bathymetry of Sulu Sea (depths in meters) (adapted from Tjia (1966)).

1. Current Circulation Pattern. The surface current pattern undergoes a seasonal change in direction; currents are from the east and northeast in February (see Fig. 4.48(a)), but they adopt a clockwise circulation pattern in August (Fig. 4.48(b)), when inflow from the west occurs north of Palawan to replace the outflow to the west found there in February.

2. Sea Surface Temperature. Figures 4.16 (a) and(b), 4.17, 4.18 and Appendix A all display the seasonal and monthly variation in sea surface temperature in areas adjacent to the Philippine Islands. Discussion of these figures is given on Page 4-20, to which the reader is referred. In the Sulu Sea the sea surface temperature in May varies from 29.0° to 29.5°C; it becomes one degree lower in August and November. The horizontal gradient is extremely small in all seasons.

3. Temperature Distribution with Depth. At locations SS2 and SS3 shown in Fig. 4.61, average T-Z soundings (Fig. 4.62) are shown (Apel et al. 1985); data from two additional stations are given (Fig. 4.63). In each case, no mixed layer is evident, and a pronounced thermocline extends from the surface (temperature at about 29°C) to about 200 meters depth. The temperature continues to decrease slowly to 500–600 meters depth and then appears uniform below, at about 10°C.

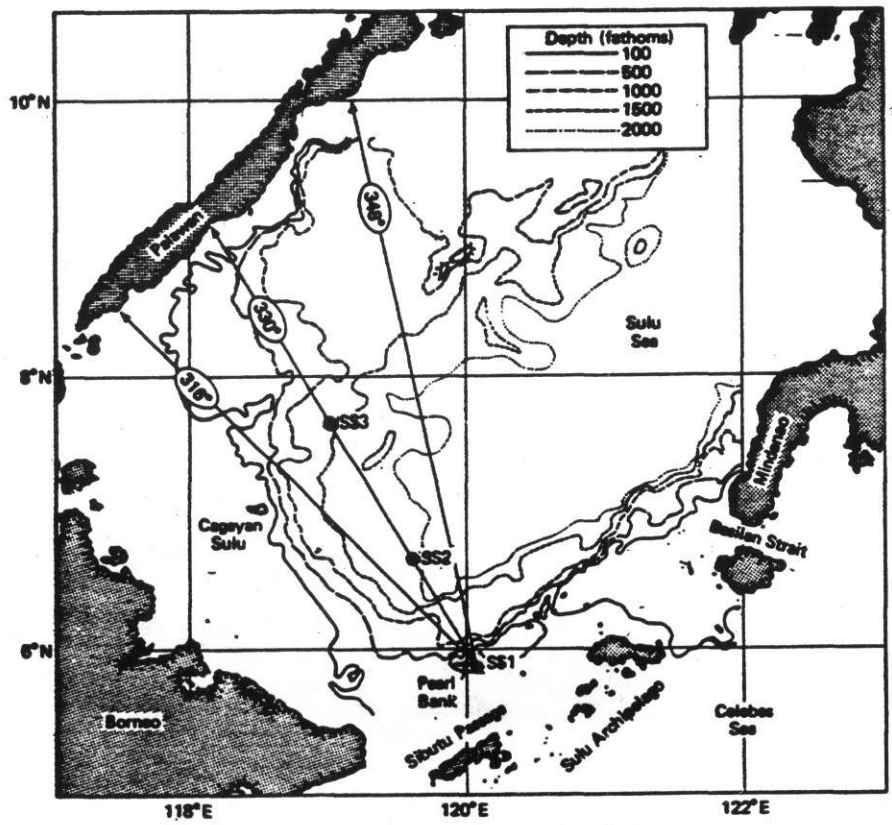

Figure 4.61: Bathymetry of Sulu Sea, showing Locations of Current Meter Moorings SS1, SS2 and SS3 and Radius from Soliton Source near Pearl Bank along 316, 330 and 348° (adapted from Apel et al. (1985)).

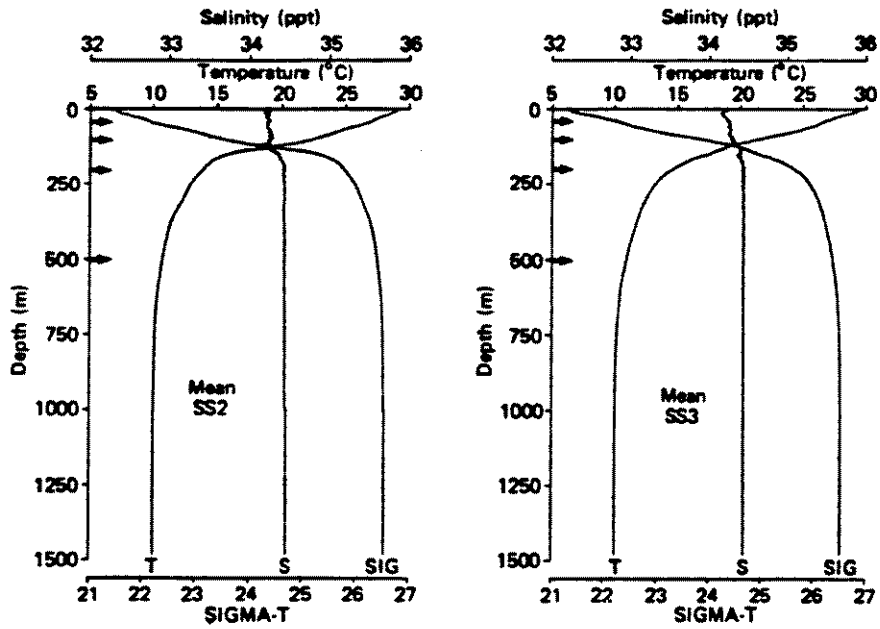

Figure 4.62: Averaged Background Profiles near SS2 and SS3 Moorings. No mixed layer of consequence existed during this period, and density is essentially temperature-controlled (adapted from Apel et al. (1985)).

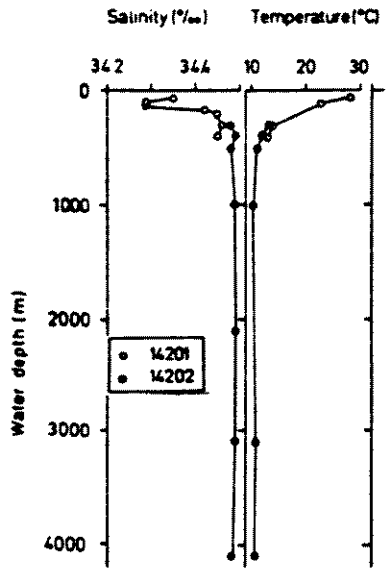

Figure 4.63: "Valdivia" Hydrographic Profiles. Data from stations 14201 (7° 38.8′N, 118° 27.9′E) and 14202 (7° 32.8′N, 121° 30.4′E) combined (adapted from Exon et al. (1981)).

4. Salinity. In February, salinity at the surface varies from >34.0 ppm along the Philippines to about 33.5 ppm along Palawan (see Fig. 4.35(a)). By August, salinity values have decreased generally and are all between 33.4 and 34.0 ppm (see Fig. 4.35(b)). The general gradient direction has shifted from westward in February to northwestward in August.

5. Salinity Variation with Depth. For the same locations noted above for Temperature/Depth profiles, salinity variation with depth is shown (see Fig. 4.62 & Fig. 4.63). In the Fig. 4.62 profiles, the salinity value at the surface (>34.0 ppm) increases irregularly with depth and becomes slightly larger near the bottom of the strong tropical thermocline (at about 200 meters); it retains that value (about 34.4 ppm) into the deep basin. The other profiles (see Fig. 4.63) experience a minimum value (about 34.3 ppm) at about 100 meters, then increase to values near 34.5 ppm at about 300 meters and deeper to the basin floor. At the south entrance to the Sulu Sea from the Celebes (Sulawesi) Sea through Sibutu Strait (see Fig. 4.60), a vertical section of salinity is given by Fig. 4.64. A salinity maximum value (>34.8 ppm) occurs at about 1200 meters depth outside the Strait, but it becomes modified and weakened as it enters the Sulu Sea, showing a very small increase with depth below 1100 meters.

6. Sediments and Turbidity Currents. The broad shelves adjacent to Palawan, Borneo and the Sulu Archipelago are covered with calcareous sand, gravel and rocks (see Fig. 4.65). Calcareous ooze and silt covers the northwestern two-thirds of the deep basin; it is assumed that turbidity currents moving along the indicated paths have carried the materials from the broad shelves into deep basins as calcareous turbidites. The shelf off Panay, Negros and Mindanao is covered with sediment (silt) that is muddy and poorly sorted; turbidity currents carried this into the adjacent deep basin region as mostly non-calcareous turbidites.

7. Seiches, Internal Waves. The Sulu Sea has had evidence of long-wave seiches travelling from SE-NW in the form of lines of surface roughness that have been photographed by satellites (Landsat-1 and Nimbus 7), by radar backscattering, by expendable bathythermographs and by echo sounder records underwater. The seiches appear to be surface evidence of large internal waves that extend from the surface to as deep as 500 meters below the surface. These features show wave lengths of 7 to 16 km, and the "crests" extend horizontally for more than 350 km. The "crests" are about 2 km wide; and they travel in packets that are about 80 km apart (see Fig. 4.66; and Figs. 4.67, 4.68, 4.69, 4.70 & 4.71).

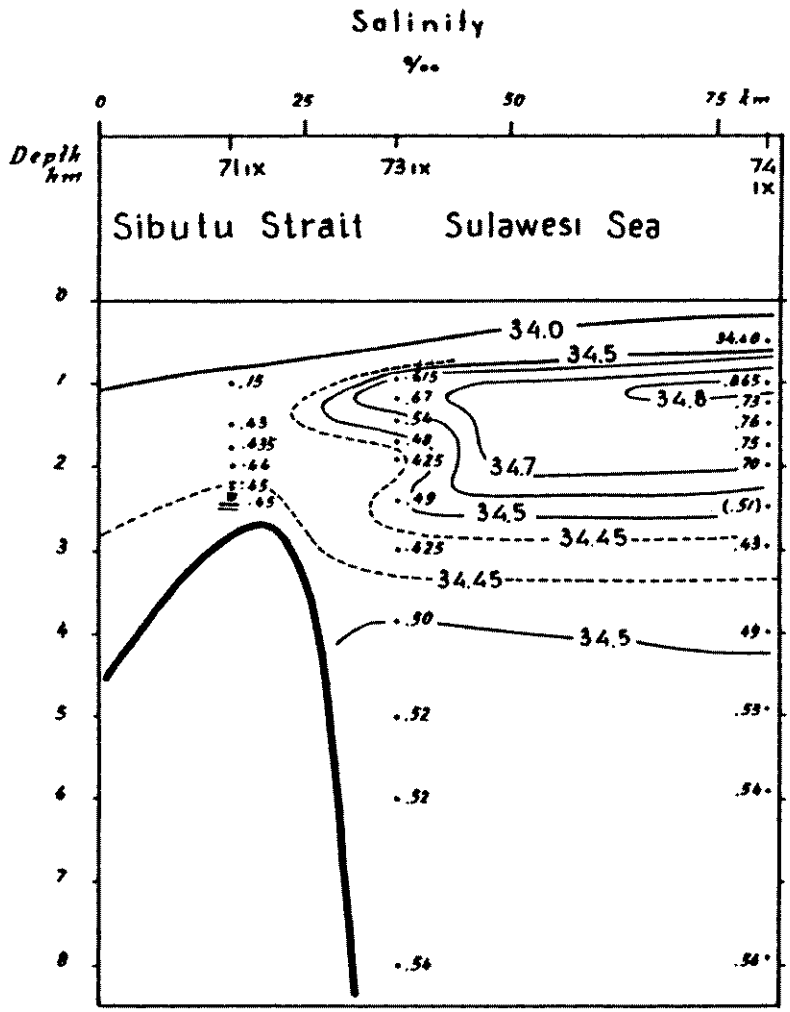

Figure 4.64: Salinity Distribution at the Entrance of the Deepest Passage Leading from Sulawesi (Celebes) Sea to Sulu Sea; depths in m x 100 (adapted from Tjia (1966)).

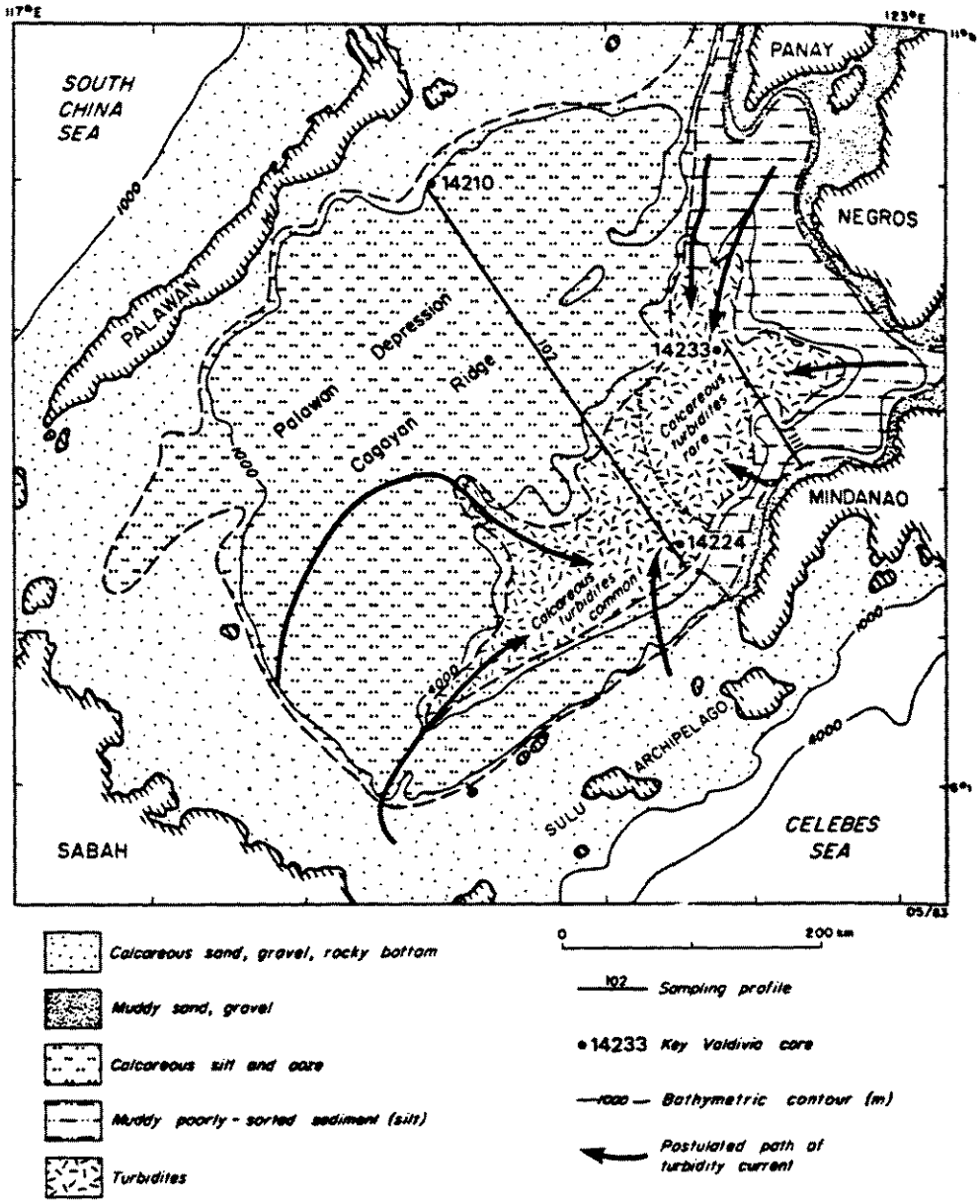

Figure 4.65: Sketch Map showing Distribution of Surface Sediment in the Sulu Sea, and Postulated Paths of Turbidity Currents in the Sulu Sea Deep (adapted from Exon et al. (1981)).

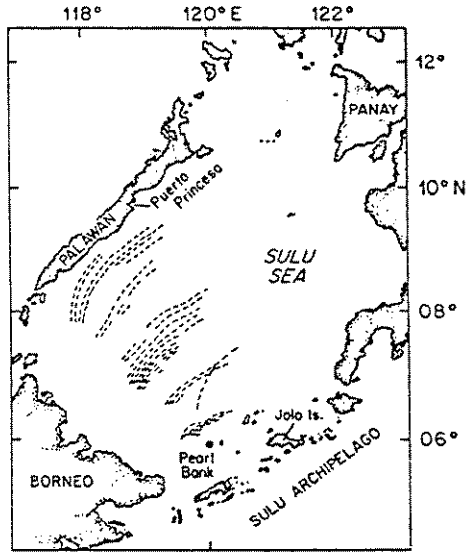

Figure 4.66: Map of the Sulu Sea showing Patterns produced by Surface Manifestations of Internal Solitary Wave Packets (adapted from Geise and Hollander (1987)).

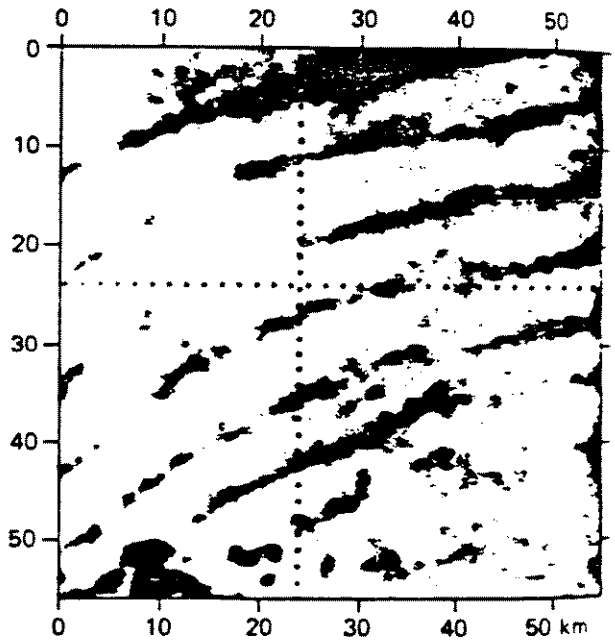

Figure 4.67: Nimbus-7 Image of Internal Solitons in Sulu Sea made during Sulu Sea Cruise on 5 May 1980. Contrast image is 55.55 km on a side; resolution is 868 m (adapted from Apel et al. (1985)).

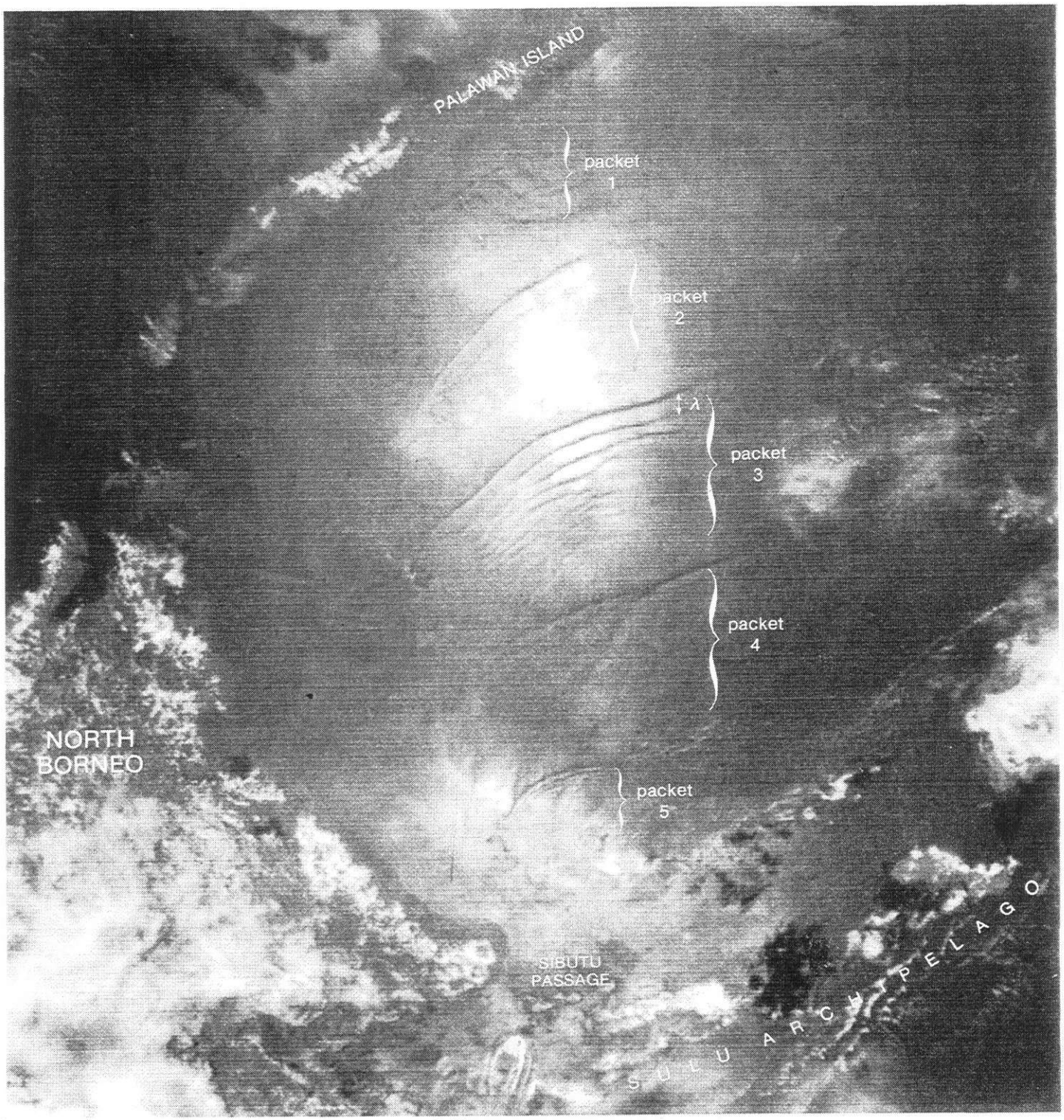

Figure 4.68: Enlarged View of DMSP VHR (Low Enhancement) Satellite Photograph which shows Internal Waves in the Sulu Sea within the Sunglint Pattern at 0419 GMT 2 April 1973. Five packets of internal waves are marked; in packet 3 the longest wave length is about 7 km, and wavelength decreases from the front to the rear of the packet (adapted from Fett et al. (1977)).

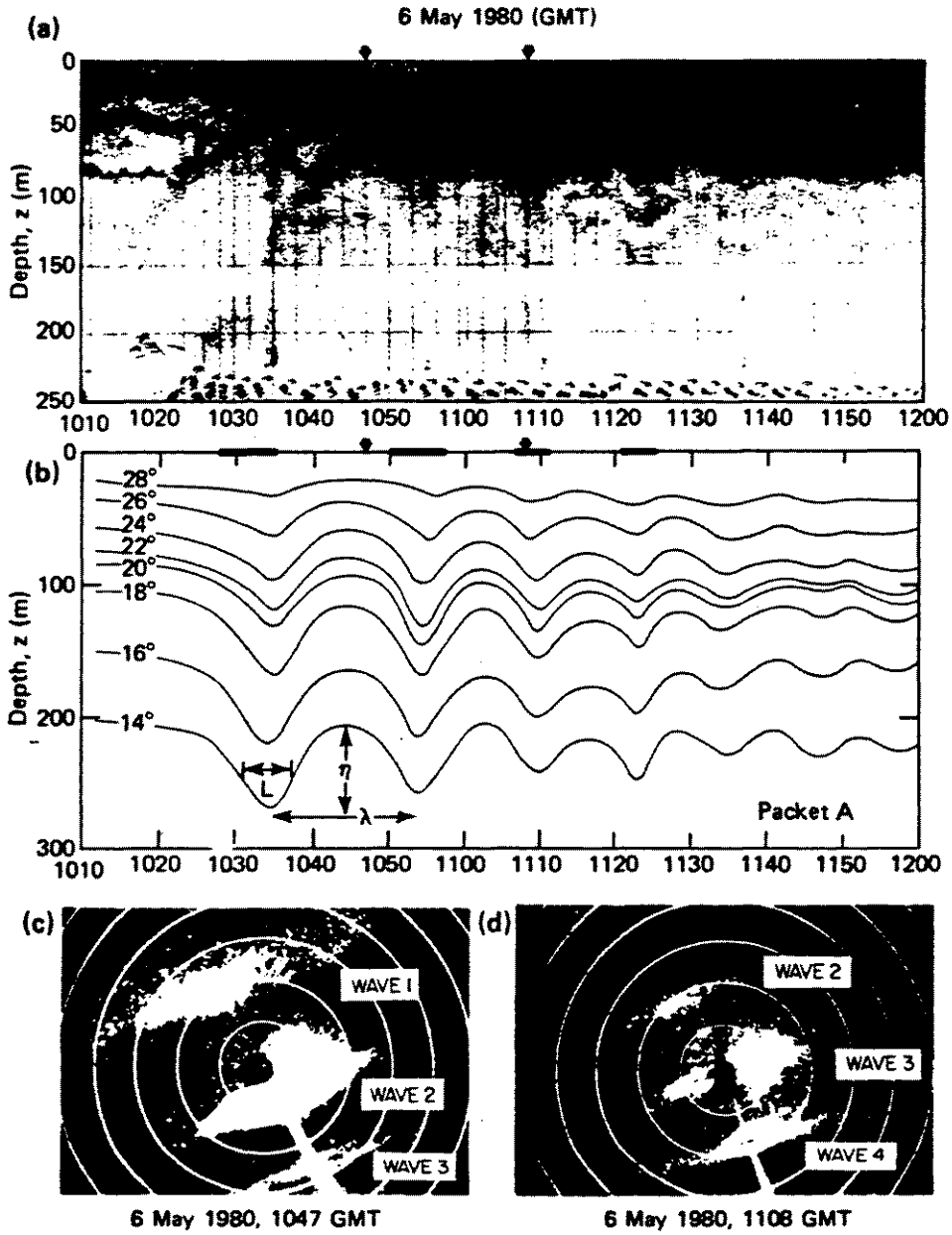

Figure 4.69: Upper: Echo-sounder Record for Packet A at a point well out in the Sulu Sea. The deep scattering layer has obscured the lead soliton. Center: Isotherm Displacements of Packet A constructed out of Repeated XBT Casts made at the Locations shown on the Upper Record. An amplitude of about 60 m was obtained at this time. Lower: Backscatter from Ship's X-band Radar PPI showing Packet A. Range rings at 1.0 n mi intervals. Surface roughness was concentrated in the darkened regions shown at z = 0 in the center plot (adapted from Apel et al. (1985)).

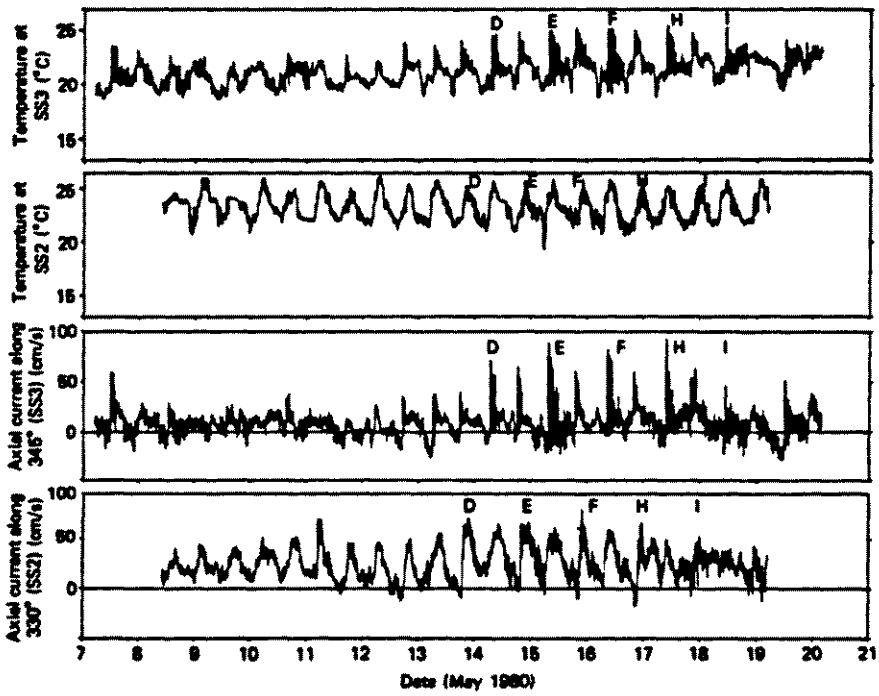

Figure 4.70: Time Series of Temperature and Axial Currents at 100 m Depths at SS3 and SS2. More energetic soliton packets are labeled (D, E, F, H and I). Note the evolution between SS2 and SS3 (adapted from Apel et al. (1985)).

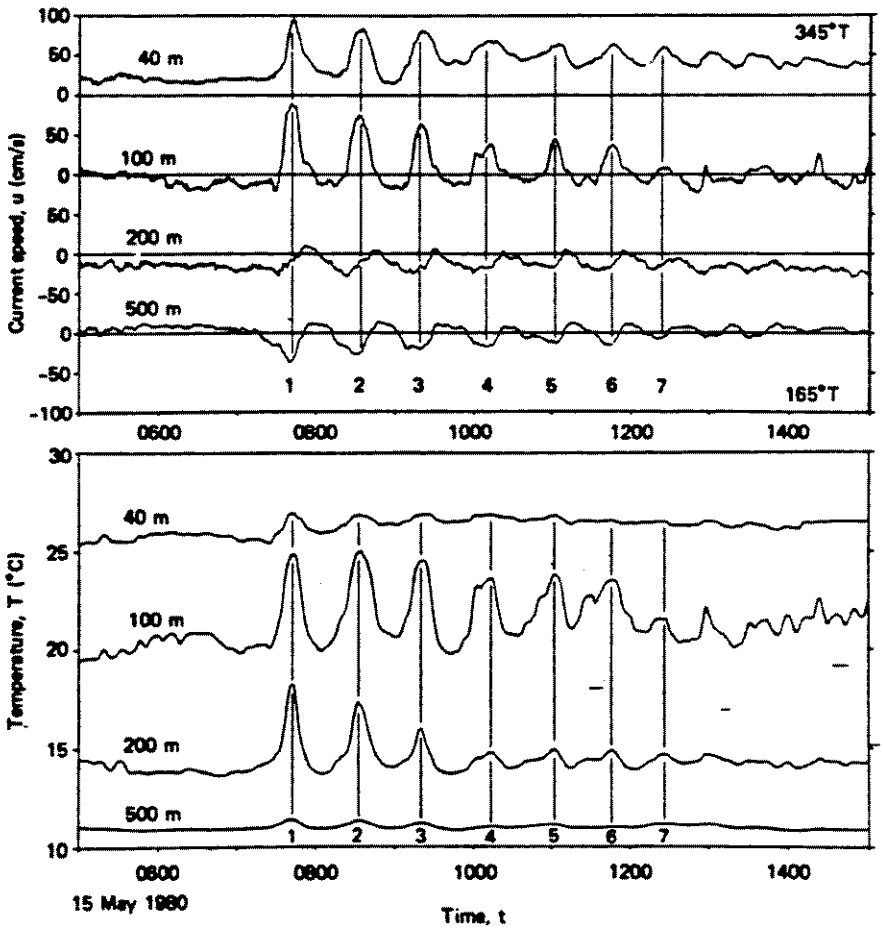

Figure 4.71: Time Series of Currents and Temperature of Packet E at SS3, at four depths. The 180° phase change in current with depth indicates the cellular nature of the streamlines (adapted from Apel et al. (1985)).

D. Luzon Strait (Bashi Channel)

This is the opening between Luzon and Taiwan at the north of the Philippine Island arc. This relatively deep connection between the Philippine and South China Seas has bathymetry as shown in Chuang (1986), Fig. 4.72.

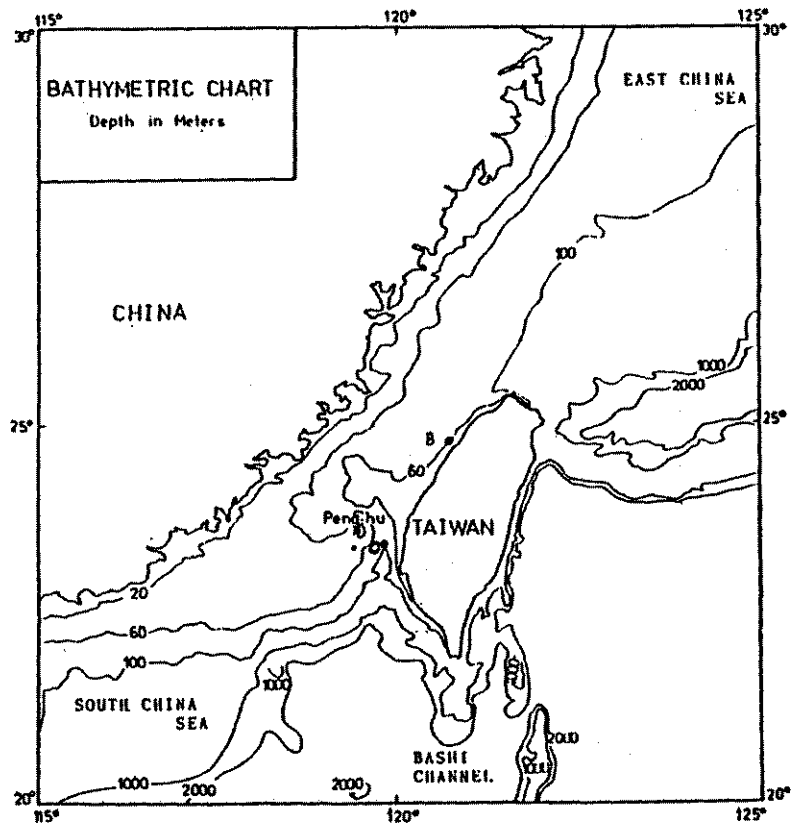

Figure 4.72: Bathymetric Chart of Taiwan Strait and Vicinity. Note Station B and Station C Location (adapted from Chuang (1986)).

1. Current Circulation Patterns. The surface currents are dominated by the presence of the strong Kuroshio Current (see Fig. 4.73; and Fig. 4.74) in both summer and winter. During summer, there appears to be some outflow from the South China Sea through Bashi Channel (or Strait) into the Philippine Sea; in winter, that is reversed. Plots of the current components along Bashi Channel appear directly related to windstress, and inversely related to sea level (see Figs. 4.75 and 4.76).

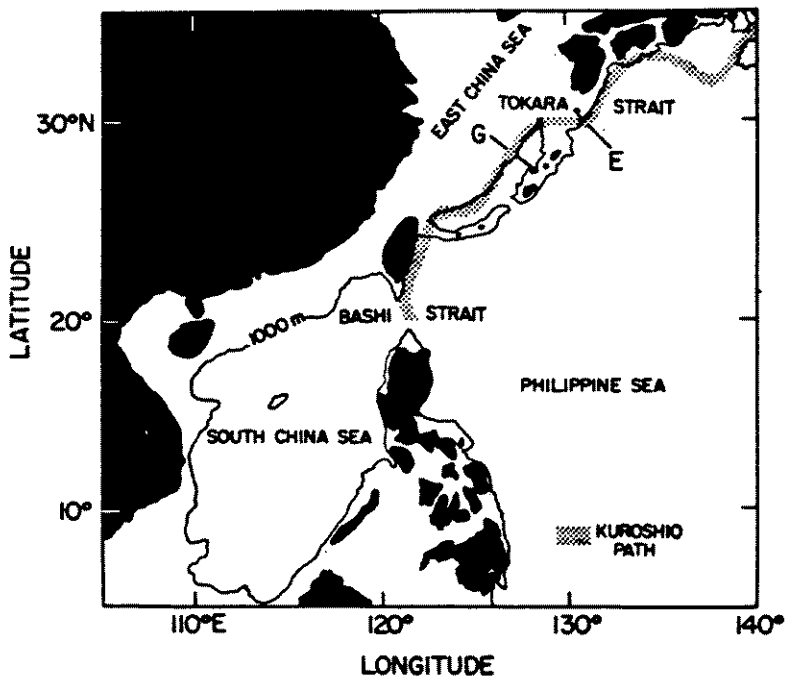

Figure 4.73: The Main Path of the Kuroshio Front and the 1000 m Bottom Bathymetry (adapted from He and White (1987)).

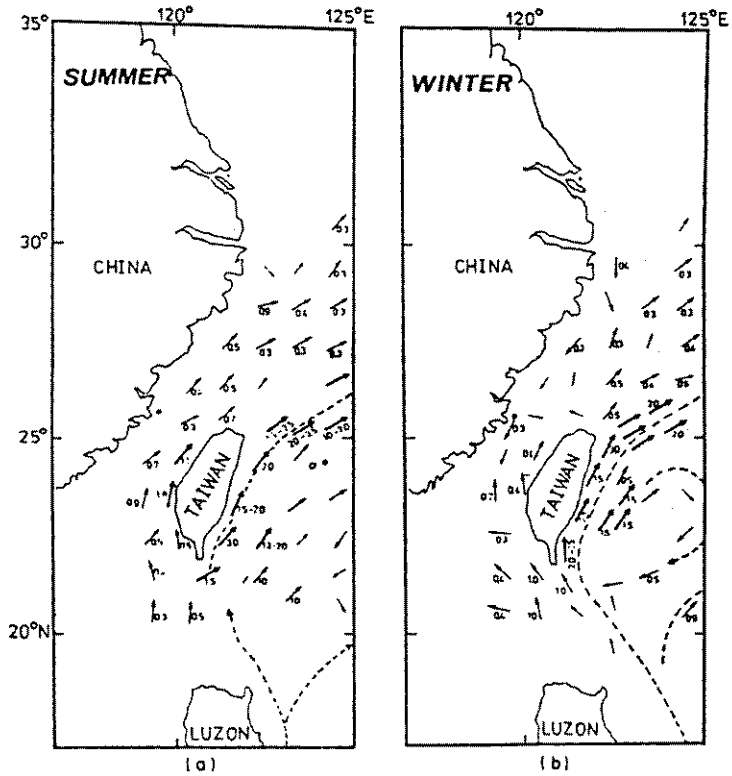

Figure 4.74: Current Chart in Knots: (a) Summer, and (b) Winter adapted from Chuang (1986)).

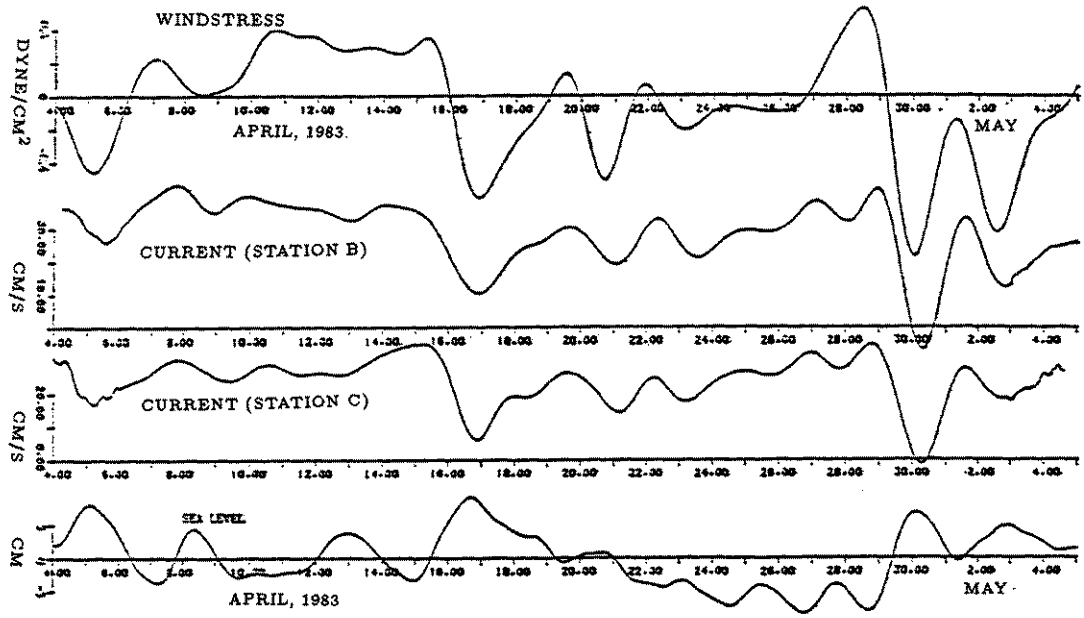

Figure 4.75: Time Series of the Filtered Along-strait Components of Windstress, Current, and Sea Level. See Fig. 4.72 for locations of Stations (adapted from Chuang (1985)).

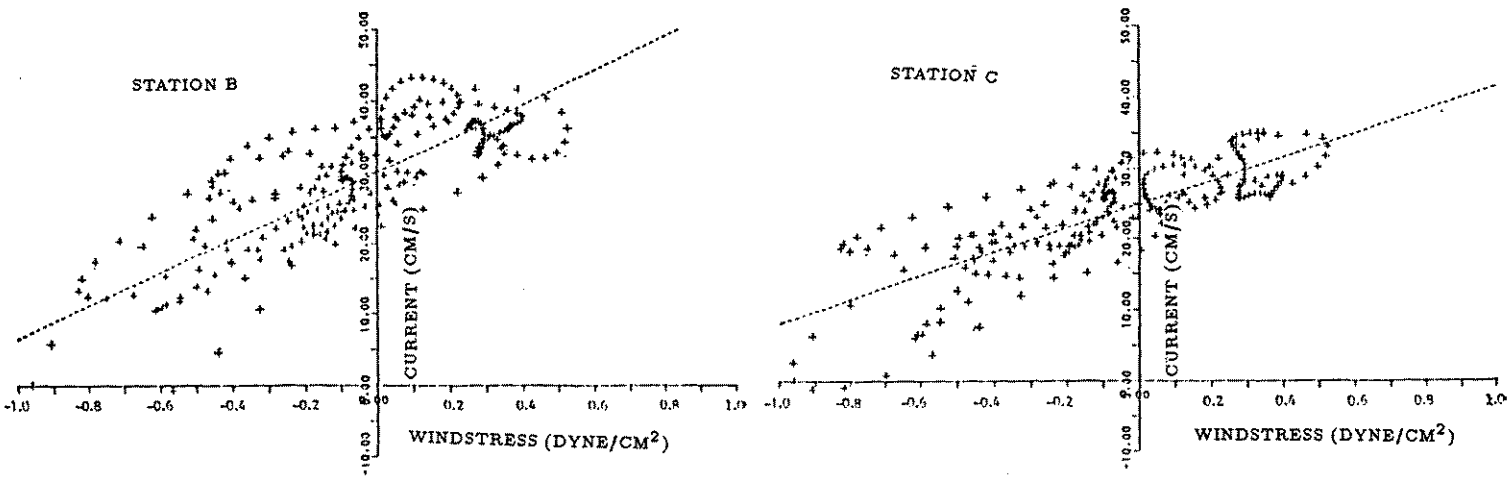

Figure 4.76: Scatter Diagrams of Windstress Versus Current Velocity (at 3-h Sampling Interval), with the Fitted Line resulting from Linear Regression Analysis plotted (adapted from Chuang (1985)).

Scatter diagrams of windstress against current velocity shows reasonable correlation. Currents calculated using zero-lagged and 4-hour lagged windstress data are shown plotted against measured currents with good results at the sampled stations B & C (Figs. 4.77 and 4.78).

Cotidal lines for diurnal and semidiurnal tide components are shown for highwater times across Bashi Strait in Fig. 4.79.

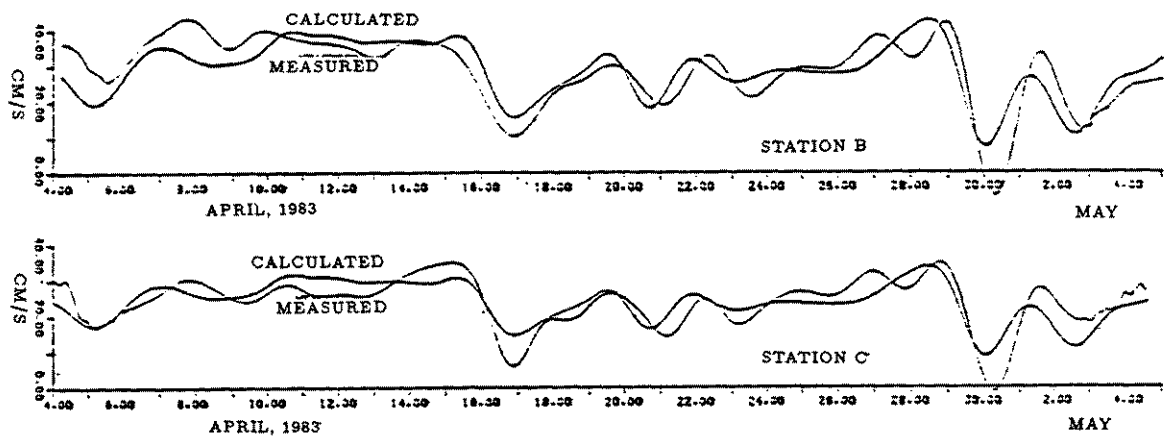

Figure 4.77: Measured Current and Calculated Current using Zero-lagged Windstress Data (adapted from Chuang (1985)).

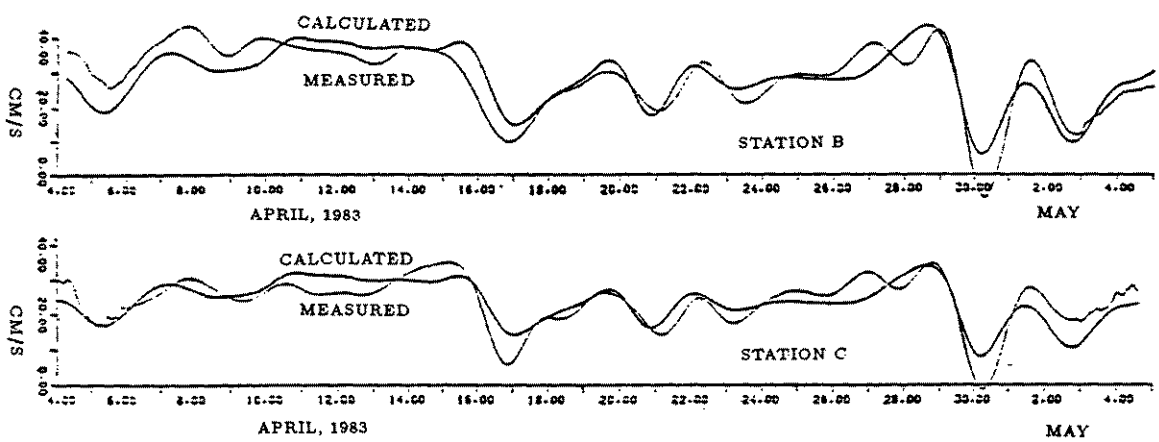

Figure 4.78: Measured Current and Calculated Current using 4-hour lagged Windstress Data (adapted from Chuang (1985)).

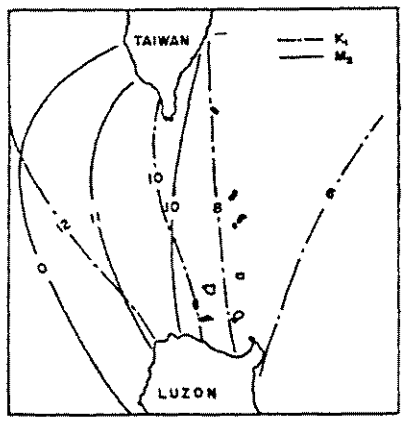

Figure 4.79: Cotidal Lines of the Diurnal Tide K_1 and the Semidiurnal Tide M_2 (adapted from Kanari and Teramoto (1981)).

2. Sea Surface Temperature. Average temperature charts (Figs. 4.17 and 4.18) show some seasonal variation in Bashi Channel. In August the temperature is essentially uniform in the Channel and very warm: almost 29°C. By November it has dropped by 2 to 2.5°C, with a gradient that shows temperature decreasing northward. In February, another decrease (by almost 2°C) has occurred, with a stronger N-S gradient present, showing the coldest temperatures of the year (about 24 to 25°C). In May, the N-S temperature gradient remains strong with values from 27 to 29°C. (Sea surface temperature for all 12 months are available in Appendix A.)

3. Temperature Variation with Depth. An E-W section of temperature in Bashi Channel is presented in Fig. 4.80 for 17–20 May 1985. Below 1000 meters, the resulting distribution reflects the lack of free exchange across the Channel.

Long-term bimonthly averages of temperature that are values averaged over the upper 200-meters of water are shown by Fig. 4.82. One feature in Bashi Channel is the strong gradient present between the warm conservative values to the east and more variable values to the west of the Channel. Annual mean values are shown in Fig. 4.81, and the strong gradient across the Bashi Channel is very much in evidence, as expected.

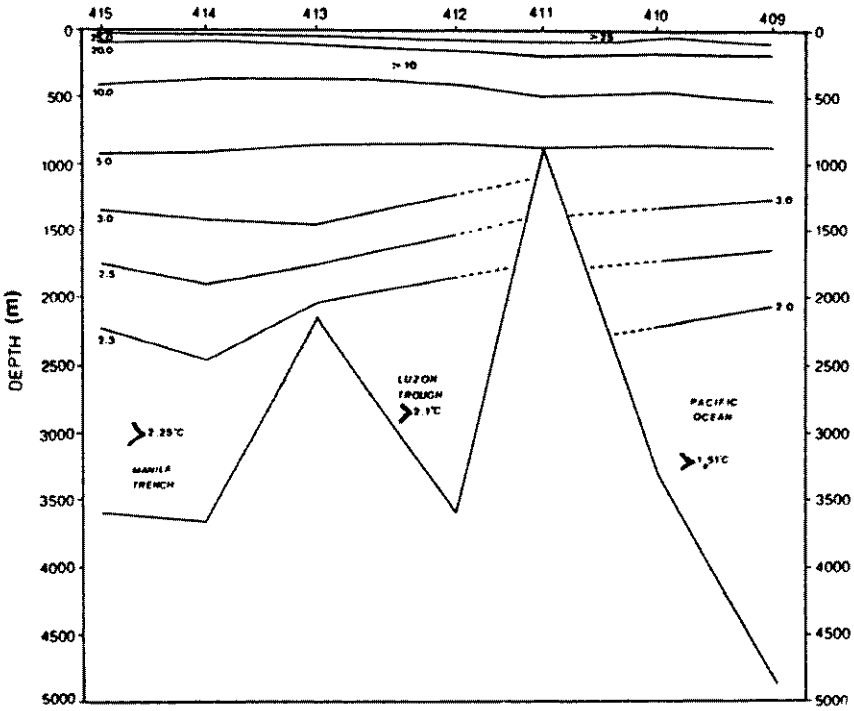

Figure 4.80: A Vertical Section of the Water Temperature (°C) in the Bashi Channel, 5/17–5/20, 1985 (adapted from Wang (1986)).

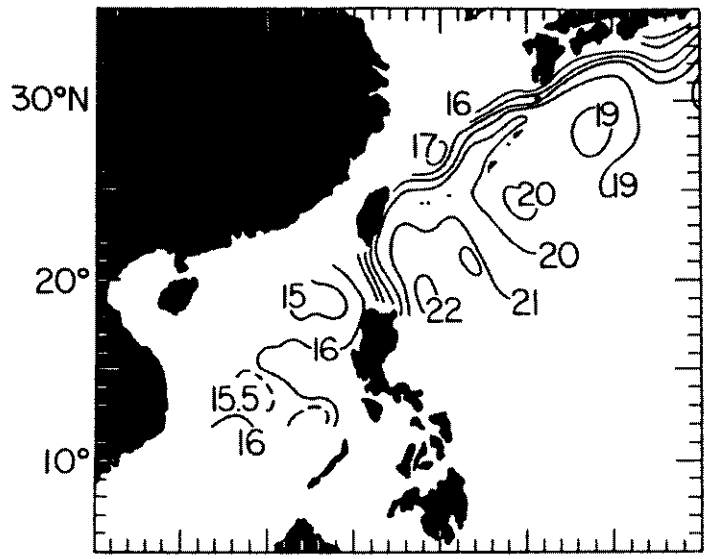

Figure 4.81: Long-term Annual Mean (1979–1982 (adapted from He and White (1987)). The contour interval is 1°C.

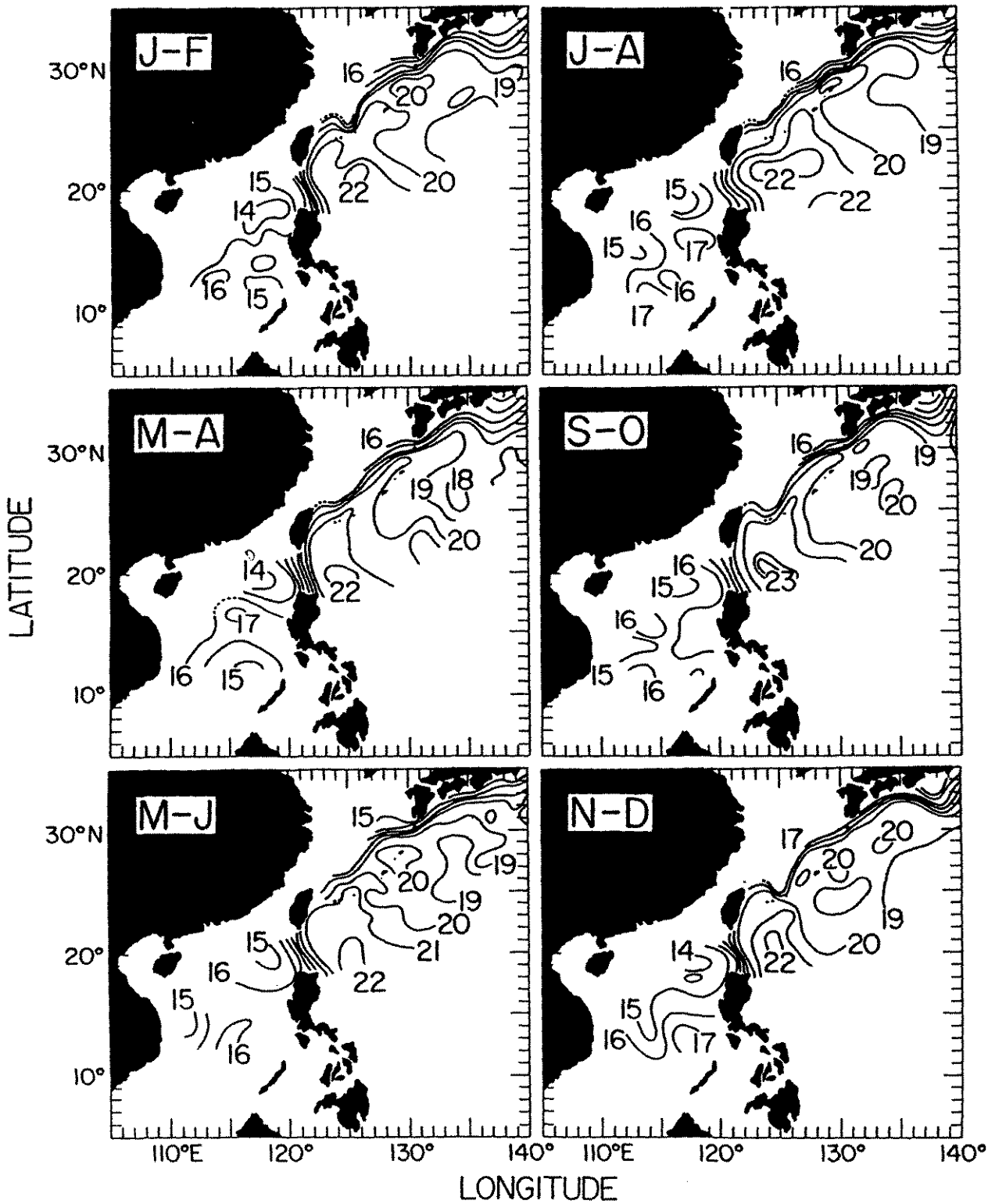

Figure 4.82: Long-term bimonthly Mean Maps of Vertically Averaged Temperature (adapted from He and White (1987)). The contour interval is 1°C.

Contours of temperatures measured at depths of 2000 db (read "meters") and at 2500 db (meters) in the Bashi Channel vicinity show some horizontal temperature variation (0.03 to 0.05°C) occurring in Figs. 4.83(a) & (b).

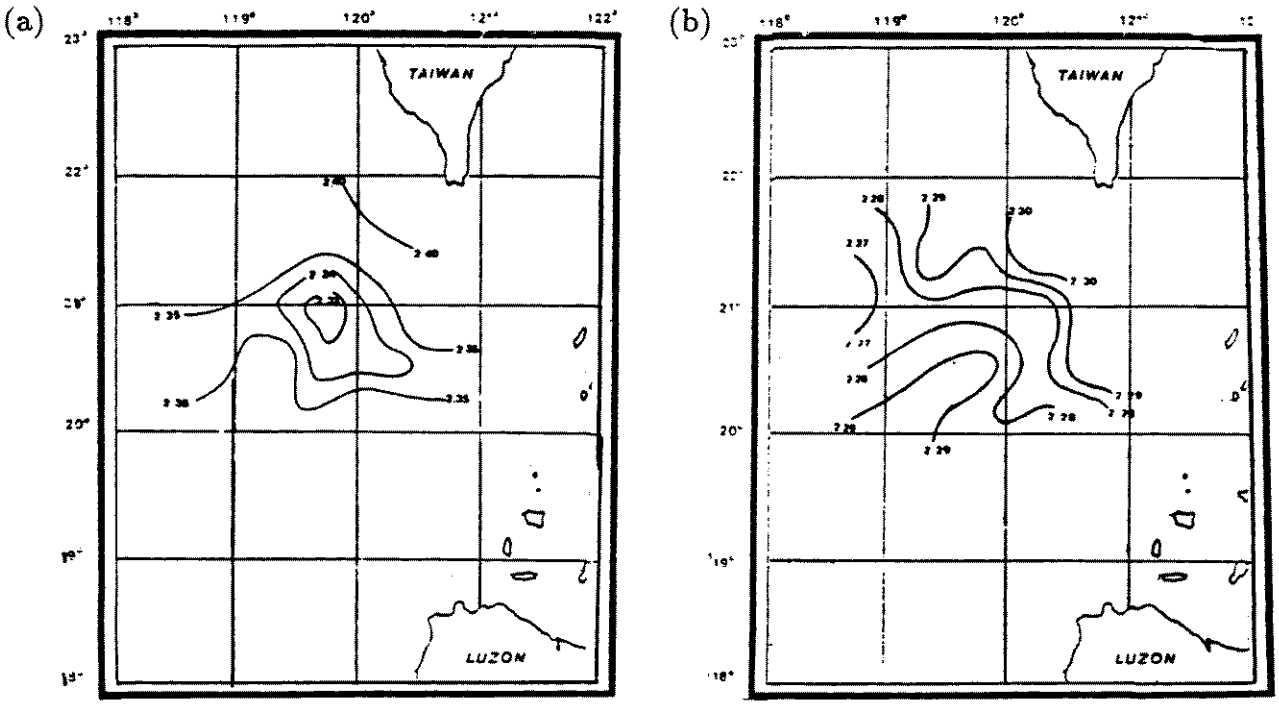

Figure 4.83: The Horizontal Distribution of Water Temperature (°C) (8/1–8/6, 1985) at (a) 2000 dB and (b) 2500 dB (adapted from Wang (1986)).

4. Salinity Variation with Depth. An E-W section across Bashi Channel from data observed during May 1985 shows sharp increases in value from the surface to the depth of the salinity maximum, at about 150 meters. Below this, values decrease to the minimum salinity core at about 500 meters depth. Below this minimum, salinity values increase slightly toward the bottom (see Fig. 4.84).

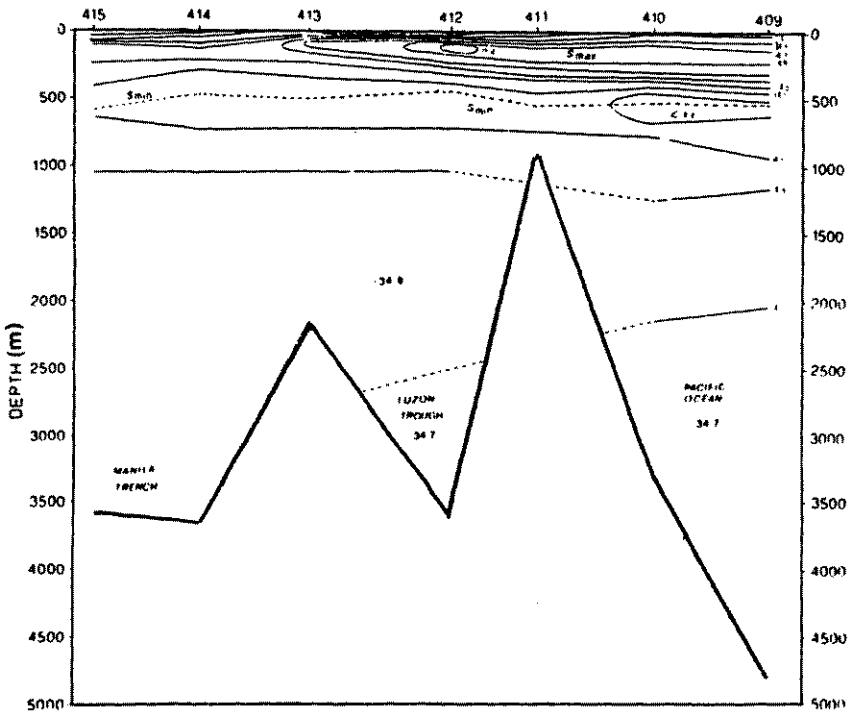

Figure 4.84: A Vertical Section of the Salinity (ppm) in the Bashi Channel, 5/17–5/20, 1985 (adapted from Wang (1986)).

Near southern Taiwan, a study reported in Fan and Yu (1981) shows sections prepared from data observed at stations whose locations are shown in Fig. 4.85. The salinity distributions along a vertical section in the Bashi Channel are shown for three seasons (August, December and April) in Fig. 4.86. The stations locations are along an east-west line (see Fig. 4.85) near southern Taiwan; the sections extend from the sea surface to 700 meters depth. A salinity maximum extends from the Pacific ocean (to the right) into Bashi Channel, centered at about 150 meters depth. In August and April, a marked salinity gradient extends from lower values at the surface down to this maximum; in December the deep mixed layer extends from the surface to about 100 meters depth in the Channel and the Pacific Ocean, and the lower values of salinity near the sea surface are not observed then; however, this does not apply to the northern South China Sea in December. There, also, the August salinity values are lower than in other parts of the section; this applies as well to the salinity maximum values observed between 100-200 meters depth.

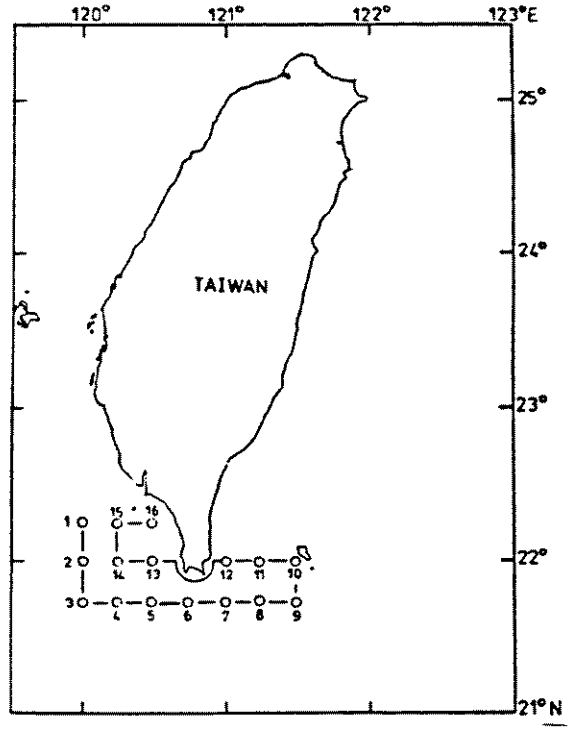

Figure 4.85: Map of Station Locations (adapted from Fan and Yu (1981)).

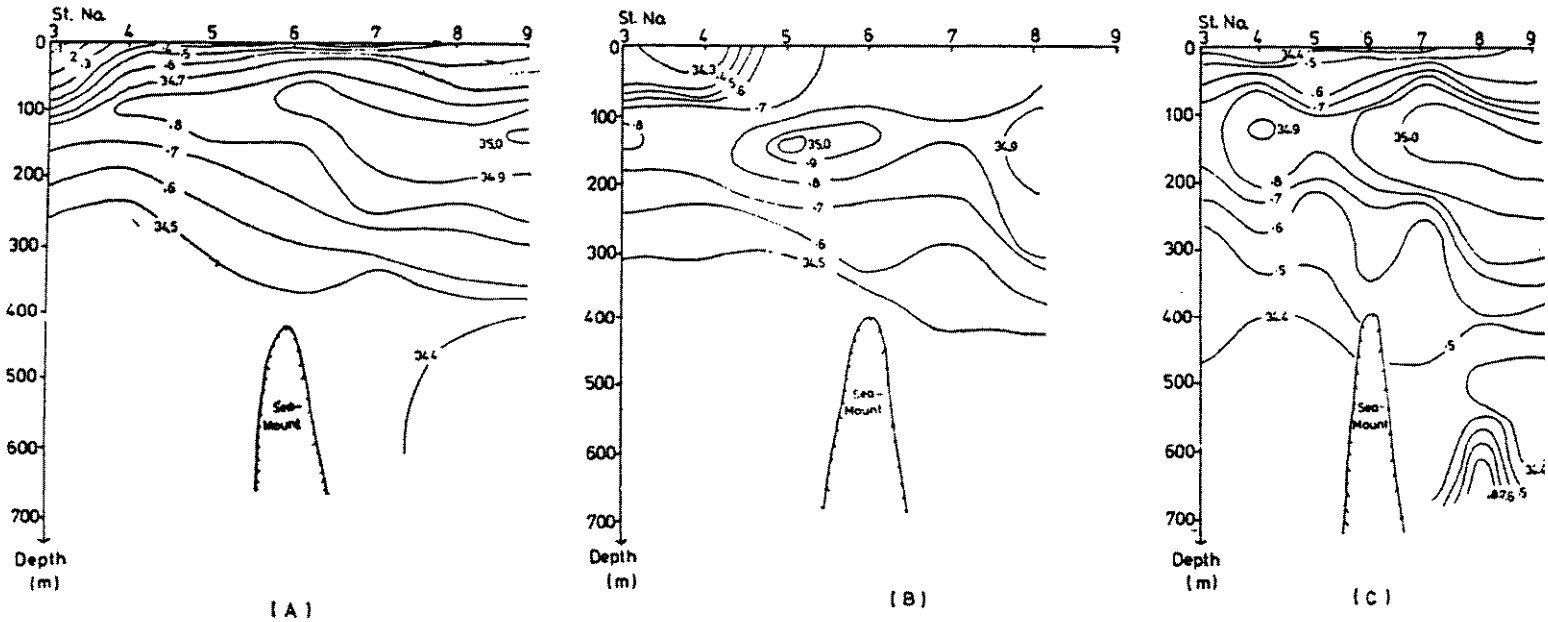

Figure 4.86: Vertical Salinity (ppm) Distribution in (A) late August; (B) middle December and (C) middle April in Bashi Channel (adapted from Fan and Yu (1981)).

5. Temperature versus Salinity. The Temperature-Salinity (T-S) diagrams for the three seasons studied in Bashi Channel by Fan and Yu (1981) are shown in Figs. 4.87-4.89; the stations locations (shown in Fig. 4.85) are nearer southern Taiwan than those in Fig. 4.86. The T-S values at 150 meters depth (near the maximum salinity value) are shown as open circles on each T-S plot. Stations 2, 13 and 14 are in the South China Sea; these show values that depart most widely from the other station plots above 150 meters depth, especially in August. Below 150 meters the station plots vary little from one another in all three seasons. This indicates a consistent watermass occurs below 150 meters, which is relatively unaffected by the seasonal influences above that depth. At great depths just west of Bashi Channel, the T-S relation for abyssal waters is clearly linear, with salinity increasing with decreasing temperature (see Fig. 4.90).

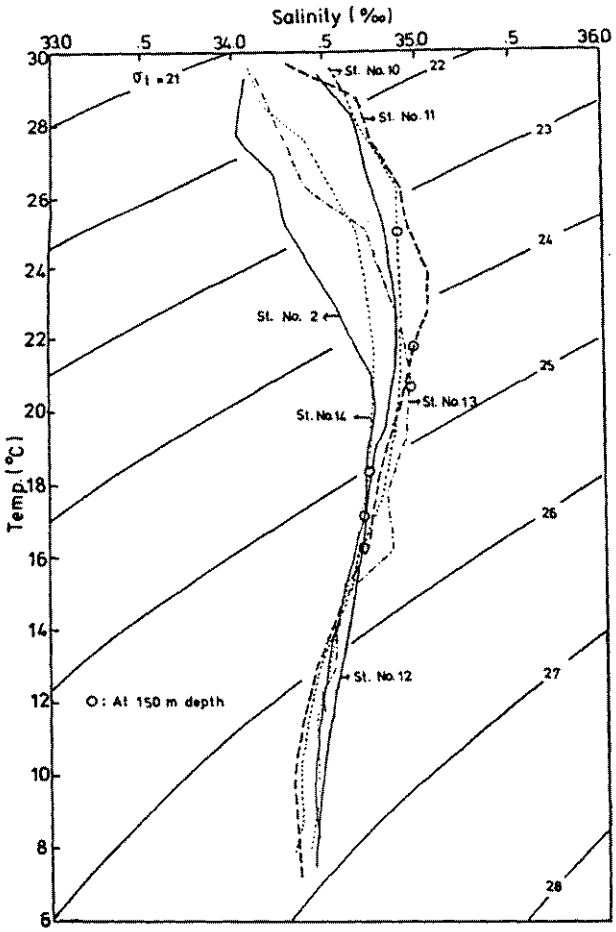

Figure 4.87: TS-diagrams for six stations in late August 1980 (adapted from Fan and Yu (1981)).

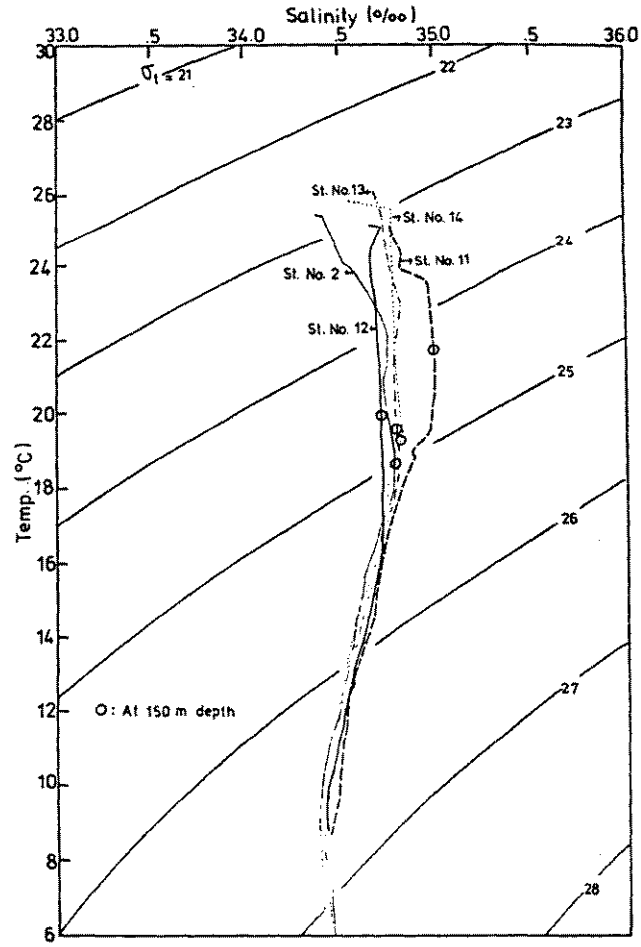

Figure 4.88: TS-diagrams for six stations in middle December 1980 (adapted from Fan and Yu (1981)).

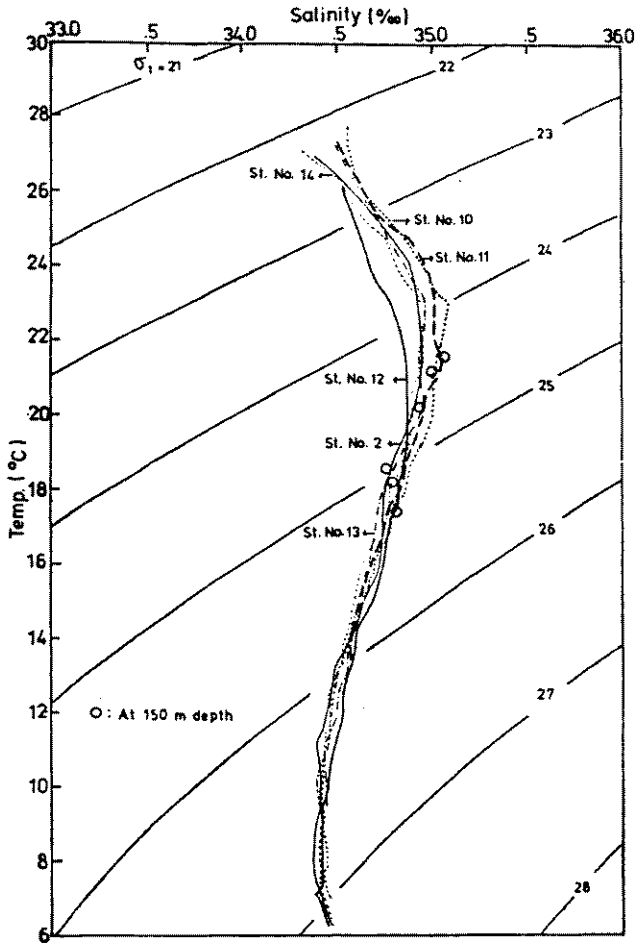

Figure 4.89: TS-diagrams for six stations in middle April 1981 (adapted from Fan and Yu (1981)).

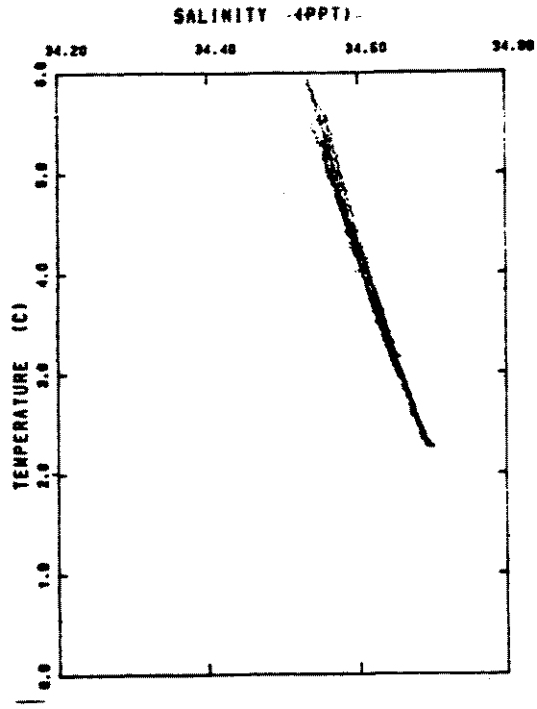

Figure 4.90: The T-S relation of the abyssal waters of the Northern South China Sea below 800 dB (adapted from Wang (1986)).

E. Shallow Seas (between islands)

The seas between the central Philippine Island group, the Visayas, are areas of coral growth. Regions of the Visayas (including Panay, Negros, Cebu, Bohol, Samar and others) where studies of coral have been made are shown on Fig. 4.91. Percentages of coral in various categories for the different types of locale in these shallow seas are shown (see Fig. 4.92). The presence of corals in a region will greatly affect the feasibility of naval operations in the area.

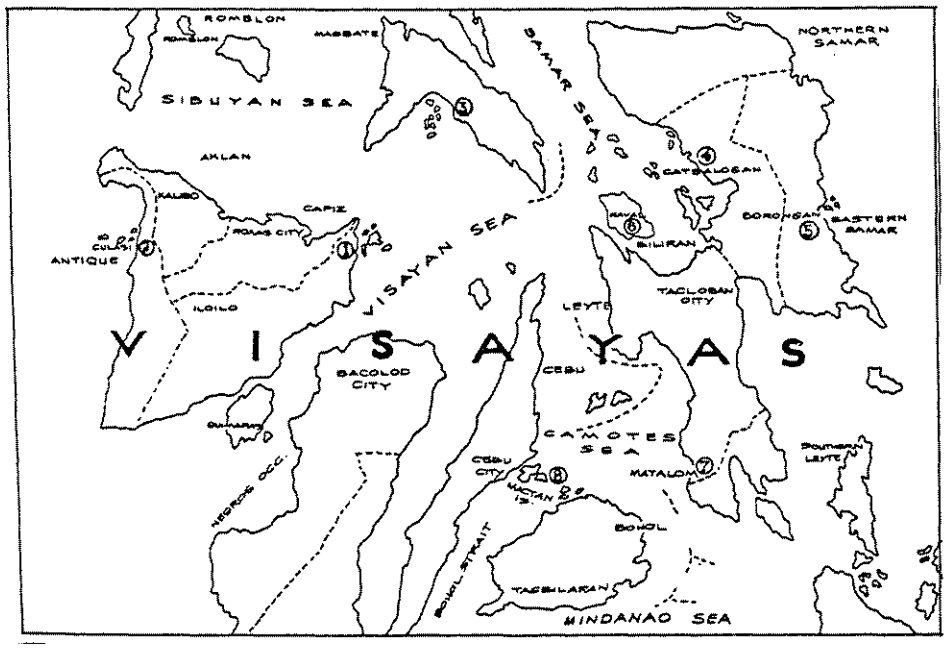

Figure 4.91: Central Philippines (adapted from Cordero (1981)).

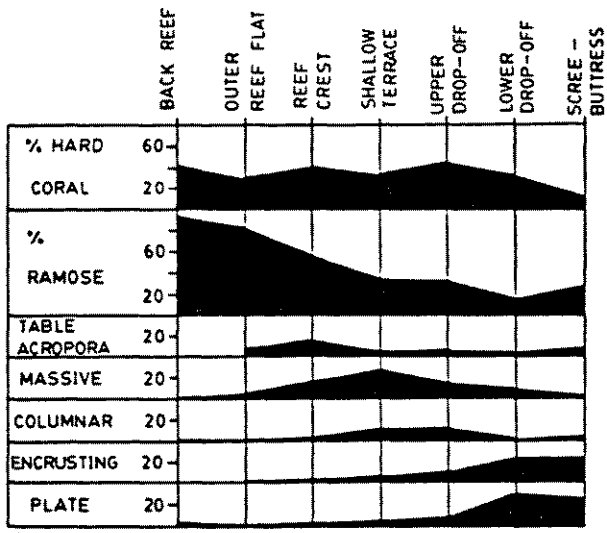

Figure 4.92: Percent Coral Cover per Biotope, and the Percent of the Cover contributed by Each of the Major Growth Forms (adapted from Ross and Hodgson (1981)). Note the clear progression from ramose to plate forms with increasing depth.

CONCLUSION. It is important to consider these ocean parameters when preparing for particular Naval operations within the Philippine Islands region. Relative significance of the ocean factors depend on the nature of the Naval operation considered—whether it is an amphibious landing, navy resupply, hurricane evacuation, weather forecasing for air operations or any of the other many possibilities.